

UNIVERSITY OF OKLAHOMA  
GRADUATE COLLEGE

TESTING STRUCTURAL ELEMENTS FOR FREE VIBRATION TO  
UNDERSTAND THEIR LINEAR DYNAMIC BEHAVIORS

A THESIS  
SUBMITTED TO THE GRADUATE FACULTY  
in partial fulfillment of the requirements for  
the degree of  
MASTER OF SCIENCE

By

ALIEU JOBE  
Norman, Oklahoma  
2018

TESTING STRUCTURAL ELEMENTS FOR FREE VIBRATION TO  
UNDERSTAND THEIR LINEAR DYNAMIC BEHAVIORS

A THESIS APPROVED FOR THE  
SCHOOL OF CIVIL ENGINEERING AND ENVIRONMENTAL SCIENCE

BY:

---

Dr. Jin-Song Pei, Chair

---

Dr. Royce W. Floyd, Co-chair

---

Dr. Philip S. Harvey Jr.



© Copyright by ALIEU JOBE 2018  
All Right Reserved.

*All Praise be to Allah*

*And to my parents,  
Aminata Jasse Jobe and Momodou Malamin Jobe*

*the love, prayers, support, guidance,  
and motivation you have given me,  
have held me high.  
Thank you!*

## ACKNOWLEDGEMENT

I would like to thank my thesis advisor Dr. Jin-Song Pei of the School of Civil Engineering and Environmental Science at the University of Oklahoma. Dr. Pei has been tremendously supportive of my journey through both academics and research. I have been doing research with her since my sophomore year and she has given me all the necessary training that a student would need to succeed. She spent countless hours reviewing my work, providing constructive feedback and answering my questions.

I would also like to thank my thesis co-advisor Dr. Royce W. Floyd of the School of Civil Engineering and Environmental Science at the University of Oklahoma. He has been a true help to me in both research and academics. His doors are always open for questions. He was always responsive and pointed me in the right direction. He was directly involved in three of the specimens that were tested in this study he designed both of the shear walls tested in this study.

My other committee member, Dr. Philip S. Harvey Jr. of the School of Civil Engineering and Environmental Science at the University of Oklahoma, has also been a strong contributor to my success. He was also directly involved with the testing of the two wall specimens and was the project principal for the timber shear wall project. He gave me beneficial advice and was always willing to answer questions.

I would like to dedicate special gratitude the entities that funded my research. The Oklahoma Department of Transportation (ODOT) not only provided the prestressed bridge girder tested in this study, but also funded the research project. The University of Oklahoma College of Engineering (COE) funded both of the shear wall projects. I was fortunate to be a two time recipient of the Honor's Research Assistant Program's (HRAP) funding for students engaged in research work The

HRAP funding sufficiently sponsored my research work on the timber joints, and thanks to the Honor's College at the University of Oklahoma for making this funding available.

Finally, a special thanks goes to the Dr. Christopher C. Ramseyer, director of Fears Structural Engineering Laboratory and Michael F. Schmitz, technical expert at the lab for making the lab and equipment available for use in this research. I would like to also than other faculty, staff and fellow students at the University of Oklahoma's Civil Engineering and Environmental Science (CEES) department who contributed to the success of this study.

# Table of Contents

<b>List of Tables</b>	<b>x</b>
<b>List of Figures</b>	<b>xii</b>
<b>1 INTRODUCTION</b>	<b>1</b>
1.1 Motivation . . . . .	1
1.2 General Technical Background . . . . .	2
1.2.1 Structural dynamics . . . . .	2
1.2.2 Modeling . . . . .	4
1.2.3 Linear dynamics . . . . .	6
1.2.4 Varieties in specimens . . . . .	7
1.2.5 Structural health monitoring . . . . .	7
1.3 Research Objectives . . . . .	12
1.4 Intended Contributions and Structure of Thesis . . . . .	12
<b>2 LITERATURE REVIEW</b>	<b>15</b>
2.1 Summary of Some Relevant Studies . . . . .	15
2.2 Summary of Relevant Literature . . . . .	17
2.2.1 Full-Scale Dynamic Testing of Bridge Structures . . . . .	17
2.2.2 Damage detection using natural frequencies (Salawu [1997] and Kato and Shimada [1986]) . . . . .	18
2.2.3 Free Vibration of Beams: Numerical Approach (Prokic et al. [2014]) . . . . .	19
2.2.4 Dynamic Analysis of Prestressed Beams . . . . .	20
2.2.5 Dynamic Studies on Masonry Walls . . . . .	23
2.3 Implications of Previous Studies on This Study . . . . .	25

<b>3</b>	<b>METHODOLOGY</b>	<b>28</b>
3.1	Scope of Work . . . . .	28
3.2	Models Specific to Study . . . . .	31
3.3	Anticipated Results . . . . .	33
3.3.1	Anticipated results: simply supported specimen . . . . .	33
3.3.2	Anticipated results: cantilever specimens . . . . .	39
3.4	General Approach . . . . .	47
<b>4</b>	<b>EXPERIMENTAL INVESTIGATION</b>	<b>52</b>
4.1	Overview of Typical Test . . . . .	52
4.2	Instrumentation and Data Acquisition . . . . .	54
4.2.1	Hammers . . . . .	56
4.2.2	Accelerometers . . . . .	58
4.2.3	SCB-68 and DAQ card . . . . .	60
4.2.4	Field calibration of accelerometers . . . . .	61
4.3	Timber Wall: Specimen Description . . . . .	62
4.4	Timber Wall: Test Setup . . . . .	64
4.5	Timber Wall: Test Procedure . . . . .	70
4.5.1	Lateral shear test . . . . .	70
4.5.2	Modal hammer test . . . . .	71
4.6	Prestressed Concrete Girder: Specimen Description . . . . .	73
4.7	Prestressed Concrete Girder: Test Setup . . . . .	76
4.8	Prestressed Concrete Girder: Test Procedure . . . . .	80
<b>5</b>	<b>DATA PROCESSING</b>	<b>83</b>
5.1	Overview . . . . .	83
5.1.1	Research Questions . . . . .	83
5.1.2	Research Approach . . . . .	84

5.2	Results and Analysis: Prestressed Concrete Girder . . . . .	92
5.2.1	Sensor layout . . . . .	92
5.2.2	Phase I demonstrated using mid-span impact . . . . .	93
5.2.3	Governing equations for Girder C relative responses . . . . .	96
5.2.4	Phase II demonstrated using mid-span . . . . .	98
5.2.5	Other phase II results and conclusion . . . . .	102
5.3	Results and Analysis: Masonry Wall . . . . .	105
5.3.1	Masonry wall setup . . . . .	106
5.3.2	Governing equations for masonry wall relative responses . . . . .	108
5.3.3	Phase II demonstrated using masonry wall . . . . .	109
5.3.4	Phase III demonstrated using masonry wall . . . . .	114
5.3.5	Masonry wall: Results conclusion . . . . .	119
5.4	Modular Code . . . . .	120
5.4.1	Architecture . . . . .	120
5.4.2	Description of individual data processing files . . . . .	121
5.4.3	Data processing inputs, outputs and their definitions . . . . .	126
5.4.4	Test nomenclature . . . . .	129
5.5	Other Analysis . . . . .	132
5.5.1	Masonry out-of-plane responses under out-of-plane impacts . . . . .	132
5.5.2	Comparison of force magnitudes between normal and gentle impacts applied on masonry wall specimen . . . . .	135
5.5.3	More details on PSD plots . . . . .	137
<b>6</b>	<b>DISCUSSION</b>	<b>140</b>
6.1	Limitations of this Study . . . . .	140
6.1.1	Instrumental limitations . . . . .	140
6.1.2	Specimen limitations . . . . .	141
6.1.3	Analysis limitations . . . . .	142

6.2	Future Work . . . . .	143
<b>7</b>	<b>CONCLUSION</b>	<b>145</b>
	<b>Bibliography</b>	<b>148</b>
<b>8</b>	<b>APPENDICES</b>	<b>153</b>
<b>A</b>	<b>EXPERIMENTAL INVESTIGATIONS OF MASONRY WALL AND TIM- BER JOINT SPECIMENS</b>	<b>153</b>
A.1	Masonry Wall: Specimen Description . . . . .	153
A.2	Masonry Wall: Test Setup and Procedure . . . . .	154
A.3	Timber Joints: Specimen Descriptions . . . . .	156
A.4	Timber Joints: Test Setup and Procedure . . . . .	157
<b>B</b>	<b>OTHER INFORMATION RELEVANT TO Chapter 5</b>	<b>159</b>
B.1	Other Specimens' Test Nomenclature . . . . .	159



# List of Tables

1	List of collected and processed datasets in this study † specificities partially done and not tested with the data yet, ‡ not sponsored by the major professor . . . . .	12
2	Summary of literature imost relevant to this study . . . . .	16
3	A brief summary of properties of all four specimens †OSB - Oriented strand board . . . . .	30
4	Estimated cross-sectional properties of Girder C using the two methods: (a) gross concrete section, and (b) transformed section . . . . .	36
5	Estimated modal frequencies for Girder C using the section properties calculated in 4 above . . . . .	37
6	Estimated fundamental frequencies and other parameters for the different anticipated modes of vibration for the masonry wall . . . . .	44
7	Estimated fundamental frequencies for the lumped mass modelled specimens in this study . . . . .	46
8	Summary of major activities in the experimental work: The initials in the table represent: AJ - Alieu Jobe (author), JSP - Dr. Jin-Song Pei, RWF - Dr. Royce W. Floyd, PSH - Dr. Phillip S. Harvey Jr., MFS - Michael F. Schmidt (lab coordinator), CWC - Conor W. Casey, CDM - Dr. Cameron D. Murray, SDT - Stephen D. Tanksley, and YPS - Yohanes P. Sugeng . . . . .	51
9	Description sensor allocation details. †“ai” stands for analog input . . . . .	68
10	Details on Impact Locations . . . . .	73
11	Accelerometers with their corresponding channel “ai” designations, resolutions, cable lengths and directions of measurement . . . . .	79
12	Locations of all sensors . . . . .	79

13	Masonry wall list of sensors IDs, channel IDs and measured acceleration, †channel 1 reserved for hammer and channel 0 is not functioning . . . . .	108
14	Damage states on the masonry wall specimen . . . . .	115
15	Mfiles' inputs and outputs . . . . .	125
16	Test IDs for Timber Wall (Test ID template = TWtest"a" "b" "c" "d")	131
17	Test IDs for Girder C specimens (Test ID template = GCtest "a" "b" "c") . . . . .	159
18	Test IDs for Masonry Wall (Test ID template = MWtest "a" "b" "c" "d") . . . . .	160
19	Test IDs explanation for tested Timber Joint specimens (Test ID template = TJtest"a" "b" "c") †see Figure 62 . . . . .	161

## List of Figures

1	SDOF model example: (a) a water tower on the campus of the University of Oklahoma (OU), and (b) SDOF model for the water tower . . . . .	5
2	Composition of this Study . . . . .	14
3	Pictures of specimens studied: (a) prestressed concrete girder; (b) masonry wall; (c) timber wall, and (d) timber joints . . . . .	28
4	AutoCAD drawings of the tested specimens highlighting overall dimensions and testing boundary conditions: (a) prestressed concrete girder, (b) masonry wall; (c) timber wall, and (d) timber joints, see Table 3 for full dimensions . . . . .	29
5	Models adopted in this study for each specimen type: (a) simple beam SDOF model, and (b) cantilever wall/beam lumped mass model	32
6	Two deflected shapes corresponding to the two different boundary conditions studied for a lumped mass cantilever SDOF model: (a) bending deflected shape, and (b) sidesway deflected shape . . . . .	40
7	Representation of a specimen design in real-world application: (a) masonry building, and (b) representative masonry wall specimen . . . . .	48
8	Representation of model in comparison with the real structure: (a) demonstrates a specimen in reality, where for the heavy top, motions along i, ii, and iii are all possible, and (b) shows the model's representation of the specimen, where only the motion along one direction can be studied at one time . . . . .	49
9	Illustrative overview of the processes involved in a typical test . . . . .	53
10	Configuration of experimental setup and data acquisition system . . . . .	55
11	Dytran modal hammer . . . . .	57
12	Dytran dynapulse impulse hammer . . . . .	57

13	Accelerometers used in this study: (a) Analog Devices (ADXL) accelerometer, and (b) Silicon Designs (SD) accelerometer . . . . .	58
14	Accelerometer mounting accessories: (a) L-bracket for SD sensors, flat bracket for mounting ADXL sensors on the prestressed concrete girder only, Loctite 410 instant adhesive to be applied on bracket before mounting and for mounting, and Loctite 7452 accelerator for accelerating the adhesive bonding power, (b) a mounted SD sensor and (c) a mounted ADXL sensor . . . . .	59
15	The National Instruments (NI) digital acquisition system utilized in this study (a) SCB-68 block; (b) DAQcard-6036E connected to the 68 pin connector, and (c) DAQ card . . . . .	60
16	Timber wall dimension detailing. All dimensions are in inches. . . . .	63
17	Timber wall lateral test setup: (a) bolted anchor for the loading system, (b) bolts to the rigid floor spaced at six feet, (c) rigid floor . . . . .	65
18	The lateral loading system for the timber wall: (a) wire potentiometer for measuring displacement; (b) hydraulic arm for applying lateral force; (c) adjustable chain for transferring lateral force and allowing slack during disengagement of loading system, and (d) s-shaped load cell for measuring applied force . . . . .	66
19	Timber wall sensor layout . . . . .	67
20	Three loading configurations for the timber wall during the modal hammer test: (a) the specimen is under no distributed load from the top; (b) the specimen is with a 4 ft long $W15 \times 50$ centered at the top, and (c) the specimen is with two 4 ft long $W15 \times 50$ placed at the top . . . . .	69
21	Timber wall impact locations where a cross head is used to indicate each impact location . . . . .	72
22	Prestressed girder dimension detailing . . . . .	75

23	Prestressed sensor layout . . . . .	77
24	Prestressed girder impact locations . . . . .	81
25	Top view of the prestressed concrete surface sanded and labeled with impact locations and side view of sensor layout: (a) Impact 15N, (b) Impact 11N, (c) Impact 0, (d) Impact 11S, (e) Impact 15S, (f) Sensor at 22.5N, (g) Sensors at 15N, (h) Sensors at 4N, (i) Sensors at 0, (j) Sensors at 11S, (k) Sensor at 22.5S . . . . .	82
26	Illustrative summary of phase I steps: (a) show the plotted results: (a.i) full relative acceleration-time history of a particular test and its corresponding PSD plot, (a.ii) zoomed plot of the major response window drawn on plot a.1 and its corresponding STFT plot, and (a.iii) zoomed plot of free vibration window on a.ii and the corresponding PSD plot where fundamental frequency, $f_n$ , is be obtained . . . . .	86
27	Illustrative summary of the Girder C's analysis procedure: (a) 3D AutoCAD drawing of specimen showing (1) the in-plane bending deflected shape, (2) the out-of-plane bending deflected shape and (3) the torsional motion about the x-axis of the specimen, (b) showing the sensors of focus for each of the response analyses. . . . .	90
28	Girder C's sensor locations showing the positions of sensors only analyzed herein . . . . .	93
29	Full in-plane absolute acceleration responses for Girder C at locations 22.5N, 0 and 22.5S (i.e., mid-span and supports), as well as the relative acceleration when specimen was excited at location 0 (i.e., mid-span) - center . . . . .	94
30	PSD for the response presented in Figure 29 . . . . .	94

31	Truncated in-plane relative acceleration response for Girder C at mid-span as well as the STFT plot when specimen was excited at mid-span - center . . . . .	95
32	Further truncated response per window in Figure 31 and its truncated PSD spectrum . . . . .	96
33	Demonstration of the rigid body motion at various sensor locations induced by support movement; a linear relationship is given by the trapezoid shown here . . . . .	97
34	A schematic to show: (a) the locations of the three in-plane sensors and center hammer impact location and (b) the first harmonic mode shape for Girder C . . . . .	99
35	Girder C's phase II analysis for in-plane responses at locations 15N, mid-span and 11S when excitation force was applied at mid-span . . .	100
36	Girder C's phase II analysis for out of plane and torsional responses at mid-span when excitation force was applied at mid-span . . . . .	101
37	Girder C's phase II analysis for in-plane responses at locations 15N, mid-span and 11S when excitation force was applied at location 15N . . .	102
38	Girder C's phase II analysis for out of plane and torsional responses at mid-span when excitation force was applied at location 15N . . . . .	103
39	Girder C's phase II analysis for in-plane responses at locations 15N, mid-span and 11S when excitation force was applied at location 11S . . .	103
40	Girder C's phase II analysis for out of plane and torsional responses at mid-span when excitation force was applied at location 11S . . . . .	104
41	Details showing impact locations from a to g where the highlighted location a and c are the main focus in this section . . . . .	105
42	Details of the mounted sensor locations on the masonry wall, refer to Table 13 for the list of the corresponding sensor details . . . . .	107

43	An illustration of the wall's bending and sidesway mode shapes in conjunction to the in-plane sensors: (a)Shows the wall with the three in-plane sensors, (b) shows the fundamental bending mode shape and (c) shows the fundamental sidesway mode shape . . . . .	110
44	Phase II IPB results for masonry the masonry wall when normal impact was applied at location a . . . . .	111
45	Phase II IPB results for the masonry wall when gentle impact was applied at location c . . . . .	111
46	Phase II OPB and TOR results for the masonry wall when normal impact was applied at impact location a . . . . .	113
47	Phase II OPB and TOR results for the masonry wall when gentle impact was applied at impact location c . . . . .	114
48	Phase III analysis illustration for the masonry wall with hand traced crack patterns that are based on the recorded ultimate crack pattern, see Table 14 for labeling description . . . . .	115
49	Summary of the masonry wall results at all five damage states when excitation force ranging from 2700 <i>lbf</i> to 3500 <i>lbf</i> (so-called normal impact) was applied . . . . .	117
50	Summary of the masonry wall results at all five damage states when excitation force approximately ranging from 900 <i>lbf</i> to 1200 <i>lbf</i> (so-called gentle impact) was applied . . . . .	118
51	Flowchart showing the overall architecture of the modular code . . .	120
52	Phase II OPB and TOR results for the masonry wall when normal impact was applied at impact location e, when torsion was anticipated	133
53	Phase II OPB and TOR results for the masonry wall when normal impact was applied at impact location f, when torsion was anticipated	133

54	Phase II OPB and TOR results for the masonry wall when normal impact was applied at impact location g, when out-of-plane bending was anticipated . . . . .	134
55	Comparison between normal and gentle impacts: force magnitudes for normal impact shown in blue, and force magnitudes for normal impact shown in blue, applied at the different damage states labeled from 1 to 5 representing elastic to ultimate state. . . . .	136
56	Figure showing the pwelch frequency plots with a free vibration window length of 0.75s . . . . .	137
57	Figure showing the default pwelch PSD plots with a free vibration window length of 0.92s . . . . .	138
58	Figure showing the default pwelch PSD plots with a free vibration window length of 0.923s . . . . .	139
59	Pictures of the masonry wall specimen . . . . .	153
60	Free-hand sketch of the masonry wall specimen by the author (not to scale) . . . . .	154
61	The masonry wall lateral test setup: (a) string potentiometer for measuring deflection; (b) hydraulic loading piston for applying lateral force; (c) load cell for measuring the applied lateral force, and (d) shear loading plate for transferring the shear load to the specimen	155
62	Connection details for the five timber joint specimens tested . . . . .	156
63	Test configuration for a typical T-shaped timber joint specimen; all dimensions are in inches . . . . .	157
64	Test configuration for a frame timber joint specimen; all dimensions are in inches . . . . .	157



## ABSTRACT

Dynamic forces such as strong seismic, wind, and impact loads can cause severe deterioration of structural elements in residential, commercial and other structural systems. In the field of structural health monitoring (SHM), inherent dynamic attributes of structures are often utilized to assess structural integrity. In modeling and testing, a free vibration refers to a vibration when a sustained excitation force is not required but a non-zero initial displacement and/or velocity is. A free vibration is useful because it reveals inherent dynamic characteristics of the structure itself, which include but are not limited to modal frequencies and mode shapes in linear analysis, as commonly used, and backbones in nonlinear analysis, which are gaining attention.

This study consisted of experimental investigation and data analysis conducted on some of the most common structural elements subjected to free vibration. The scope of the experimental work was extensive spanning two years and involving a real-world prestressed concrete bridge girder tested after four decades of service, a half-scale reinforced masonry wall, a full-scale timber shear wall, and a number of scaled timber connection specimens. All tests were conducted using a modal hammer. A large amount of quality data was collected for future studies using nonlinear techniques (e.g., backbones). The data analysis in this study, however, had a reduced scope focused on only two test specimens; the bridge girder and masonry wall. The goal was to achieve a good understanding of modeling using collected data, and develop a detailed and general linear dynamics data processing and result analysis procedure - paired with modular code - for the two specimens considered in-depth and other test specimens to follow.

Such an in-depth study for a seemingly straightforward free vibration test is motivated as follows: First, a modal hammer test in fact generates both forced and free vibration; using only the free vibration portion of the data is the most proper for exacting fundamental frequency. Next, all models have their applicable range. The A real-world specimen has more than one degree of freedom. Thus, other degrees-of-freedom will be checked using the experimental data to better understand what the extracted fundamental frequency represents for each specimen. The procedure and code developed during this research are demonstrated using the real-world bridge girder and half-scale masonry wall, the two specimens with significance for SHM.

# 1 INTRODUCTION

## 1.1 Motivation

Like humans, structures do not last forever. From the moment they are built, structures begin their aging process. Structural aging is generally accelerated by environmental effects such as wind forces, seismic and temperature fluctuation. The ASCE Infrastructure Report Card for America's infrastructures ([ASCE \[2017\]](#)) indicated that infrastructures in the nation have an average grade of D+. It was also noted that "deteriorating infrastructure is impeding our ability to compete in the thriving global economy, and improvements are necessary to ensure our country is built for the future" ([ASCE \[2017\]](#)). These necessary improvements are certainly not helped by the alarming increment in the negative effects that deteriorate structures at a quicker pace. In Oklahoma, specifically, seismicity has grown exponentially within the last decade as data have shown that the number of magnitude 3+ earthquakes has risen from 1.5 per year prior to the year 2008 to about 2.5 per day in 2015 ([Andrews and Holland \[2015\]](#)). Tornadoes, on the other hand, have also done plenty of damage in the state.

The number of alarming effects that impact the structures is the key influence of this study. This study strives to contribute to the resiliency of structures by providing both data and a better understanding of structural behaviors under certain dynamic circumstances. Specimens tested in this study represent some of the most common structural elements currently used including: a prestressed bridge girder, a masonry shear wall, a timber shear wall and a number of timber joint models. The prestressed concrete girder is a retired component extracted from a demolished bridge after serving for over forty years. The masonry and timber shear walls are laboratory-fabricated specimens designed by other researchers to

study the behaviors of typical lateral force resisting elements used in schools and residential homes, respectively. The timber joint specimens are a set of inexpensive models that represent some of the commonly used stud to plate connections types in timber construction. These timber joints were first built and studied by Sugeng [2006] and Mai et al. [2008] for nonlinear dynamics.

The *goal* of this study is to begin a series of studies to understand quantitatively the behaviors of the selected structural elements under free vibration. Free vibration is believed to be unavoidable in a structural response after every induction of dynamic loads until the vibration dies out. This, in addition to the fact that free vibration reveals some inherent properties of structures, promotes the author's decision to conduct free vibration analysis. The structural elements will be tested with representative data analyzed. The test data is not only useful for this study, but for future studies as well. By applying digital signal processing (DSP) techniques learned from electrical engineering and concepts in structural engineering, the author performs refined data analysis to the test data. The computer programs and the analysis tools developed in this study, will directly benefit future free vibration tests.

## **1.2 General Technical Background**

### **1.2.1 Structural dynamics**

Structural dynamics is a field of study with numerous engineering applications. Examples of the applications include structural engineering (as in this study), mechanical engineering and aerospace engineering. In structural engineering, dynamics can be defined as a time varying behavior of structures. Just like any object in motion, structures under dynamic loads will have a certain displacement, ve-

locity and acceleration. There are numerous types of external forces that building structures are exposed to, and some of the most common ones are wind, seismic and impact forces. Structural properties such as mass, stiffness and damping are inherent properties often used to predict structural responses under dynamic conditions.

Mass, denoted as  $m$ , is a well-known concept and can either be lumped or distributed. The product of mass and acceleration,  $m\ddot{u}$ , is an inertia force according to the Newtons second law of motion. Stiffness, denoted as  $k$ , is defined as the amount of force required to give an object a unit displacement. The product of stiffness and displacement,  $ku$ , produces the spring force according to the Hooke's law. Stiffness can be measured experimentally, and estimated theoretically and numerically. Damping, denoted as  $c$ , is the structure's ability to attenuate its motion. Damping force is often considered proportional to velocity, i.e.,  $c\dot{u}$  is the so-called linear viscoelastic damping force, the first approximation of a really complicated effect.

The forces associated with,  $m$ ,  $c$ , and  $k$ , sum up to produce an internal resistance force called the restoring force. The restoring force balances out any external force - at any time instance - through the force equilibrium equation shown below, according to the Newtons second law of motion.

$$m\ddot{u} + c\dot{u} + ku = P \tag{1.1}$$

where  $P$  represents the external force acting on the structural system. Equation (1.1) is a general equation of motion used to define most simplified dynamic systems.

### 1.2.2 Modeling

Modeling is the act and art of quantitatively reconstructing a real-world phenomenon for a certain purpose. One cannot anticipate a model to capture all attributes of a real-world system because a model is created to only serve a particular purpose.

Real-world structures and test specimens are complicated. They possess many attributes, at least, due to their constitution of composite materials. Taking a building as an example, the different aspects could include, sub-structure, super-structure, mechanical electrical system, cladding, etc. If an engineer were to model a building, it would be impossible to model all aspects simultaneously. As a matter of fact, there may or may not be a real need of doing so given the purpose of the investigation that motivates the modeling. In another general example, a car has multiple systems, each of which performs a specific function. It is impractical to model the entire car at once, instead, the engine system can be modelled as the Rankine cycle, the suspension system as a dynamic system and the transmission system as a pulley system. It is more common and practical to model one system at a time for a thorough understanding.

Structural dynamic systems could be modelled at three levels in analysis: single degree-of-freedom (SDOF), multiple degrees-of-freedom (MDOF) and continuous systems. An SDOF model typically represents the simplest form of a dynamic system. An MDOF model assumes that the system has multiple governing frequencies and corresponding "mode shapes." An MDOF models is more complex thus more accurate than an SDOF model, making it a better representation of a real world structure in general. The same can be said about a continuous model with respect to an MDOF model. This is because, intuitively, a real world structure would be the closest to a continuous system, than to an MDOF system, and last, to an SDOF system. Both SDOF and MDOF models are discrete models - in contrast

to continuous models (Anderson and Naeim [2012]).

An SDOF model is created by greatly simplifying a continuous system. This simplification is useful in determining the fundamental frequency of the system. The fundamental frequency is the lowest frequency at which a dynamic system inherently oscillates when vibrating freely.

One way of the ways of simplifying a continuous structure into an SDOF model is by lumping its mass at a proper coordinate. An example is illustrated in Figure 1.

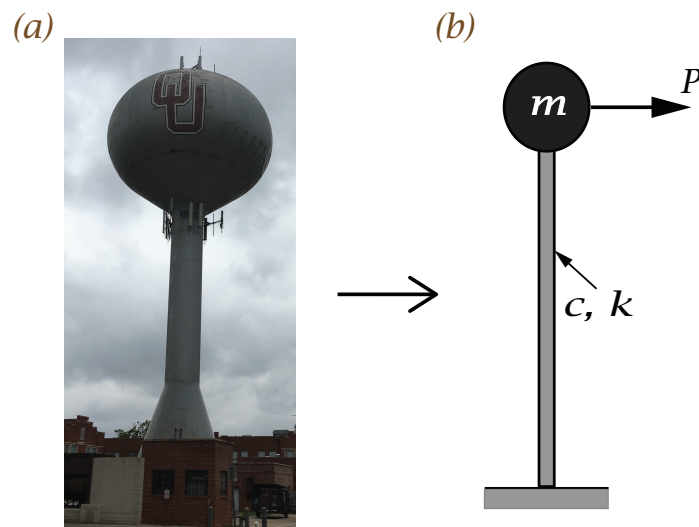


Figure 1: SDOF model example: (a) a water tower on the campus of the University of Oklahoma (OU), and (b) SDOF model for the water tower

In this figure, a water tower and its corresponding SDOF model are presented. In this SDOF system, the fundamental frequency can be estimated using Equation (1.2):

$$f_n = \frac{1}{2\pi} \sqrt{\frac{k}{m}} \quad (1.2)$$

where  $f_n$ ,  $k$  and  $m$  represent fundamental frequency (in Hz), stiffness, and mass,

respectively.

Although not the key focus of this study, an MDOF model is generally used to analyze both simple and complex structures. Modal frequency is the frequency at which a structure resonates (Chopra [2012]). In MDOF modelling, modal frequencies cannot be mentioned without mentioning mode shapes. The number of modal frequencies is the same as the number of degrees-of-freedom. Each modal frequency corresponds to a mode. A mode shape is the deflected shape of a certain dynamic system at any discretized mode or degree-of-freedom. Since continuous systems are typically discretized into MDOF systems in analysis, the masses and stiffnesses are individually lumped at discrete points, and are typically represented in matrices for analysis purposes. In order to determine the modal frequencies and their corresponding mode shapes, finite element method is one of the popular schemes utilized. Without trying to achieve perfect estimations of structural dynamic properties, the “close-enough” approximations of a systems modal frequencies are acceptable for designing and/or monitoring.

In the real world, neither SDOF nor MDOF systems exist, since they are discretized forms of continuous systems. However, they are used to simplify continuous systems for analytical purposes.

### **1.2.3 Linear dynamics**

Structural members generally have a unique way of responding to dynamic forces. Since most structural members are made from composite materials (such as concrete, masonry and wood), the prediction of their behaviors is complicated. Structures can be modelled linearly or nonlinearly relative to excitation forces. Linear dynamic system can be defined as systems where the resisting forces are proportional to the motion (Chopra [2012]). This study conducts linear analysis only on



tested structural members. However, the data collected can be utilized to conduct nonlinear analysis in the future. Modal analysis is popular in linear dynamics. The digital signal processing (DSP) tools to be applied in this study are linear analysis tools as well. The understanding gained from linear dynamics will help predict structural behaviors in serviceability condition.

#### **1.2.4 Varieties in specimens**

This study involves different types of materials, structural types, specimen scales, and test boundary conditions. In this study, four different structural members are tested: a prestressed concrete girder, a masonry wall, a timber wall and some timber joint specimens. Each of the members are supported during testing. Since these tests are conducted to mimic real-world scenarios, the specimens were set up accordingly. The prestressed concrete girder is a 46 *ft* long pre-existing bridge girder and was simply supported across bridge piers in-service to support vertical loads. Hence, it is tested as a simply supported specimen. The two wall specimens represent vertically standing structural systems of buildings that primarily resist lateral loads. Thus, they are tested as cantilever upright systems as they appear in the real-world. Among the tested specimens are a set of timber connections that were designed to mimic common connection types used in timber construction (Sugeng [2006]). They are also tested as cantilever upright systems.

#### **1.2.5 Structural health monitoring**

SHM is a process of implementing a damage identification strategy for aerospace, civil, and mechanical engineering infrastructure (Worden et al. [2007]). Although having its primary roots in aerospace engineering as a means of tracking and monitoring flexible space structures, structural health monitoring (SHM) technol-

ogy rapidly moved into civil engineering to protect civil infrastructure such as bridges and buildings from extreme loads of earthquake and winds to serviceability (Housner et al. [1997]).

In the current era of architecture, there is high competition in building heights and distinct physical appearances. These pose higher challenges in maintaining building resistance against dynamic forces and manifest the need for structural monitoring and control. As it can be compared with a cardio monitor in hospitals, SHM keeps a live feed of structural health performance. In other words, “SHM refers to the use of in-situ, nondestructive sensing and analysis of system characteristics, including structural response for the purpose of detecting changes, which may indicate damage or degradation” (Lynch and Loh [2006]).

Basic components involved in a SHM system include the following:

**Sensing** incorporates traditional engineering techniques such as measuring strain, acceleration, velocity, displacement, rotation, and other parameters into revolutionary technology such as newly improved sensors, high resolution data acquisition, digital communications technology, and real-time computational capabilities to ensure a complete and uninterrupted flow of data between the structure and its monitor (Housner et al. [1997]). In this study, rugged commercial sensors and modal hammers are utilized to measure acceleration and impact force, respectively.

**Data acquisition** is the process of collecting test data. Systems that are designed primarily to facilitate data acquisition are called Data Acquisition Systems (abbreviated as DAQ or DAS). These systems can typically perform functions such as data collection, data display, data transformation and data storage (Yu et al. [2008]). Nowadays, the majority of DAQs are fully digitized and can range from being completely manual, i.e., will function based on

user prompts, to fully automated, i.e., will continue to acquire data without user prompts. Automated DAQs are usually pre-programmed by the user to complete the desired task in their absences. They are mostly utilized in SHM since SHM requires a continuous flow of data in order to monitor the structural system. Laboratory testing, on the other hand, mostly requires manual or semi-automatic DAQs. This is because experimental specimens are typically put to test in a shorter duration than structures in service, and thus do not require continuous monitoring.

DAQs are generally composed of two key components, namely: hardware and software. These two work hand in hand to collect analog data and convert it into digital signals, which are then processed for analysis of results. In this study, a semi-automated DAQ is utilized and it is comprised of both hardware and software that are products of National Instruments (NI).

**Testing** involves all laboratory and in-situ techniques employed to put the structural elements on trials and study their performances. Laboratory dynamic testing is systematically carried out after a careful design process in this study. The author's main focus is to induce dynamic excitation forces to study the specimens' behaviors without causing any unintended damage. The factors to be decided could be called operational parameters ([Lynch and Loh \[2006\]](#)).

**Data processing** involves synthesizing the collected data using computer programs to analyze and present results that are readable. Data processing systems are highly digitized. The tools mostly utilize a series of algorithms that work collaboratively to make the data readable in a certain way. In this study, a modular code is developed to process the test data. This modular code is designed to automatically generate results and does not require robust com-

puter tools.

Indeed, structures, including bridges, aircrafts, ships, and other utility structures, have been engineered to ensure economic and industrial success (Lynch and Loh [2006]). Therefore, the need to protect them is in the best interest of society. This is where damage identification of structures, a widely studied subject under SHM, plays a key role. Worden et al. [2007] studied the literature published in the prior two decades and derived some fundamental axioms of SHM geared towards damage identification. The eight fundamental axioms are described as follows:

**Axiom I:** explains that all materials have inherent micro defects. Worden et al. [2007] depicts that fabricated materials such as metals and fiber-reinforced plastic are never perfect single crystals with perfect periodic lattice.

**Axiom II:** is described as the most basic axiom by the authors. It suggests that for samples to be tested for damage, one must have a similar sample that is in normal condition to compare it with.

**Axiom III:** categorizes damage detection into supervised and unsupervised learning modes, the concepts from machine learning to infer general information and predict new events based on data collected from structures. This axiom states that identifying the existence and location of damage can be conducted unsupervised, but identifying severity can only be done under supervised learning.

**Axiom IVa:** portrays that sensors are only capable of collecting data. Detecting damage entirely relies on the data processing.

**Axiom IVb:** reveals the concern of sensor sensitivity being a disadvantage in addition to its advantages. This axiom suggest that the more sensitive a sensor is to damage detection, the more sensitive it is to environmental changes.

**Axiom V:** states that the time and length variation of the damage detection affects required sensing capabilities. For example, a rigid structural member that is being tested for free vibration requires a high sampling rate due its rapid response.

**Axiom VI:** denotes a trade-off between sensitivity to damage and noise rejection capabilities of a sensor. It is hard to achieve both at the same time. This relates axiom IVb above in the sense that the sensitivity to damage is directly proportional to its sensitivity to noise.

**Axiom VII:** relates the size of a damage to the frequency of the excitation and reveals that the damage size is inversely proportional to the frequency range.

This study is focused on structural testing and data processing. Thus, this study is a direct application of a number of the fundamental axioms by [Worden et al. \[2007\]](#) stated above. This study involves analyzing damaged structures, hence it can directly relate to axioms III, IVa and VII. The disadvantage of sensors discussed in axioms IVb and VI is encountered in this study and discussed in Section 6.1. Axiom V can be related to this study as sampling rate and other operational parameters are carefully decided for testing.

As a field of study, SHM keeps expanding every day. There are numerous subjects under SHM yet to gain maturity. Newly designed SHM systems feature wireless sensing protocols as well as automated control systems that can counteract abnormal dynamic behavior. [Lynch and Loh \[2006\]](#) studied the importance of wireless sensor and sensor networks in structural health monitoring. The paper notes that wireless is not only a financial saver for project owners, they help expand the scope of structural monitoring and facilitate regular upgrades to optimize their functionalities.

### 1.3 Research Objectives

This study involves both testing and analyses. One of the key objectives of this research is to design an experimental methodology to enable the collection of clean and well-organized free vibration response data from all tested specimens that are made up of different construction materials and of different scales. The data is to be used by the author in SDOF linear dynamic models, and by future researchers in this team in nonlinear dynamic modeling.

Another key objective of this research is to conduct linear SDOF analyses on the data collected from the prestressed girder and masonry wall through developing a modular MATLAB code. These specimens are two typical examples chosen to showcase the capability of the modular code that can be utilized by future researchers in studying the remaining specimens and other types of structures subject to free vibration.

### 1.4 Intended Contributions and Structure of Thesis

Table 1 is a summary of the data inventory showing the number of test datasets acquired from the experimental investigation and the number of processed set for analyses.

Table 1: List of collected and processed datasets in this study † specificities partially done and not tested with the data yet, ‡ not sponsored by the major professor

Specimen	Acquired Datasets	Mfiles	Processed Dataset
Prestressed concrete girder	18	Yes	18
Masonry wall	114	Yes	13
Timber wall ‡	331	Yes †	0
Timber joints	30	Yes †	0

Every successful analysis is preceded by a successful physical test. This study follows a systematic manner for testing structural elements for free vibration response. The author carefully designs and conducts all tests to ensure proper data acquisition. The data acquired in this project is not only used by the author, but will be used by future researchers to conduct different analyses on the same structural element.

A simplified SDOF approach is adopted for analyzing the data in this study, which mainly relies on the knowledge of structural engineering and tools in DSP. A modular code is developed, thoroughly explained and documented in this study, to facilitate data processing by future researchers.

As it can be seen in Figure 2 this thesis is comprised of two main parts: experimental investigation and data processing. The experimental investigation portion involves all four types of specimens and includes a setup portion and a testing portion. The setup entails preparing both the data acquisition system and the specimens for testing. A bulk of the time spent on the experimental investigation was concentrated on setup to ensure a proper execution of the experimental procedures saving data for sensor calibration. Data processing involves the development of a modular code using MATLAB<sup>®</sup> to thoroughly analyze the two specified specimens using SDOF models. MATLAB<sup>®</sup> is a mathematical programming software developed by Mathworks<sup>®</sup>. The code generated in this study is prepared for all four specimens and similar specimens in the future but only applied to and validated using the two specified specimens.

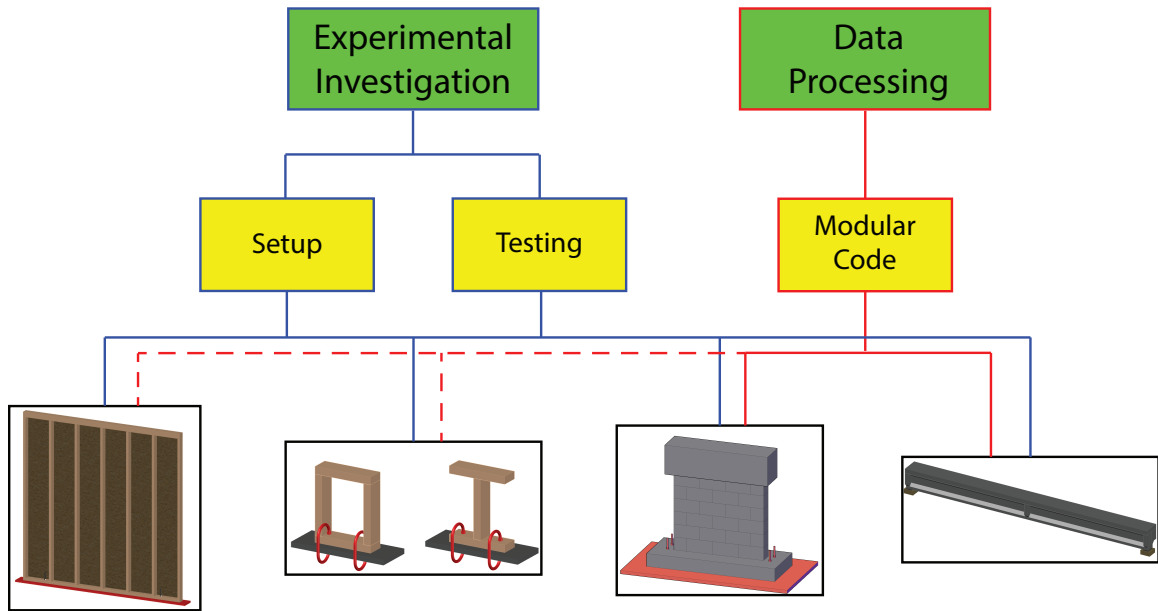


Figure 2: Composition of this Study

Chapter 1 of this thesis offers the motivation, a general technical background, and clearly defined research objectives of this study. Chapter 2 presents a summary of some relevant publications. Chapter 3 presents the general methodology employed in this study. Chapter 4 presents an overview of a typical test, details of the data acquisition used, and descriptions, test setups and procedures for the timber wall and prestressed concrete girder tested in this study. Chapter 5 present the overall analysis approach conducted for the prestressed concrete girder and masonry wall specimens, as well as details of the modular code. Chapter 6 presents the limitations of this study and future work recommendations. Chapter 7 offers concluding remarks. Appendix A contains descriptions, test setups and procedures for the masonry wall and timber joint specimens. Finally, Appendix B.1 contains tables for the nomenclature adopted for three of the specimens, a completion of what is presented in Section 5.4.4.



## **2 LITERATURE REVIEW**

### **2.1 Summary of Some Relevant Studies**

While a technical background of this thesis has been discussed in Chapter 1, this chapter presents a review of some publications on dynamic testing and analysis. Papers were selected based on their direct relevance to the focus of this study. This review was conducted to study some relevant testing methods, analysis and/or results. The chapter mainly offers summaries of the reviewed papers while examining each of them in important aspects that could be applied to this study and/or future work.

Table 2 provides a summary of these papers in terms of testing procedure, analysis procedure and/or scope.

Table 2: Summary of literature most relevant to this study

Studies relevant to prestressed concrete Girder										
Reference	Specimen		Setup		Loading methods	Free vibration				Analysis scope
	Type	Span/Height, <i>ft</i>	Boundary conditions	Support		Excitation	Magnitude, <i>lbf</i>	$f_n$ estimation	$f_s, (Hz)^1$	
Grace and Ross [1996]	Post-tensioned girders with web openings	16.5	Simply supported	N/S	Impact, log-decrement, and destructive static loading	Actuator sudden impact	300	FFT	N/S	System identification of damaged structure
Jacobs et al. [2007]	Post-tensioned girder	55	Simply supported	Air spring bellows	Destructive quasi-static loading and impact free vibration	Mass drop <sup>2</sup>	254 <sup>3</sup>	SPICE <sup>4</sup>	256	System identification of damaged structure and instrumentation feasibility study
Prestressed concrete girder in this study										
N/A	Pretensioned girder	45 <i>ft</i>	Simply supported	Elastomeric pads	Non-destructive impact free vibration	Modal hammer <sup>5</sup>	Varied <sup>6</sup>	FFT and STFT	10,000 <i>Hz</i>	Linear SDOF $f_n$ identification
Studies relevant to masonry wall										
Paquette and Bruneau [2003]	Un-reinforced masonry wall <sup>7</sup>	9 <i>ft</i>	Cantilever wall	Bolted on strong floor	Pseudo-dynamic seismic induction <sup>8</sup>	MTS hydraulic actuator	Varied	N/A	N/A	Behavior of masonry wall under earthquake loads
Masonry wall in this study										
N/A	Reinforced masonry wall	6 <i>ft</i>	Cantilever wall	Bolted on strong floor	Destructive static and impact free vibration	Modal hammer	Varied	FFT and STFT	10,000 <i>Hz</i>	SDOF damage detection through changes in $f_n$

<sup>1</sup>  $f_s$  refers to sampling rate which is the rate at which the DAQ samples test data in a second

<sup>2</sup> mass is dropped from a height of 3.3 *ft*

<sup>3</sup> weight of dropped mass

<sup>4</sup> a system identification software developed at K.U. Leuven and based on the stochastic subspace identification method Peeters [2000]

<sup>5</sup> see Section 4.2.1 for description

<sup>6</sup> Manually controlled hammer force varied from test to test

<sup>7</sup> four sided full-scale wall (two wythe solid bricks) with dimensions 13.5 × 18.7 *ft*, built with a door and window on either of the sides in loading plane

<sup>8</sup> The time history La Malbaie with varying amplification factors were induced laterally at the diaphragm

## 2.2 Summary of Relevant Literature

### 2.2.1 Full-Scale Dynamic Testing of Bridge Structures

Dynamic field tests have been carried out on bridges since the late 19th century (Salawu and Williams [1995]). Although they were mainly conducted as part of safety inspection and involved monitoring vibration in the earlier days, it is mostly conducted nowadays to: improve analyses and design procedures, assess design for code provisions and monitor in-service behaviors of bridges (Salawu and Williams [1995]).

Salawu and Williams [1995] presented a review of the different dynamic tests but mainly categorized them into two: ambient vibration testing and forced vibration based on the degree of control the user has over the input excitation. Ambient vibration testing was defined as testing systems where the input loading is not under the control of the test engineer and these include wind, vehicular and any other service loads. Forced vibration, on the other hand, involves experiments where the force is known and controlled by the experimentalist.

The following is a list of the reasons for conducting full-scale dynamic testing according to Salawu and Williams [1995]:

- It can contribute to the increase in database for the dynamic behavior of similar structures
- It can be a troubleshooting tool to verify that structural behavior conforms to what is expected
- It can validate theoretical models of structures to check assumptions with regards to boundary conditions

- It can be used to assess structural integrity when higher load levels are foreseen
- It can monitor the overall condition of a structure through a SHM
- It can determine the integrity of structures after an overload and can pinpoint the type of loading induced on a structure

### 2.2.2 Damage detection using natural frequencies (Salawu [1997] and Kato and Shimada [1986])

Structural damage can be detected through various methods. Salawu [1997] denotes that frequency analysis is one of the popular and inexpensive ways of detecting structural damage as he reviewed its use as a diagnostic parameter in structural assessment procedures. As an inherent property of structures, a change in natural frequencies is a sensitive indicator of structural integrity, thus it can be used to monitor structural condition (Salawu [1997]).

Salawu [1997] discussed the relationships between frequency changes and structural damage and reviewed various methods for measuring damage using fundamental frequencies. The presence of damage or deterioration can alter the fundamental frequencies of structures because deterioration causes abnormal reduction in stiffness which then lowers the fundamental frequencies (Salawu [1997]).

Kato and Shimada [1986] monitored the changes in dynamic parameters during the failure process of a prestressed concrete bridge, and observed small change in vibrational characteristic while the prestressing wires were in elastic state despite concrete cracking. Kato and Shimada [1986] noticed a sudden decrement in the fundamental frequency occurred when the strands exceeded their elastic limit.

Salawu [1997] argues that utilization of theoretical damage models could introduce uncertainties to results, and denotes that civil engineering structural damages are better off being analyzed solely through measured data without any prior theoretical data. Salawu [1997] concluded that the method of detecting structural damage through fundamental frequencies can be a potential approach for routine integrity assessment of structures but they may not be sufficient in uniquely identifying damage locations.

### 2.2.3 Free Vibration of Beams: Numerical Approach (Prokic et al. [2014])

Numerical methods are well established ways of analyzing structural systems. They provide a great deal of flexibility and usually do not encounter constraints like experimental analyses do if developed properly and maturely. Following an approach, first proposed by Hajdin [1958] and later used in further studies by other researchers, Prokic et al. [2014] used numerical methods in the free vibration analysis of fictitious beams. Prokic et al. [2014]'s approach was applied to a set of second-order ordinary differential equations of variable coefficients, with arbitrary boundary conditions. The numerical method used by Prokic et al. [2014] is based on numerical integration rather than numerical differentiation.

In demonstrating the applicability of their approach on a transversely vibrating uniform Timoshenko beam, Prokic et al. [2014], chose to analyze the cantilever glass-epoxy composite beam of Han et al. [1999] clamped on the left end. With up to forty intervals, Prokic et al. [2014] was able to replicate the first six fundamental frequencies produced by Han et al. [1999] with less than 0.5% error. The beam model studied by Mirtalaie et al. [2012] where the analysis not only considered bending, but torsion and shear was also solved by Prokic et al. [2014] with differences of less than 0.2%.

Prokic et al. [2014] concluded that the numerical approximations used in their study were, in most cases, accurate for a fairly low number of integration intervals. It was also noted that the proposed method can serve as a convenient alternative to similar numerical techniques in the analysis of problems defined in a similar manner.

#### 2.2.4 Dynamic Analysis of Prestressed Beams

Three papers are found and reviewed herein:

**“Prestress force effect on vibration frequency of concrete bridges” (Saiidi et al. [1994])**

Saiidi et al. [1994] studied the effect of prestress force on the fundamental frequencies of concrete bridges based on measured data. Saiidi et al. [1994] noted that theoretical prediction showed that the increment in axial compressive force from prestressing steel decreases the fundamental frequencies of the specimen and vice versa.

Experimental measurements by Saiidi et al. [1994] showed an opposite trend as conducted both field and laboratory tests to confirm their observations. It was their understanding that, as the prestress force decreases, more micro-cracks open which softens the beam leading to a lowered fundamental frequency. Saiidi et al. [1994], hence, developed an empirical equation, Equation (2.1), that estimates the effective rigidity of the beam based on the presence of prestress force.

$$EI_e = \left( 1 + 1.75 \frac{N}{f'_c} \right) EI_g \quad (2.1)$$

where,

$EI_e$  = effective flexural rigidity

$N$  = axial compressive force

$f'_c$  = compressive strength of concrete

$EI_g$  = original flexural rigidity

Test data signified that the effect of prestress force on fundamental frequencies is quiet small but the method can be carried out in order to estimate the amount of prestress losses that has occurred for a bridge after years of service (Saiidi et al. [1994]).

**“Dynamic characteristics of post-tensioned girders with web openings” (Grace and Ross [1996])**

As summarized in Table 2, Grace and Ross [1996] conducted an experimental and theoretical investigation on the dynamic characteristics of post-tensioned concrete girders with web openings under repeated cyclic loading. Girders with cross-sections including rectangular, I and T were fabricated for testing purpose. Web openings were placed on the specimens to mimic utility openings in girders under service conditions. Modal frequencies were measured prior to and post tensioning the beams, and throughout the cyclic test.

Theoretical values for the modal frequencies were determined under prestressing load conditions only. It was observed that experimentally obtained modal frequencies fairly conformed to the theoretical values with the exception of one of the I-girders (Grace and Ross [1996]).

Experimental results by (Grace and Ross [1996]) showed that placement of one or two web openings barely affected the modal frequencies of the specimens as the greatest percentage difference obtained was 4%. It was also observed that modal

frequencies for the specimens with one web opening were about the same as those with two web openings. Significant reduction was seen on the second modal frequency values from inducing one and two web openings. Reductions of up to 8.9% and 16.5% of the second modal frequencies was observed for one and two web openings, respectively. [Grace and Ross \[1996\]](#) suggested that this observation could be due to the coincidence of the locations of web openings and the nodal point of the second mode shape at the mid-span of the specimens. After inducing several millions of cycles of fatigue loading, [Grace and Ross \[1996\]](#) noticed slight decrease in all of the specimens' fundamental frequencies which indicates slight decrease in stiffness as a result. An interesting observation was that the I-sections had the least decrement in modal frequencies, thus [Grace and Ross \[1996\]](#) concluded that due to the presence of the top and bottom flanges, the I-sections maintained more of their inherent stiffness throughout the fatigue loading.

Results of a parametric study conducted by [Grace and Ross \[1996\]](#) indicated that parabolic shaped strands caused higher modal frequencies and additional increase in prestress force caused further increase in the modal frequencies. Pure axial prestress force induced by straight strands had an opposite effect.

**“Testing of a prestressed concrete girder to study the enhanced performance of monitoring by integrating optical fiber sensors” ([Jacobs et al. \[2007\]](#))**

To investigate the monitoring technology of concrete members using integrated fiber optic, [Jacobs et al. \[2007\]](#) conducted static and dynamic laboratory tests on a post-tensioned I-shaped concrete girder with a total length and span of about 58 *ft* and 55 *ft*, respectively, as summarized in Table 2. They measured strain, deflection and acceleration. From the measured acceleration history, [Jacobs et al. \[2007\]](#) calculated the mode shapes, modal frequencies and damping using a system



identification software called SPICE.

The specimen was post-tensioned using seven parabolic strands. During the quasi-static tests, the load was applied to four points within the span and bending deflection was measured at six locations. During the static loading of the specimen, a number of extensive concrete cracks were observed on the specimen prior to the yielding of prestressing strands.

For the dynamic setup, the girder was lifted from its static supports and then supported by two air spring bellows at each end but with a shorter span. The shorter span allowed the possibility of applying excitation force at one overhanging end of the beam and not within the simply supported span. The excitation force was applied using a 250 *lb* mass dropped from a height of about 3 *ft*. The impact plane was offset from the neutral axis of the beam in order to excite both bending and torsion responses. A damper was placed on the impact location to act as a mechanical low-pass filter.

After the initial dynamic test, a total of seven damage levels of static loading cycles were performed. Six of the static tests were followed by dynamic tests. The dynamic results allowed [Jacobs et al. \[2007\]](#) to study frequencies up to 128 *Hz*. Within this range, eight modes were found: four torsional and four bending modes. [Jacobs et al. \[2007\]](#) observed a slight decrease in eigenfrequencies with increased damage on the specimen. Reinforcement yielding caused significant decrease in the modal frequencies.

## 2.2.5 Dynamic Studies on Masonry Walls

**“Pseudo-dynamic testing of unreinforced masonry building with flexible diaphragm” ([Paquette and Bruneau \[2003\]](#))**

As summarized in Table 2, Paquette and Bruneau [2003] tested full-scale unreinforced masonry (URM) wall under a seismic loading by inducing pseudo-dynamic excitation. Their specimen was a 9ft tall four-sided wall enclosing a total rectangular area of around 250 ft<sup>2</sup> with a window and door openings on the two parallel walls oriented in-plane to its loading axis. The wall was designed to study the flexible-floor/rigid-wall interaction and the impact of wall continuity at the corners on the wall's seismic behavior.

Based on theoretical analyses conducted by Paquette and Bruneau [2003], the anticipated behaviors of the specimen included pier rocking behavior, bed joint sliding, diagonal tension and toe crushing. The test setup for the experiment featured a single degree-of-freedom (SDOF) system induced by a single actuator acting on the diaphragm center span. Prior to testing, a series of pseudo-dynamic simulated free vibration tests were conducted by Paquette and Bruneau [2003] to determine the vibrating period and damping ratio of the specimen. During testing, the time history of La Malbaie, Canada earthquake was applied to the specimen in multiple trials starting with the first 10 seconds of a quarter scale of the ground shaking. In the first trial, elastic behavior was observed but as half scaled ground shaking was applied stiffness softening was observed. The full-scale of the La Malbaie created additional cracking with increased openings. When one and half scaled ground shaking was applied, some cracking noise was observed as new cracks were seen. Rocking of the door pier also occurred as a result of the 1.5 multiplier. The specimen was then subjected to a double scaled La Malbaie. At the wall's ultimate capacity, severe cracking was observed to separate due to the combination of rocking and sliding motion. Cracks openings as wide as half inch was observed by Paquette and Bruneau [2003].

Considering hysteresis in their analysis process, Paquette and Bruneau [2003]

was able to conclude that the combined rocking and sliding mechanism induced by the pseudo-dynamic force caused large deformations without significant strength reduction in the masonry specimen. The elastic phase of the diaphragm was not exceeded, they noted. [Paquette and Bruneau \[2003\]](#) also noted that some theoretical seismic response procedures such those in FEMA 273 and 306 predicted similar behaviors as what was experimentally observed, although the codes did not account for the presence of continuous corners. This resulted in the understanding that continuity had negligible effect on the lateral strength of the shear wall.

### **2.3 Implications of Previous Studies on This Study**

The papers summarized above in Section 2.2 have key findings that directly apply to this study. These implications are given herein:

Full-scale dynamic tests are conducted in this study. In conjunction to the motivations stated in Section 1.1, the reasons stated by [Salawu and Williams \[1995\]](#) give additional motivation for conducting the full scale dynamic tests on the retired bridge girder. According to definitions given in [Salawu and Williams \[1995\]](#), this study can be categorized as a forced vibration test where a modal hammer is used to induce an excitation force, and the free vibration response is analyzed.

In this study, natural frequencies will be analyzed using the free vibration data of the specimens, some of which will be tested through different damage states. Hence, based on findings by [Salawu \[1997\]](#) and [Kato and Shimada \[1986\]](#), it is expected that the fundamental frequencies will decrease through the damage states. Thus a decrement in the fundamental frequency will be anticipated during analysis of the masonry wall specimen.

Although, in this study, specimens are tested and analyzed using a modular

code rather than numerically, the approach used by [Prokic et al. \[2014\]](#) could be a possible application in future studies. Results of the numerical approach could be compared with the results of the current study.

Part of the analysis in this study is extracting the fundamental frequency of a prestressed concrete girder that has served and was retired after more than forty years. Over the years of service, time dependant prestress losses have occurred. Thus the understanding gained from [Saiidi et al. \[1994\]](#) would assist analyzing the obtained results.

A few implications of the study conducted by [Grace and Ross \[1996\]](#) apply to the prestressed concrete girder in this study. First, cyclic loading is denoted by [Grace and Ross \[1996\]](#) that it causes a slight reduction of modal frequencies of a prestressed beam. Since the girder tested in this study undertook cyclic vehicular loading for more than forty-years, the experimentally obtained fundamental frequency of the girder is expected to slightly less than the theoretically estimated based on [Grace and Ross \[1996\]](#)'s observations. Secondly, as it is observed by [Grace and Ross \[1996\]](#) that the presence of holes have very little effects on the beams' modal frequencies and that I-sections tend to retain most of their inherent stiffnesses, the AASHTO Type II prestressed girder tested in this study is expected to have little to no change in the fundamental frequency due to the presence of core openings, should there be any. Core openings are openings drilled in a beam to extract a sample of the concrete for material analysis after structural testing is completed.

Similar to observations in [Grace and Ross \[1996\]](#), [Jacobs et al. \[2007\]](#)'s observation of a slight decrease in modal frequency due to damage can be expected in the masonry wall analysis of this study. [Jacobs et al. \[2007\]](#) studied the torsional motion of the girder and stated that a similar decrement is observed in the torsional

response of the girder. This study aims at figuring out what an identified natural frequency means, in-plane bending, out-of-plane bending, or torsion?

As suggested by [Paquette and Bruneau \[2003\]](#), the continuity of the wall's corners does not affect the lateral strength of the wall. Although this study is conducted on a masonry wall with a non-continuous corner, the need to study the effect of continuous corners its in-plane and out-of-plane responses is recommended for future studies and results obtained should be compared with the results of this study.

### 3 METHODOLOGY

#### 3.1 Scope of Work

In this study, some of the most crucial elements in commonly seen structures are under investigation in terms of test specimens. The specimens, as presented in the Figures 3 and 4, include a real-world AASHTO Type II girder that had served more than forty years, a half-scale masonry wall, a full-scale timber wall and a number of timber joint specimens. Unlike the first one, the remaining three specimens were built solely for testing purposes.

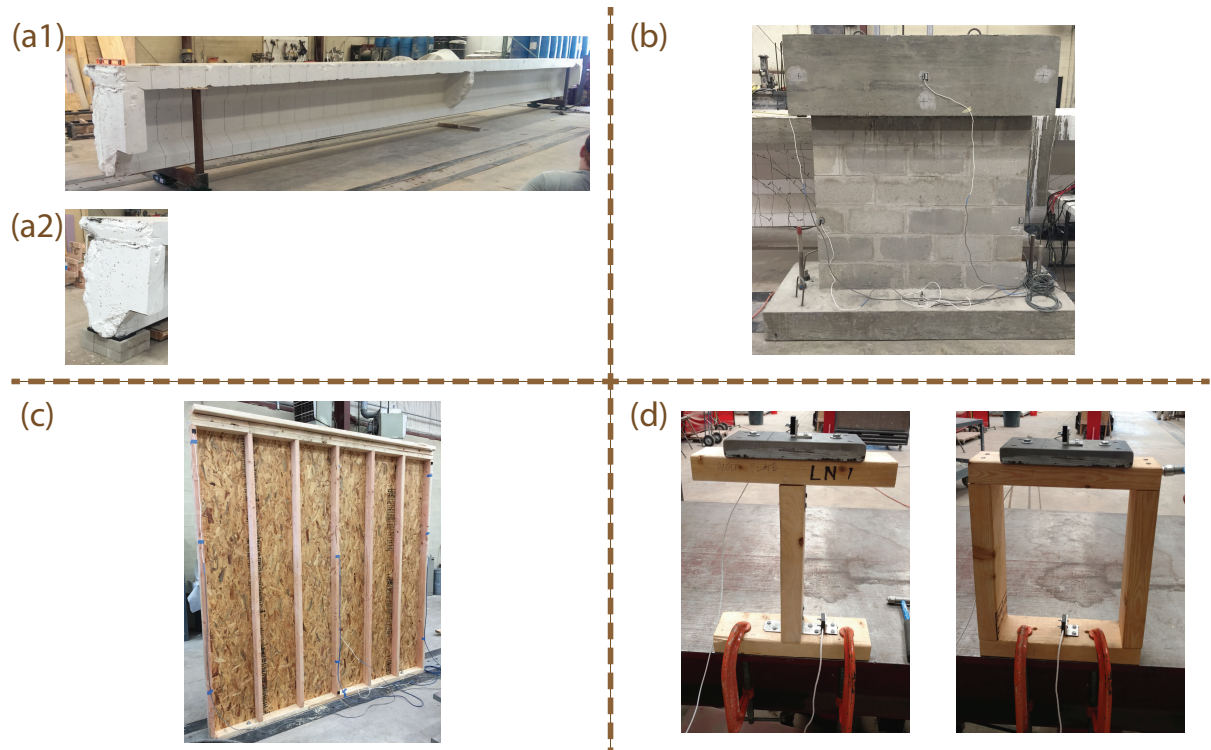


Figure 3: Pictures of specimens studied: (a) prestressed concrete girder; (b) masonry wall; (c) timber wall, and (d) timber joints

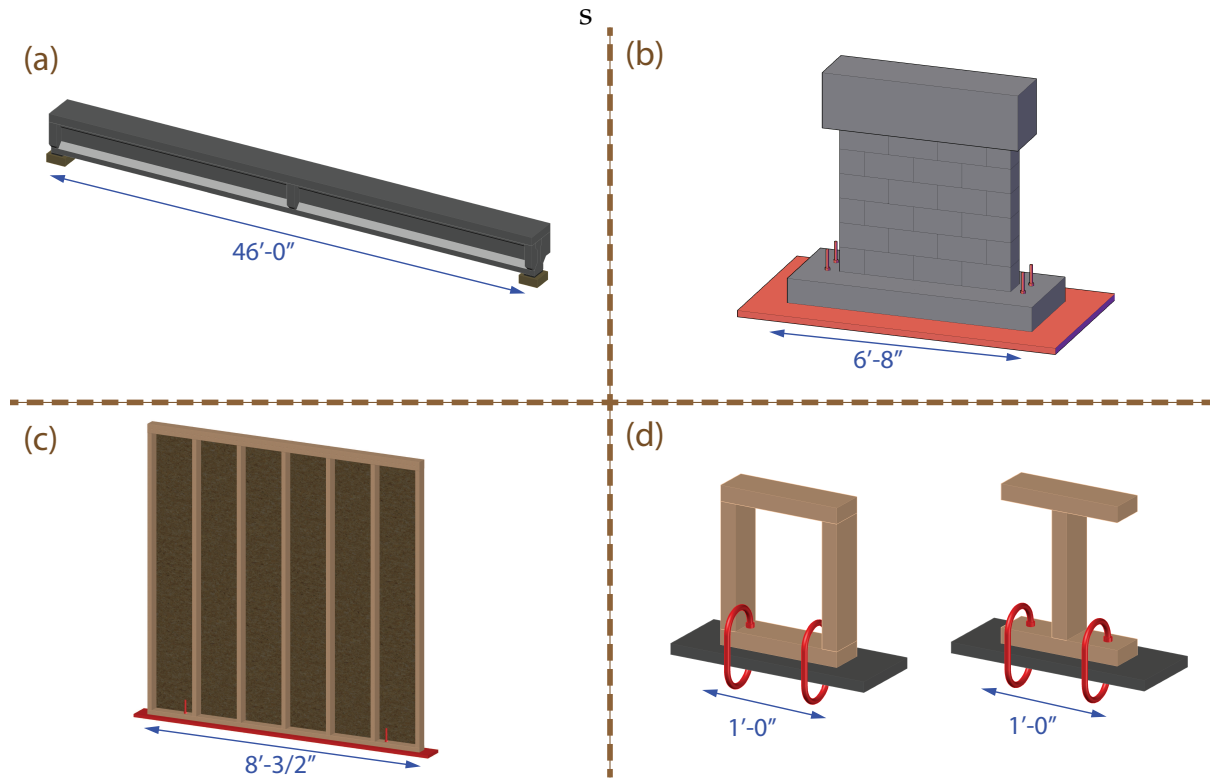


Figure 4: AutoCAD drawings of the tested specimens highlighting overall dimensions and testing boundary conditions: (a) prestressed concrete girder, (b) masonry wall; (c) timber wall, and (d) timber joints, see Table 3 for full dimensions

**Pre-stressed concrete girder (GC):** This is a full-scale 46 *ft* long specimen extracted from a real-world bridge that was demolished. The girder itself was not pre-damaged.

**Masonry wall (MW):** This is a half-scale reinforced masonry wall with a reinforced concrete top and base. The specimen was fabricated for experimental purpose.


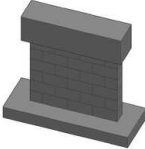

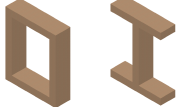
**Timber wall (TW):** This is a full-scale timber shear wall specimen also fabricated for experimental purpose.

**Timber joints (TJ):** These include a number of timber joint specimens that were

built by Sugeng [2006] and Mai et al. [2008] to mimic some popular connection types used in timber constructions and generate data for nonlinear dynamic analysis.

As represented in Table 3, the scope of this study is bounded by four specimens. For each of the specimens, Table 3 provides a brief summary of the type of structure, origin, its construction materials, nature, boundary conditions and dimensions. Full descriptions of the specimens can be found in Sections 4.6, A.2, 4.3 and A.3 respective of the order of presentation in Table 3.

Table 3: A brief summary of properties of all four specimens †OSB - Oriented strand board

Specimen	Prestressed Concrete	Masonry Wall	Timber Wall	Timber Joints
Schematic				
Struct. Type	Girder	Wall	Wall	Joint
Origin	Retired	Fabricated	Fabricated	Fabricated
Constr. Material	Pretensioned prestressed concrete	Reinforced masonry	OSB† sheathed timber shear wall	Wood and various connectors
Nature	Real-world AASHTO Type II girder	Half-scale lab specimen <sup>9</sup>	Full-scale lab specimen	Lab specimens
Boundary Con'd	Simple beam	Cantilever wall	Cantilever wall	Cantilever column
Dim.	46'-0" × 3'- $\frac{1}{2}$ " × 3'-9"	6'-8" × 2'-6" × 6'-2"	8'- $\frac{3}{2}$ " × 0'-4" × 8'- $\frac{1}{8}$ "	1'-0" × 0'-3 $\frac{1}{2}$ " × 1'-3"

The scope of work of this project can be categorized into two: experimental



investigation and data processing.

**Experimental investigation** refers to the tasks of specimen design and fabrication (if applicable), instrumentation and testing. As suggested by their origins, not all the specimens were designed and fabricated by the author. However, all specimens were tested for free vibration by the author, when an excitation force was induced using a modal hammer. The instrumentation setup and testing procedure was carefully designed and executed for both proper acquisition of clean data, for linear, and nonlinear data analysis in the present and future work, respectively.

**Data processing** refers to the generation of results from the measured data leading to a better understanding of the specimens' structural behaviors. To complement the experimental investigation, a major portion of this study, data analysis, is directed towards studying two tested specimens: the prestressed concrete girder and the masonry wall. The data processing, in this study, is facilitated by a modular code that is developed to study the SDOF models adopted for the specimens. Data analysis serves two purposes: (1) to study the behavior of the two specimens under free vibration, and (2) document and demonstrate the use of the modular code for analyzing other structures tested in a similar way.

### **3.2 Models Specific to Study**

Specimens of different nature are tested in this study. Models are created for each type of specimen beforehand. These models are tailored toward the main focus of this research. They are then utilized to extract meaningful results that are more likely to answer the research questions. Figure 6 presents illustrations of the mod-

els used in this study.

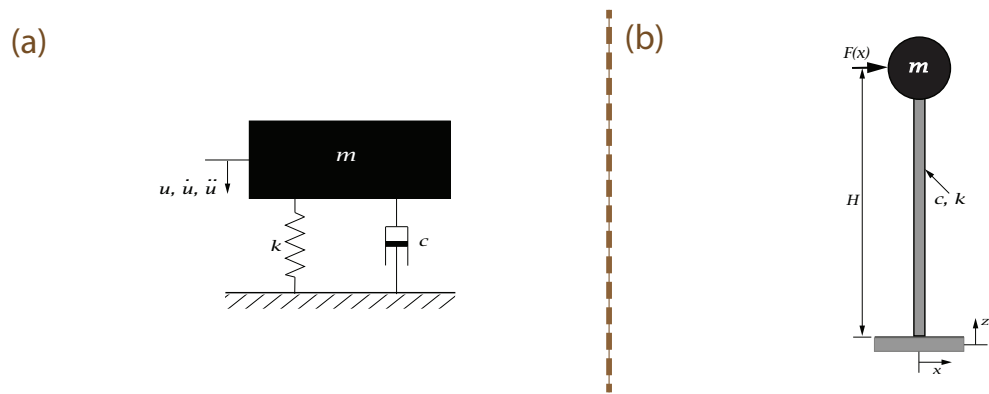


Figure 5: Models adopted in this study for each specimen type: (a) simple beam SDOF model, and (b) cantilever wall/beam lumped mass model

**Simply supported beam SDOF model:** As illustrated in Figure 6(a), this model is used to represent a typical simply supported beam with mass uniformly distributed across the length as an sdof system. It is adopted for the prestressed concrete girder in the analysis portion of this study.

**Cantilever wall/beam model with lumped mass:** As illustrated in Figure 6(b), this model represents a system with lumped mass at the top and has a massless shaft with flexural rigidity and damping ratio. This model is used to represent the masonry wall, timber joints, and the timber wall specimen.

### 3.3 Anticipated Results

#### 3.3.1 Anticipated results: simply supported specimen

For a simply supported beam (typical for the prestressed concrete girder with span,  $L$ , constant flexural rigidity,  $EI$ , density,  $\rho$ , and cross-sectional area,  $A$ ), the modal frequencies can be estimated using Equation (3.1) which assumes a continuous model. Results obtained from the continuous beam formula will be compared with the fundamental frequency obtained from an SDOF estimation.

$$\omega_i = \left(\frac{i\pi}{L}\right)^2 \sqrt{\frac{EI}{\rho A}} \quad (3.1)$$

where

$\omega_i = i^{th}$  modal frequency,

$i =$  a positive integer,

$L =$  span,

$E =$  Young's modulus (modulus of elasticity) of the material assuming the beam is made of a homogenous material,

$I =$  moment of inertia of the cross section,

$\rho =$  density of material, and

$A =$  cross sectional area.

The parameter values of the governing quantities in Equation (3.1) are estimated one by one as follows:

**Span,  $L$ :**

Although the total length of the girder is 46 *ft*, it was supported on elastomeric pads in such a way that the span was 45 *ft*.

**Modulus of elasticity of concrete,  $E_c$ :**

According to [American Concrete Institute \[2014\]](#), the elastic modulus of concrete,  $E_c$  can be estimated using Equation (3.2).

$$E_c = 33w_c^{\frac{3}{2}}\sqrt{f'_c} \quad (3.2)$$

where

$w_c$  = air-dry weight of the concrete (*pcf*), and

$f'_c$  = compressive strength of concrete (*psi*).

[Floyd et al. \[2016\]](#) conducted compressive tests on six cores acquired from Girder C with three from the deck and three from the web. The average  $f'_c$  was 6,452 *psi* and its magnitude puts Girder C's concrete on the high strength category (greater than 6,000 *psi*). Hence, according to recommendations by [Russell et al. \[1977\]](#) and [Precast/Prestressed Concrete Institute \[2010\]](#), Equation (3.3) would produce a more accurate estimation for the Young's modulus of high-strength concrete.

$$E_c = \left(40,000\sqrt{f'_c} + 10^6\right) \left(\frac{w_c}{145}\right)^{\frac{3}{2}} \quad (3.3)$$

Normal weight concrete was utilized on the specimen as confirmed by [Floyd et al. \[2016\]](#). Thus,  $w_c$  is assumed to be 145*pcf* and a Young's modulus,  $E_c$  of 4,213 *ksi* is obtained using Equation (3.3) and adopted for this analysis.

### Density of reinforced concrete, $\rho$ :

Density is defined as the amount of matter in a unit volume. It is the ratio of the unit weight of the material to acceleration due to gravity,  $g$  as shown in Equation (3.4). The imperial form of  $g$ ,  $386.09 \frac{in}{s^2}$  is used.

$$\rho = \frac{w_c}{g} \quad (3.4)$$

### Estimating moment of inertia, $I$ and cross sectional area, $A$ :

In estimating the area moment of inertia for the girder,  $I$ , two methods are employed. In the first method, the presence of steel is ignored and a *gross section* of concrete only is considered. The second method takes the steel into account by using the *transformed section* approach, which converts the area of steel into an equivalent area of concrete based on the ratio of their Young's moduli.

Floyd et al. [2016] tested two prestressing strands obtained from Girder A, another specimen that was extracted from the same bridge as Girder C, and determined an average ultimate tensile strength,  $F_u$ , and modulus of elasticity,  $E_s$  of 283.6 *ksi* and 26,350 *ksi*, respectively. Assuming that  $E_s$  is the same for strands used in both girders, a section transform coefficient of  $n = 6.254$  is obtained from the ratio  $\frac{E_s}{E_c}$ . Table 4 presents the set of section properties obtained.

Table 4: Estimated cross-sectional properties of Girder C using the two methods: (a) gross concrete section, and (b) transformed section

Section Property	Strong Axis (xx)		Weak Axis (yy)
	Gross section	Transformed section	
Area, $A$ (in <sup>2</sup> )	697.5	710.4	697.5
Centroid, $\bar{y}$ or $\bar{x}$ (in)	27.45	27.03	11.24
Moment of Inertia, $I_{xx}$ or $I_{yy}$ (in <sup>4</sup> )	158,971	165,622	45,724

Gross section is only considered for the weak axis moment of inertia. The properties of the section about its weak axis are also presented in Table 4 above.

The values acquired from both methods for strong axis were utilized to estimate two different sets of strong axis modal frequencies for Girder C are given in Table 5. With about a 4 percent increase in its strong axis moment of inertia after applying transformed section, transformed section is expected to be more accurate due to a closer depiction of the reality. The weak axis modal frequencies are also presented in Table 5.

Table 5: Estimated modal frequencies for Girder C using the section properties calculated in 4 above

Modes (i)	Strong Axis (xx)				Weak Axis (yy)	
	Method (a)		Method (b)		$\omega_i (\frac{rad}{s})$	$f_i$
	$\omega_i (\frac{rad}{s})$	$f_i (Hz)$	$\omega_i (\frac{rad}{s})$	$f_i (Hz)$		
1	69.94	11.13	71.39	11.36	37.51	5.97
2	279.78	44.53	285.58	45.45	150.05	23.88
3	629.52	100.19	642.55	102.26	337.61	53.73
4	1119.14	178.12	1142.31	181.80	600.20	95.53
5	1748.65	278.31	1784.86	284.07	937.81	149.26
6	2518.06	400.76	2570.20	409.06	1350.45	214.93
7	3427.36	545.48	3498.32	556.78	1838.12	292.55
8	4476.56	712.47	4569.24	727.22	2400.81	382.10
9	5665.64	901.71	5782.94	920.38	3038.52	483.60
10	6994.62	1113.23	7139.44	1136.28	3751.26	597.03

Considering the girder as an SDOF system with the mass lumped at the mid-span, the relationship between fundamental frequency, mass and stiffness is governed by Equation (3.5).

$$f_n = \frac{1}{2\pi} \sqrt{\frac{k}{m}} \quad (3.5)$$

where  $f_n$ ,  $k$ , and  $m$  represent fundamental frequency, stiffness, and mass, respectively.

The stiffness for Girder C can be estimated using Equation (3.7):

$$k = \frac{48EI}{L^3} \quad (3.6)$$

where

$E$  = Young's modulus of the material,

$I$  = moment of inertia of inner cross-section and

$L$  = span.

Using the moments of inertia obtained from the transformed section properties, the stiffness about the strong axis is obtained.

The mass of the specimen is estimated by  $\frac{W}{g}$ , where self weight  $W$  is estimated by multiplying the assumed unit weight of the specimen, 150 *pcf* (unit weight of reinforced concrete) by the cross sectional area and half length of the girder.

Eventually, this estimation produces a fundamental frequency of 11.28 *Hz*. This number validates the first modal frequency acquired using the beam formula.

To rule out a possible torsional motion in the data analysis to be presented in Section 5.2, the fundamental torsional frequency of the girder is estimated by using Equation (3.7):

$$f_n = \frac{1}{2L} \sqrt{\frac{GJ}{\rho I_p}} \quad (3.7)$$

where

$L$  = span of the girder,

$G$  = shear modulus of the assumed isotropic material of the entire girder,

$J$  = torsional constant of the assumed uniform cross-section along the span,

$\rho$  = density of reinforced concrete,

$I_p$  = polar moment of inertia of the assumed isotropic material of the entire



girder.

Shear modulus,  $G$ , is estimated using Equation (3.8),

$$G = \frac{E}{2(1 + \nu)} \quad (3.8)$$

where the assumed isotropic material has a Young's Modulus,  $E$ , estimated using Equation (3.3) and a poisson's ration,  $\nu$ , of 0.15 (Wight [2016]).

$I_p$  is estimated as the sum of the moments of inertia about the strong and weak axes of the specimen.  $J$ , for the girder is estimated as an open section using Equation (3.9) (Boresi and Schmidt [2003]).

$$J = \frac{1}{3} \sum_{i=1}^n b_i t_i^3 \quad (3.9)$$

where  $b$  and  $t$  are the larger and smaller dimensions, respectively, of the individual rectangular sections that the girder is comprised of.  $J$  is estimated to be  $12,159 \text{ in}^4$  for the girder.

A fundamental torsional frequency of  $20.05 \text{ Hz}$  is estimated for the girder.

### 3.3.2 Anticipated results: cantilever specimens

A lumped mass cantilever SDOF model with two different boundary conditions, as illustrated in Figure 6, is adopted for a number of the tested specimens in this study.

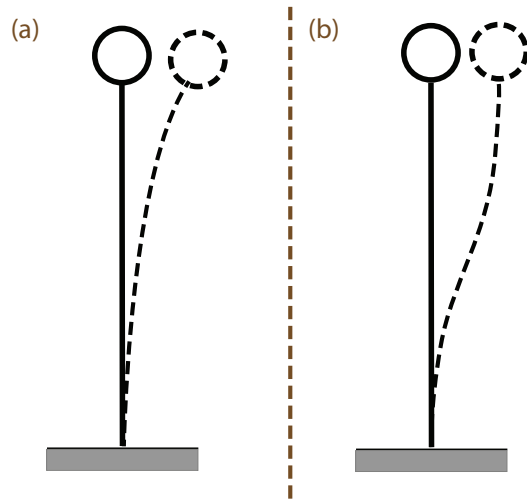


Figure 6: Two deflected shapes corresponding to the two different boundary conditions studied for a lumped mass cantilever SDOF model: (a) bending deflected shape, and (b) sidesway deflected shape

The bending mode occurs when the top mass is free to rotate thereby causing a quarter-sine deflected shape. Sidesway, on the other hand occurs when the top mass is assumed to have very little rotation. The sidesway has an inflection point at about half of the wall height and appears to have a half-sine deflected shape.

The masonry wall, timber wall and timber joint specimens are first modeled as lumped SDOF models with the same fixed-free boundary condition. Thus, the estimations of their theoretical results follow a similar procedure.

The properties (including both mass and stiffness) are calculated in order to estimate the fundamental frequencies of all the cantilever specimens using the SDOF model. Equation (3.10) is used to estimate mass:

$$m = \rho Al \tag{3.10}$$

where

$m$  = lumped mass,

$\rho$  = density of the lumped material by using Equation (3.4),

$A$  = cross-sectional area of the beam or wall section for mass estimation and

$l$  = proper length for estimating the lumped mass.

Stiffness is estimated for each specimen depending on the assumed deflected shape; see Figure 6. The fundamental frequencies are estimated using Equation (3.5). For the three types of specimens, the estimation for their fundamental frequencies are detailed as follows:

#### **Masonry wall:**

For the masonry wall, the lumped mass is assumed to comprise the mass of the concrete block on top and half of the mass of the masonry wall. A total lumped weight of 2400 *lbf* was estimated.

Stiffness, for the masonry wall, is estimated for both in-plane and out-of-plane responses. For in-plane responses, two possible deflected shapes are analyzed: bending and sidesway, as represented in Figure 6(a) and (b), respectively.

Bending controls when the lumped mass is free to rotate, while sidesway controls when the top mass is unable to rotate. As the fixity of the top mass is more or less an unknown, both the bending and sidesway stiffnesses are estimated using Equations (3.11) and (3.12), respectively (Chopra [2012]).

$$k = \frac{3EI}{h^3} \quad (3.11)$$

$$k = \frac{12EI}{h^3} \quad (3.12)$$

where

$k$  = stiffness of the wall,

$E$  = Young's modulus of the material,

$I$  = moment of inertia associated with the correct bending axis

$h$  = height from the top of the fixed base to the center of the lumped mass on top.

For the out-of-plane motion of the wall, bending is assumed to control, thus, its stiffness is estimated using Equation (3.11).

$EI$  is obtained from the combined flexural rigidities of both masonry wall and its reinforcing rebars. For in-plane bending of the wall, the transformed section is used to calculate  $EI$ . Based on the information given about the wall's construction, the author neglected deformation compatibility of the wall and the rebars in the sidesway mode due to an imperfect bond between the two. Thus, the rebars are assumed to act independently from the masonry and deform laterally rather than bending about the centroid of the wall. With three #3 bar reinforcements, the total stiffness of the wall is estimated as the sum of that of the three rebars acting as separate columns within the wall and that of the masonry wall itself.

The stiffness of each rebar is calculated using Equation (3.12) and multiplied by three to obtain the total stiffness contribution of the reinforcement. For each bar, the moment of inertia is estimated to be  $9.71 \times 10^{-4} \text{ in}^4$  and an assumed Young's modulus,  $E_s$  of 29,000 *ksi* (that of mild steel) is utilized. For the masonry wall as well, Equation (3.12) is utilized to estimate its stiffness for the sidesway mode.

The Young's modulus of masonry,  $E$  is estimated to be 40,250 *psi* using Equa-

tion (3.13) (Masonry Standards Joint Committee [2008]):

$$E_m = 900\sqrt{f'_m} \quad (3.13)$$

where  $f'_m$  is the compressive strength of the masonry unit and was estimated to be 2,000 *psi* according to Floyd [2017]. This estimation is based on the assumption of a partially grouted masonry wall, which accounts for the opened hollow portions of the wall as well as the partial grout. It should be noted that sidesway case can also be estimated using either gross or transformed section. A more detailed analysis of the effect of the voids within the wall and interaction of the composite materials as well as analyzing the wall as a deep beam should be considered in future research.

To ensure a thorough analysis of results, the torsional fundamental frequency for the masonry wall is estimated using Equation (3.14) (Rao [2007]):

$$\omega_n = \frac{1}{4h} \sqrt{\frac{GJ}{\rho I_p}} \quad (3.14)$$

where

$h$  = height of the from the top of the base to the center of the top mass,

$G$  = shear modulus,

$J$  = torsional constant of the assumed uniform cross-section along the height of the wall,

$\rho$  = density of the lumped material,

$I_p$  = polar moment of inertia of the cross-section

Shear modulus,  $G$ , for the wall, is also estimated using Equation (3.8), with assumptions of an isotropic masonry wall with a Young's modulus  $E$  as esti-

mated using Equation (3.13) and poisson's ratio,  $\nu$  of 0.165 (Narayanan and Sirajuddin [2013]).

$I_p$  is estimated as the sum of the moments of inertia of the strong and weak axes assuming a solid rectangular cross section of the wall.  $J$ , for the masonry wall is also estimated with assumptions of a solid wall for simplicity and consistency using Equation (3.15) (Boresi and Schmidt [2003]). Thus the hollows of the masonry wall should be taken into account in future studies when in-depth torsional analyses are conducted.

$$J = k_1 b h^3 \tag{3.15}$$

where  $k_1$  is determined based on the ratio of  $b$  and  $h$ , and  $b$  and  $h$  represent the lengths of the long and short sides, respectively, of the rectangular wall cross section. A  $k_1$  value of 0.303 is obtained based on the  $\frac{b}{h}$  ratio of 7.34 in conjunction with torsional parameters provided in Boresi and Schmidt [2003].  $J$  is estimated to be 7,522  $in^4$ .

Table 6, provides a summary of the estimated modal parameters for the masonry wall.

Table 6: Estimated fundamental frequencies and other parameters for the different anticipated modes of vibration for the masonry wall

Response mode	$k \left( \frac{lb}{in} \right)$	$m \left( \frac{lb \cdot s^2}{in} \right)$	$\omega_n \left( \frac{rad}{s} \right)$	$f_n \text{ (Hz)}$
In-plane bending	132,580	6.22	146.0	23.24
In-plane sidesway	291,030	6.22	216.4	34.44
Out-of-plane bending	1,350	6.22	14.73	2.34
Torsion	–	6.22	70.06	11.15

### Timber wall

The wall was tested with three different setups: the first only consists of the wall by itself and was denoted as *setup (a)*, the second consists of a 4 ft steel W-section centered at the top of the wall - denoted as *setup (b)*, and the third setup consists of two 4 ft W-sections – *setup (c)*. These three setups are further described in Section 4.4. Similar to the masonry wall, sidesway is assumed to control the in-plane response of the timber wall under setup (b) and (c). For simplicity, however, the specimen is analyzed using the sidesway assumption for all three setups. The weights of the three setups consisted of half of the wall for the first setup and half of the wall plus the weight of the added steel section for the second and third setups. The lumped weights for the three setups were estimated to be  $w_{(a)} = 115 \text{ lbf}$ ,  $w_{(b)} = 315 \text{ lbf}$  and  $w_{(c)} = 515 \text{ lbf}$ , respectively.

The timber wall specimen consists of seven studs and two OSB sheathing panels. The total stiffness combines that of all the studs and sheathings. The individual stud stiffnesses are estimated using Equation (3.12), above. The moment of inertia of the  $2 \times 4$  studs are the same as that of the timber joint specimens ( $I = 0.984 \text{ in}^4$ ), and the Young's modulus of  $E = 1,200,000 \text{ psi}$  – that of a No. 2 Douglas Fir – is also utilized (American Wood Council [2014]). As for the OSB sheathing panels, the bending rigidity,  $EI$  of  $78,000 \text{ lb in}^2$  per foot of panel width (Ame [2015]) is used.

### Timber joints

The tested timber joint specimens consist of two different shapes: a T-shaped and a frame model. A steel block of weight  $w = 8.93 \text{ lbf}$  was used as the lumped weight for all the timber joint specimens while the timber self-weights are neglected. With only one  $2 \times 4$  vertical lumber in the T-shaped model as opposed to two in the frame model, half the stiffness of the frame

model is expected in the T-shaped model. The timber joint specimens are also analyzed as sidesway specimens (see Figure 6). Given that the lumped mass for the timber joints – particularly the T-shaped model – is more free to rotate than that of the other specimens, the bending mode may be significant and should be analyzed in future studies when in-depth analysis of the timber joints is conducted. As described by Sugeng [2006], the specimen was designed using Grade 2 Spruce-Pine-Fir timber, hence its modulus of elasticity is 1,400,000 *psi* (American Wood Council [2014]). The moment of inertia for a single 2 × 4 about its weak axis (as it was loaded) is calculated to be about 0.984 *in*<sup>4</sup>. Using a height of 14 *in* (from the bottom of shaft(s) to the center of the steel block), two stiffness values are obtained for the two models:  $k_{t-shape} = 4441 \text{ lb/in}$  and  $k_{frame} = 8882 \text{ lb/in}$ .

Table 7, represents the computed fundamental frequency for the masonry wall, timber joints and timber wall.

Table 7: Estimated fundamental frequencies for the lumped mass modelled specimens in this study

Specimen	Timber Joints		Timber Wall		
	Frame	T-shaped	(a)	(b)	(c)
$f_n(\text{Hz})$	2.39	1.69	3.14	1.90	1.49



### 3.4 General Approach

While Chapter 5 will detail data analysis in this study, the main approach involved in the experimental investigation follows three steps:

#### Step 1 - Creating a model:

For each specimen, a model is created for a certain analytical aspect of it. Models establish a certain path towards answering research questions; this path leads in the design and testing processes. Although no model can represent all aspects of the structure, it can be a good representation of a particular aspect of interest.

Figure 7 presents an illustrative example of a tested specimen's representation of a real-world scenario using the masonry wall as an example. The reinforced masonry wall studied in this paper represents the shear wall of a masonry building between two door openings. The timber wall similarly represents the shear wall components of a timber building. More information on the modeling aspect of the prestressed concrete girder and the timber joint specimens can be found in [Floyd et al. \[2016\]](#) and [Sugeng \[2006\]](#), respectively.

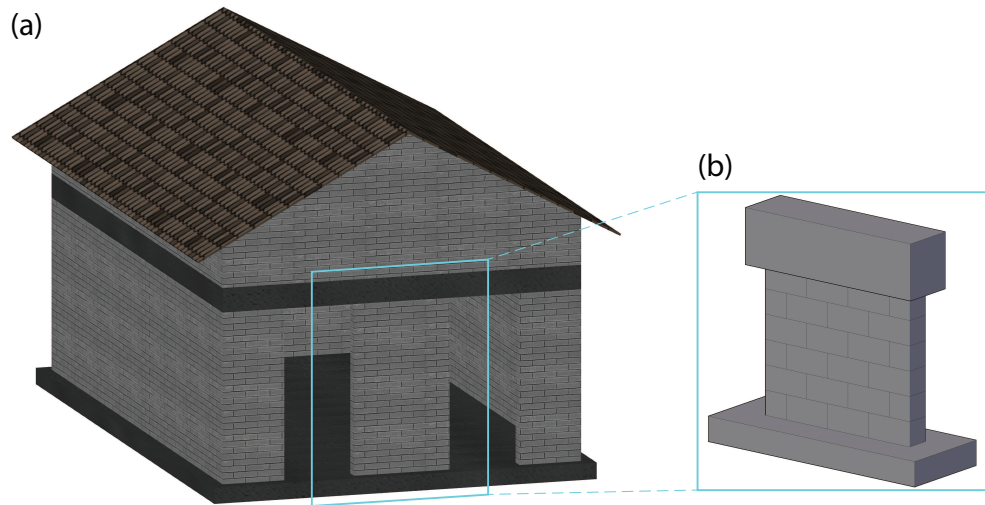


Figure 7: Representation of a specimen design in real-world application: (a) masonry building, and (b) representative masonry wall specimen

Using the masonry wall specimen as an example, when loaded in its in-plane direction with an excitation force that may not be precisely in-plane, the author anticipates not only in-plane motion, but out-of-plane and torsional motions as well. When an SDOF model is created to study this specimen, that model can only be used to analyze one direction of responses. An illustration of this limitation is shown in Figure 8. In this study, all models are SDOF models. With the limitation in mind, other DOFs will be checked.

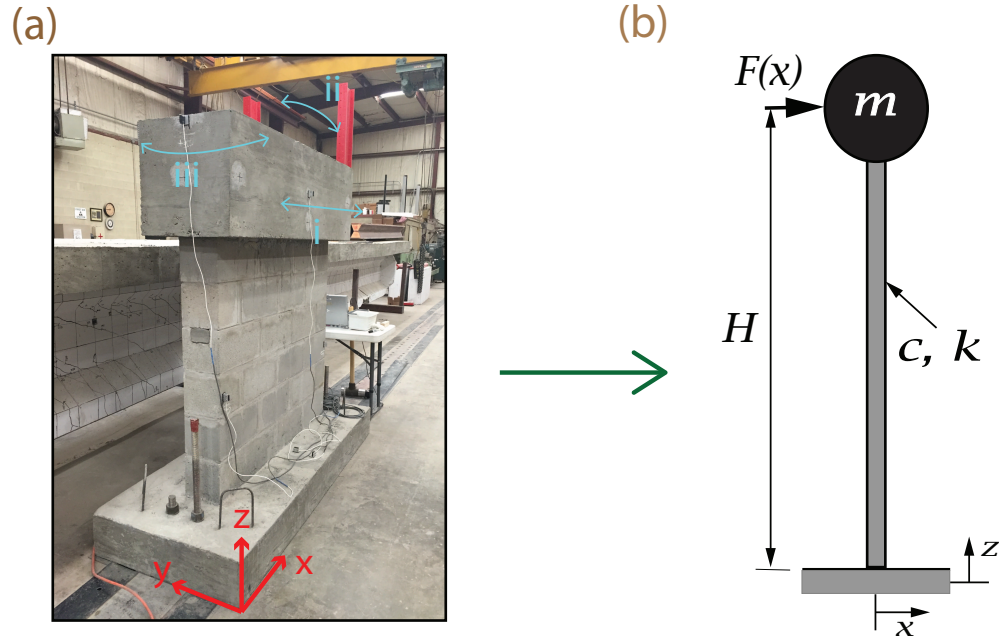


Figure 8: Representation of model in comparison with the real structure: (a) demonstrates a specimen in reality, where for the heavy top, motions along i, ii, and iii are all possible, and (b) shows the model's representation of the specimen, where only the motion along one direction can be studied at one time

### Step 2 - Specimen design and fabrication (when applicable):

Since Girder C is a retired specimen, its design and fabrication conducted in the 1960's. See Table 8 for more information on the history of the design and fabrication of the specimens as well as the participants. Designing a specimen takes a number of factors into consideration. These factors include: scale, materials and connections. In this study, it was intended to create a close representations of real-world structural elements. Some of the specimens are of full-scale and others were not. Girder C and the timber wall specimen are full-scale specimens. The masonry wall is a half-scale specimen and the timber joint specimens are representatives of the common types of connections used in industry (Sugeng [2006]). The design of the specimens

was not conducted by the author, but was conducted by faculty members and/or students. The author did, however, participated in the fabrication of the timber wall specimen, the experience of which will be documented in Section 4.3.

### **Step 3 - Testing specimens:**

Testing offers the chance to analyze the structural behavior. Again, a close representation of real-world conditions are to be generated during testing. These conditions include the types of loading (location and magnitude) and boundary conditions.

Specifically for the two wall specimens, different damage states are created to emulate structures that are deep in their deterioration process. These are the occasions where other researchers conducted destructive static loading on the specimens parallel to its dynamic modal hammer tests conducted by the author. Testing methods utilized in this study will be discussed in-depth in Chapter 4.

In this study, several structural elements are tested in a similar way. For a single specimen even, numerous identical procedures are employed in its testing. Table 8 is a road map summarizing the design, fabrication and test month, duration, and participants for all specimens.

Table 8: Summary of major activities in the experimental work: The initials in the table represent: AJ - Alieu Jobe (author), JSP - Dr. Jin-Song Pei, RWF - Dr. Royce W. Floyd, PSH - Dr. Phillip S. Harvey Jr., MFS - Michael F. Schmidt (lab coordinator), CWC - Conor W. Casey, CDM - Dr. Cameron D. Murray, SDT - Stephen D. Tanksley, and YPS - Yohanes P. Sugeng

Specimen	Design and Construction			Experimental Setup and Testing		
	Date	Duration	Participants	Date	Duration	Participants
Prestressed Girder	~ 1960's	No info.	No info.	Jun 2015	One Month	AJ, JSP, CMD, CWC, MFS and SDT
Masonry Wall	Feb 2016	~ 2 Months	RWF, CWC, PSH and MFS	Mar 2016	One Day	AJ, JSP, PSH, RWF, CWC and MFS
Timber Wall	Jun 2016	One Week	RWF, AJ and MFS	Jul 2016	One Week	AJ, RWF, PSH, CWC and MFS
Timber Joints	~ 2007	~ 2 Months	YPS	May 2016	One Week	AJ and MFS

## 4 EXPERIMENTAL INVESTIGATION

This chapter details the instrumentation and test procedures on representative specimens in this study. As previously mentioned, four types of specimens were tested. This chapter will cover the experimental procedures for two specimens: the prestressed girder (Girder C) and the timber wall. Of the four specimens, Girder C is one of its kind due its simply supported boundary conditions and its. The remaining three specimens are modeled as cantilever upright specimens. Of the three cantilever specimens, the timber wall is considered to have the most complicated test setup and procedure, thus, it is used for illustration purpose to detail the experimental procedures of a typical cantilever specimen. Brief descriptions of the nature, test setup and procedure of each of the masonry wall and timber joint specimens can be found in Appendix A.

### 4.1 Overview of Typical Test

As mentioned previously, the general methodology used in this study includes experimental investigation and data processing. Experimental investigation involves designing the tests, setting up the equipment and conducting the modal hammer test. Serving as an overview of a typical test, Figure 9 is an illustration of the sequential overview of the data acquisition path in this study. Following the figure are brief descriptions of the sequence.

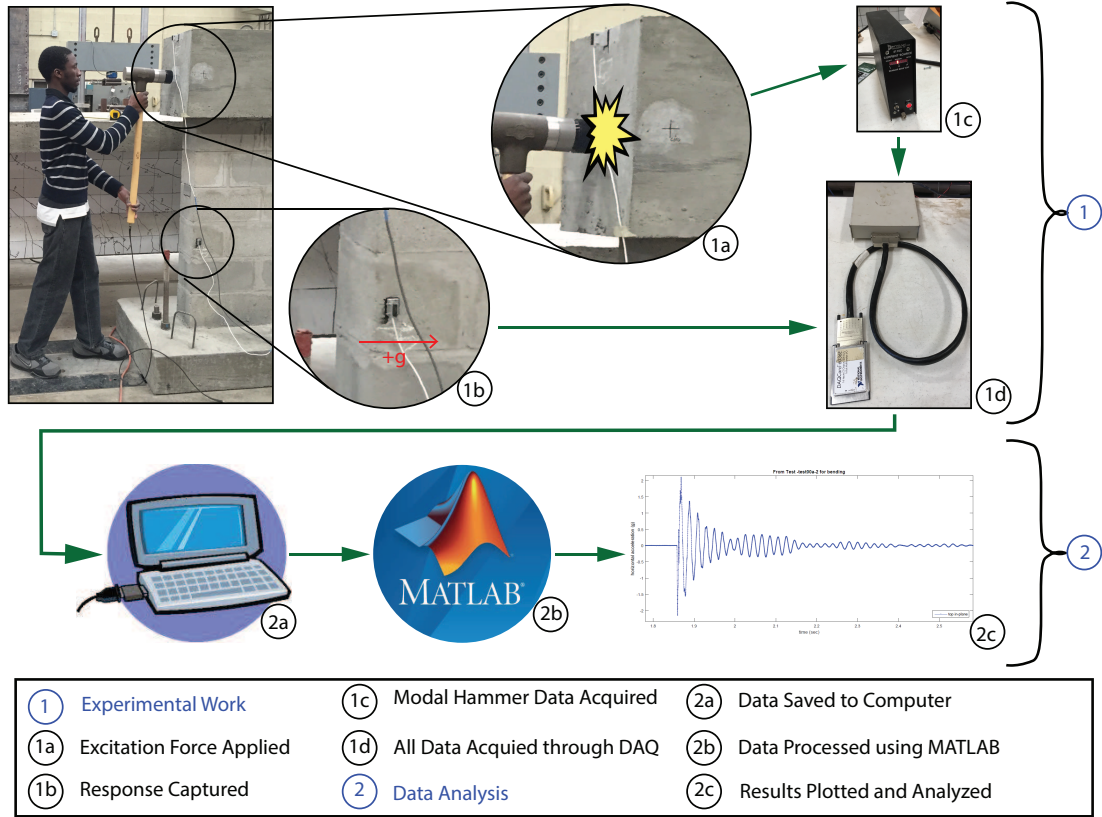


Figure 9: Illustrative overview of the processes involved in a typical test

First a modal hammer was used to manually apply an excitation force (Figure 9-1a) to induce a vibration of the specimen. The modal hammer is equipped with a force sensor that enables the recording of the magnitude of the excitation force. The hammer was intentionally controlled by the author so that the excitation force was of moderate and consistent magnitude. The reason is that too large of a force could cause unintended (hardly seen or existed) damage to the specimen and too low of a force may not be enough to overcome the noise level. For the masonry wall specimen sometimes however, the force intensity was dialed down for the interest of studying the specimen’s behavior under a low excitation force with the intended practical application to residential buildings in mind. The hammer was powered

using a Dytran 4110C current source. The hammer force signal was received by the current source and then fed directly into an NI SCB-68 block, which is connected to the data acquisition computer through a 68 pin DAQ connector.

Second, accelerometers were utilized to record the acceleration of the specimen at different locations of interest. The acceleration data was fed directly into the SCB-68 block.

LabVIEW<sup>®</sup> from NI was utilized to facilitate data acquisition. Operational parameters to be specified included sampling rate, number of channels, channel assignments to respective sensors, etc. The operational parameters were specified under LabVIEW's block diagram and tests were run under the front panel window. LabVIEW program files are known as "VI" files which stands for virtual instrument. The VI files used in this study were inspired by Dr. Peng F. Tang's original design which enables automation of test duration and file saving. The author further improved the files and tailored them to fit the current testing protocols. For the timber wall testing, Dr. Philip S. Harvey assisted in further enhancing the "VI" files.

MATLAB<sup>®</sup> will be employed to process the data after proper acquisition and storage. Details of the data processing procedure are discussed in Chapter 5.

## **4.2 Instrumentation and Data Acquisition**

This section reviews key components of the data acquisition system utilized in this study. Figure 10 illustrates the data acquisition system highlighting the connectivity of the individual components.



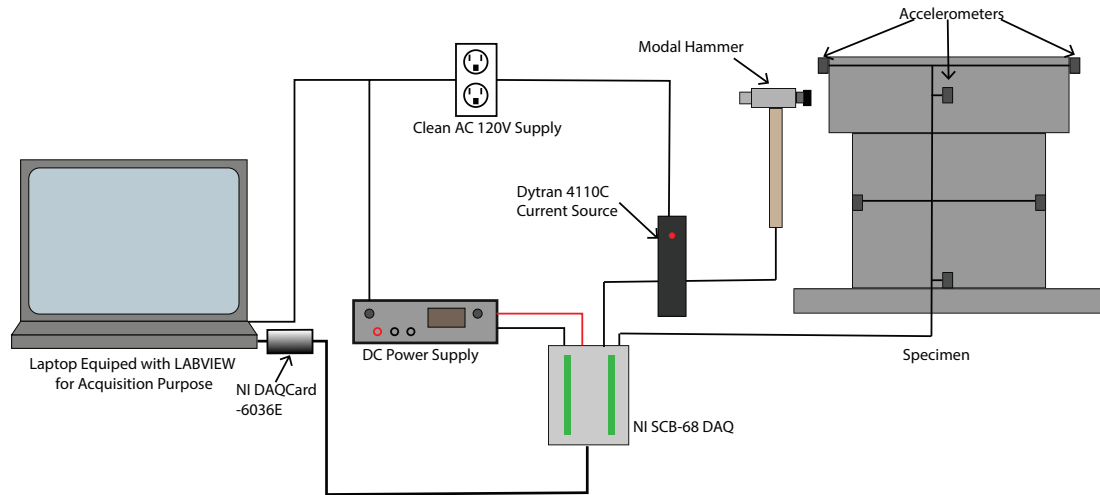


Figure 10: Configuration of experimental setup and data acquisition system

The two major components of the instrumentation are the modal hammer and accelerometers. The modal hammer was used to excite the specimen and the accelerometers to record the acceleration responses at designated locations. The remaining components, shown in Figure 10, are behind the scenes to facilitate data collection during testing.

For each test, there were two data paths that eventually converged. First, the modal hammer force data was fed through the power supply, the Dytran 4110C current source, and then into the SCB-68 block. The second path was the acceleration data, which was fed directly into the SCB-68 block. The block and the accelerometers were powered with about 10 V DC by a DC power supply. From the block, data flowed through a 68-pin connector into the DAQcard-6036E, which fed the data into the data acquisition computer. The computer was equipped with software packages such as “NI LabVIEW” and “Measurement and Instrumentations” to facilitate data acquisition process. The overall system was connected to a clean 120 V AC power receptacle (outlet). The reason for a clean electrical supply is to avoid other electrical noise from interfering with the sensitive data acquired

from tests. The receptacle's circuitry is isolated from that of other receptacles that power other equipments in the lab. This isolation creates a shield from the majority of the electrical noise induced by other lab equipments, although the presence of noise was observed on some tests.

For all specimens, trials were conducted prior to the actual test. This was done to mitigate any possible source of malfunction in the instrumentation. Most of the problems encountered during trials were related to electrical noise distorting the sensor signals.

#### 4.2.1 Hammers

Two different hammers were used in this experimental investigation: a big hammer and a small one, both of which are products of Dytran.

The big hammer, referred to as the modal hammer in this study, is designed to excite large, heavy structures and machines such as buildings, bridges, trucks and other massive structures (Dytran Instruments, Inc. [b]). The "Impulse Hammer", as named by the manufacturer is a 12 *lb* sledge hammer equipped with an integral piezoelectric force sensor at the tip. This sensor utilizes self-generating quartz crystals to output voltage signal at a sensitivity of  $1.0 \frac{mV}{lbf}$ . The output signal is proportional to the impact force of the hammer (Dytran Instruments, Inc. [b]).

The modal hammer is designed for a maximum nominal impact force of 5000 *lbf* which is equivalent to a maximum voltage output of 5 *V*. As shown in Figure 11, the hammer comes equipped with four different color-coded tips that are distinguished based on their hardness or softness. Each of these tips has a suitable application for recommended use (Dytran Instruments, Inc. [b]). The modal hammer is powered with 12 *V DC* using the 4110C current supply, which is also a product of Dytran. The hammer was used to excite the prestressed concrete girder, the

masonry wall and the timber wall during testing.



Figure 11: Dytran modal hammer

The small hammer used in this study is also a product of Dytran. Named “Dytrapulse Impulse Hammer,” it is also equipped with a force sensor that uses a quartz sensing element with a maximum allowable force of 1000 *lb* (Dytran Instruments, Inc. [a]). The force sensor has a voltage sensitivity of 10  $\frac{mV}{lb_f}$  (Dytran Instruments, Inc. [a]). This hammer was used only in this study to excite the timber joints specimens. As shown in Figure 12, the small hammer also comes with different heads with different levels of hardness.



Figure 12: Dytran dynapulse impulse hammer

## 4.2.2 Accelerometers

Accelerometers are sensors that measure acceleration of a body. They can be uniaxial (i.e. measure in a single axis), biaxial (i.e. measure in two axes) or triaxial (i.e. measure in three axes). In this study, they are the key facilitators of the experimental investigation. Two brands of analog uniaxial accelerometers were utilized in this study: a Silicon Designs (SD) brand and an Analog Devices (ADXL) brand, as shown in Figure 13.

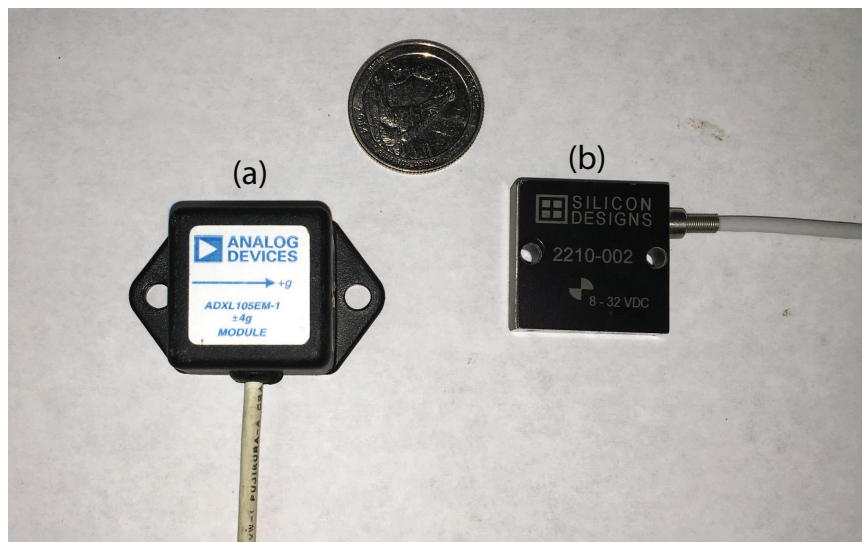


Figure 13: Accelerometers used in this study: (a) Analog Devices (ADXL) accelerometer, and (b) Silicon Designs (SD) accelerometer

The SD accelerometers are manufactured by Silicon Designs Inc. and are characterized by their high drive low impedance buffering (Silicon Designs, Inc. [2006]). Two different models of sensors were utilized in the study: a  $\pm 2g$  range and a  $\pm 5g$  range. The  $\pm 2g$  range was preferred and used for most of the experimentation first and foremost, due to the accelerometer's high resolution. There is a limitation due to measurement saturation when acceleration beyond its range is encountered during the timber joint tests.

The ADXL accelerometers made by Analog Devices have options for both uniaxial or triaxial. During the time of testing, only uniaxial  $\pm 4g$  range ADXL modules were available. They were only used during the testing of Girder C due to a limited number of available SD sensors.

Since two brands of accelerometers were utilized, each of which required a different mounting method, two different mounting brackets were fabricated. Figure 14 presents photos of the sensor mounting accessories.



Figure 14: Accelerometer mounting accessories: (a) L-bracket for SD sensors, flat bracket for mounting ADXL sensors on the prestressed concrete girder only, Loctite 410 instant adhesive to be applied on bracket before mounting and for mounting, and Loctite 7452 accelerator for accelerating the adhesive bonding power, (b) a mounted SD sensor and (c) a mounted ADXL sensor

The sensors were mounted on the brackets using small screws and bolts and



the brackets were mounted on the specimens using the Loctite 410 adhesive. Loctite 7453 accelerator was sprayed on the brackets before the adhesive was applied in order to accelerate the curing process of the adhesive. For the timber joint specimens, only L-brackets were used for mounting and were mounted to the specimen using screws. For the timber wall specimens, the sensors were directly mounted to the specimen using wood screws.

#### 4.2.3 SCB-68 and DAQ card

The SCB-86 and DAQ card are the key in the data collection and modulation. Figure 15 presents photos of the components of the DAQ unit used in this study.

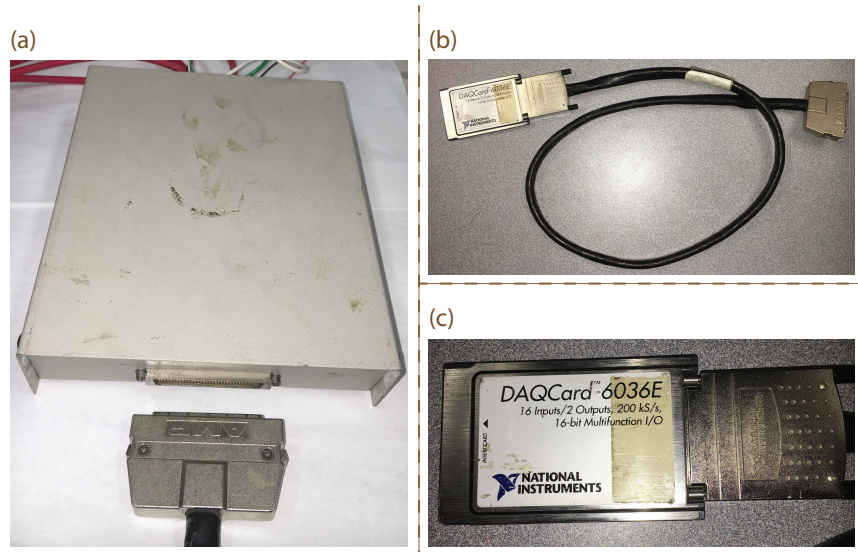


Figure 15: The National Instruments (NI) digital acquisition system utilized in this study (a) SCB-68 block; (b) DAQcard-6036E connected to the 68 pin connector, and (c) DAQ card

The SCB-68 block is a shielded input/output (I/O) connector block manufactured by National Instruments (NI). The SCB-68 block interfaces I/O signals to plug-in data acquisition (DAQ) devices with a 68-pin connector (National Instru-

ments). The block is limited to two configurations: a sixteen-channel single-ended mode and an eight-channel differential mode. Two units of the SCB-68 block were available and one was configured in single-ended mode and the other in differential mode. Thus, both configurations were utilized in the study. The first configuration was utilized in testing the prestressed concrete girder and the latter was utilized on the remaining specimens. Due to its size, the prestressed concrete girder required a comprehensive setup to record it in-plane and out-of-plane motion along multiple locations. However, the DAQ is limited to a maximum of fifteen single-ended channels that can accommodate accelerometers. With the single-ended mode comes another limitation that only half the resolution of the sensors can be utilized.

Another crucial component of the acquisition system is the DAQcard. The DAQ device used in this study is the DAQcard-6036E, which is a digital I/O card – also manufactured by NI. The DAQcard modulates the analog data from the SCB-68 block into useful digital signals that are fed into the data acquisition computer where it is stored for processing.

#### **4.2.4 Field calibration of accelerometers**

Prior to every test, and sometimes after, field calibration was conducted on the sensors. The purpose of the calibration is to record the positive and negative “g” voltage readings for each of the accelerometers used. It was conducted by placing the accelerometer on a horizontal surface with its measuring axis facing vertically down and then running the acquisition system for a short time. The same procedure was repeated for the opposite end of the sensor’s measuring axis. When the measuring axis faces vertically down, gravity will have full effect on the accelerometer and thus the reading should represent either positive or negative “g”.

Repeating the procedure on the opposite end will ensure the recording of both positive and negative “g” readings for the sensor. These reading are inputs of the modular code and are know as the sensitivity values later discussed in Section 5.4.

### **4.3 Timber Wall: Specimen Description**

The timber wall specimen tested in this study was designed to mimic shear walls that are most commonly used in typical timber homes. The specimen is designed based on the International Building Code (IBC) 2009, and with nominal dimensions of 8 × 8 feet (height × width). The 8 feet height is a standard dimension from floor to ceiling for a typical home. See Figure 20 for the overall dimensions and other details to be explained herein.



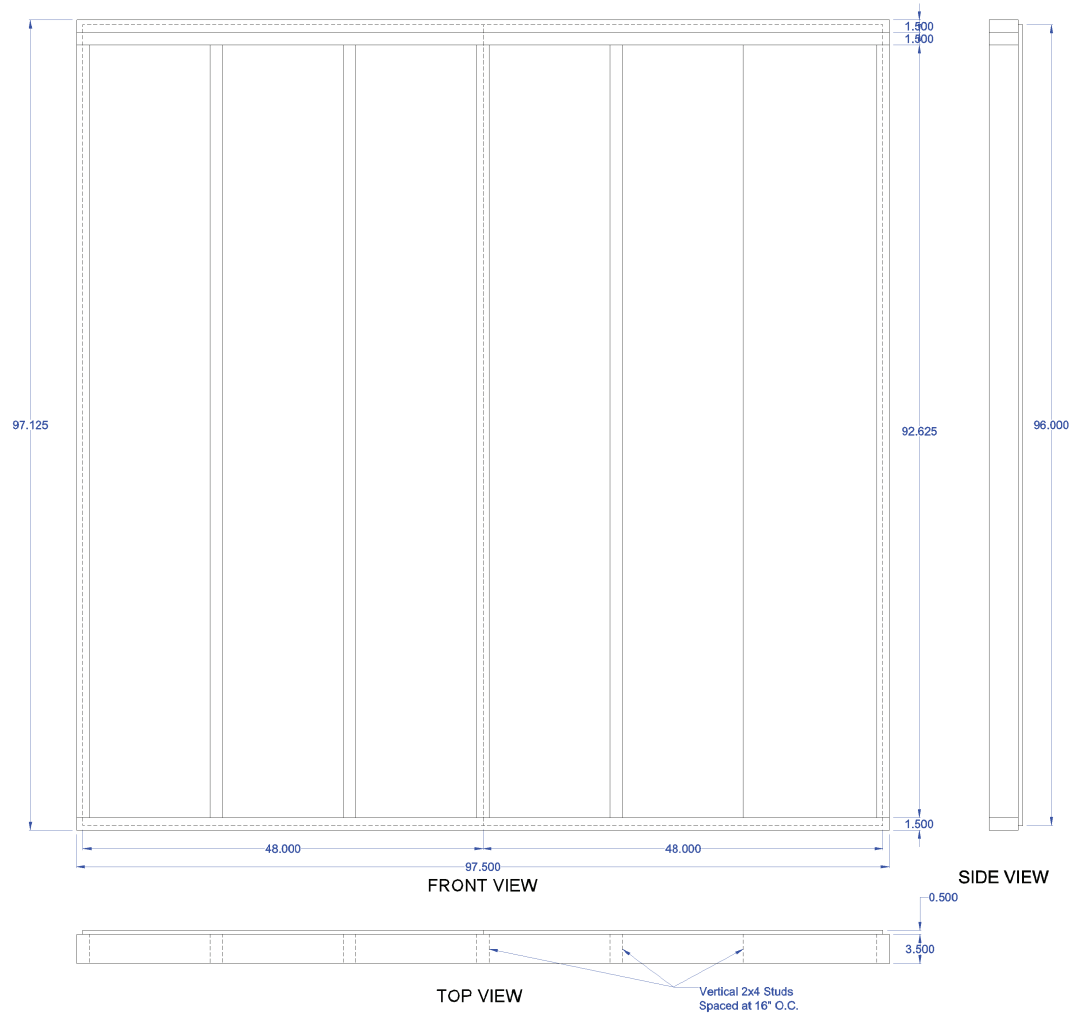


Figure 16: Timber wall dimension detailing. All dimensions are in inches.

The wall is framed using  $2 \times 4$  dimension lumber and it consists of a single horizontal plate at the bottom, double at the top and seven vertical studs spaced at 16 in on center (O.C.). Nails are utilized in all of the specimen's connections. The stud (vertical elements) of the framing are connected to the plates (horizontal elements) using two 16d end nails at each joint. The two top plates are nailed together using 10d spaced at 24 in O.C. Although designed as described above, a  $2 \times 6$  plate is placed nailed at the top to accommodate the placement of a W-sections (as added mass in the form of distributed load) during testing. Two  $4 \times 8$

feet  $\frac{3}{8}$  in thick Oriented Strand Board (OSB) are nailed on one side of the framing using 10d common nails spaced 4 in O.C. at its edges and 6 in O.C. in field. The wall sheathing is designed based on [City of Moore \[2014\]](#).

#### 4.4 Timber Wall: Test Setup

In this study, the timber wall specimen was tested both statically and dynamically, specifically, modal hammer tests for the latter. The intermittent modal hammer tests were performed by the author in between a series of destructive shear loadings. During the experimental procedures, the timber wall specimen was mounted on a rigid floor (at Fear Lab structural engineering high bay) using two 0.5 in anchor bolts spaced at 6 ft on center. The specimen was maintained at the same location through all tests.

To apply lateral load by pulling as shown in [Figure 17](#), a hydraulic jack was mounted on a rigid column, attached (in series) to the load cell which was then hooked on to a steel plate mounted at the top of the specimens. This plate was mounted with four bolts at the top of the specimen in such a way that the center of the hook was directly aligned to anchor bolt on the base closest to the loading system. To measure the deflection as the specimen was loaded, a string potentiometer (wirepot) was mounted on the rigid column underneath and parallel to the loading system. The wirepot was then hooked to the specimen at the end of the  $2 \times 6$  plate as illustrated in [Figure 18](#).

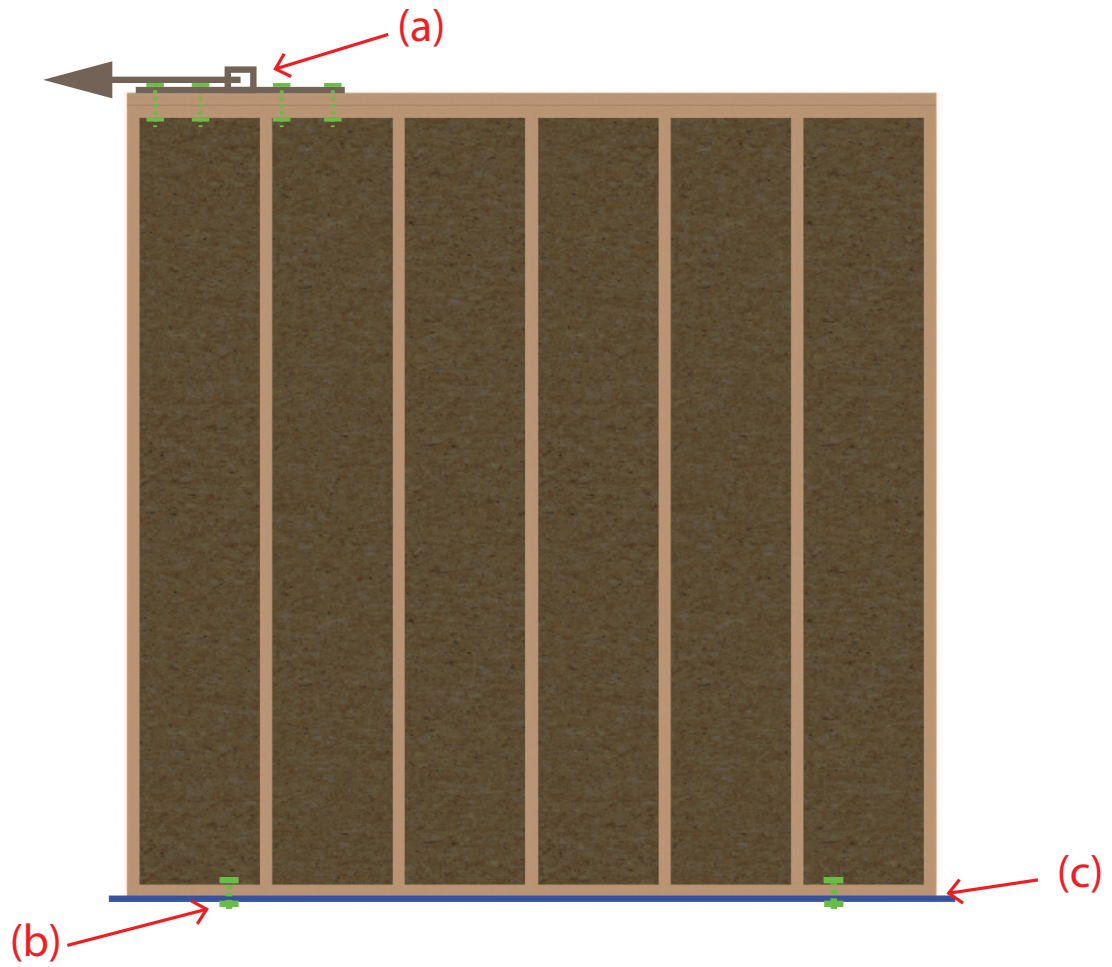


Figure 17: Timber wall lateral test setup: (a) bolted anchor for the loading system, (b) bolts to the rigid floor spaced at six feet, (c) rigid floor

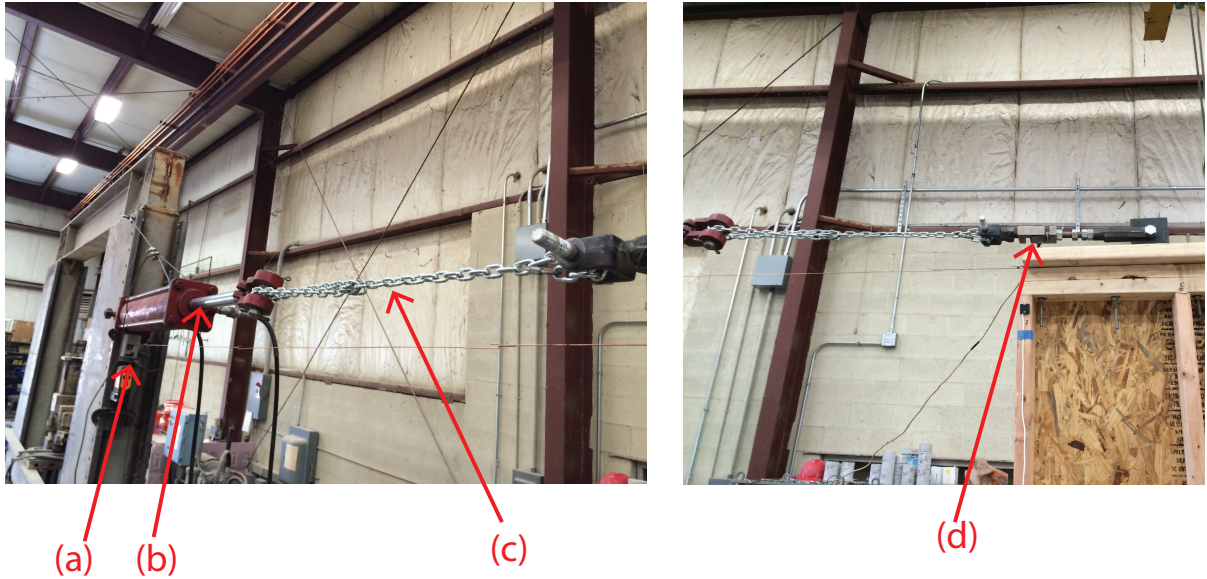


Figure 18: The lateral loading system for the timber wall: (a) wire potentiometer for measuring displacement; (b) hydraulic arm for applying lateral force; (c) adjustable chain for transferring lateral force and allowing slack during disengagement of loading system, and (d) s-shaped load cell for measuring applied force

For all hammer tests, six accelerometers were mounted at different locations of interest on the specimen as illustrated in Figure 19, where the arrows indicate the positive direction of measurement. The sensor layout was designed to capture in-plane, out-of-plane and torsional responses. Accelerometers were mounted at the base of the specimen to correct rigid body motion in the data analysis. The numeric numbers assigned to the accelerometers in Figure 19 are actually the analog channel IDs, which are given in Table 9. Accelerometer IDs assigned by the manufacturers, and the mounting locations and orientations, are also specified in Table 9.

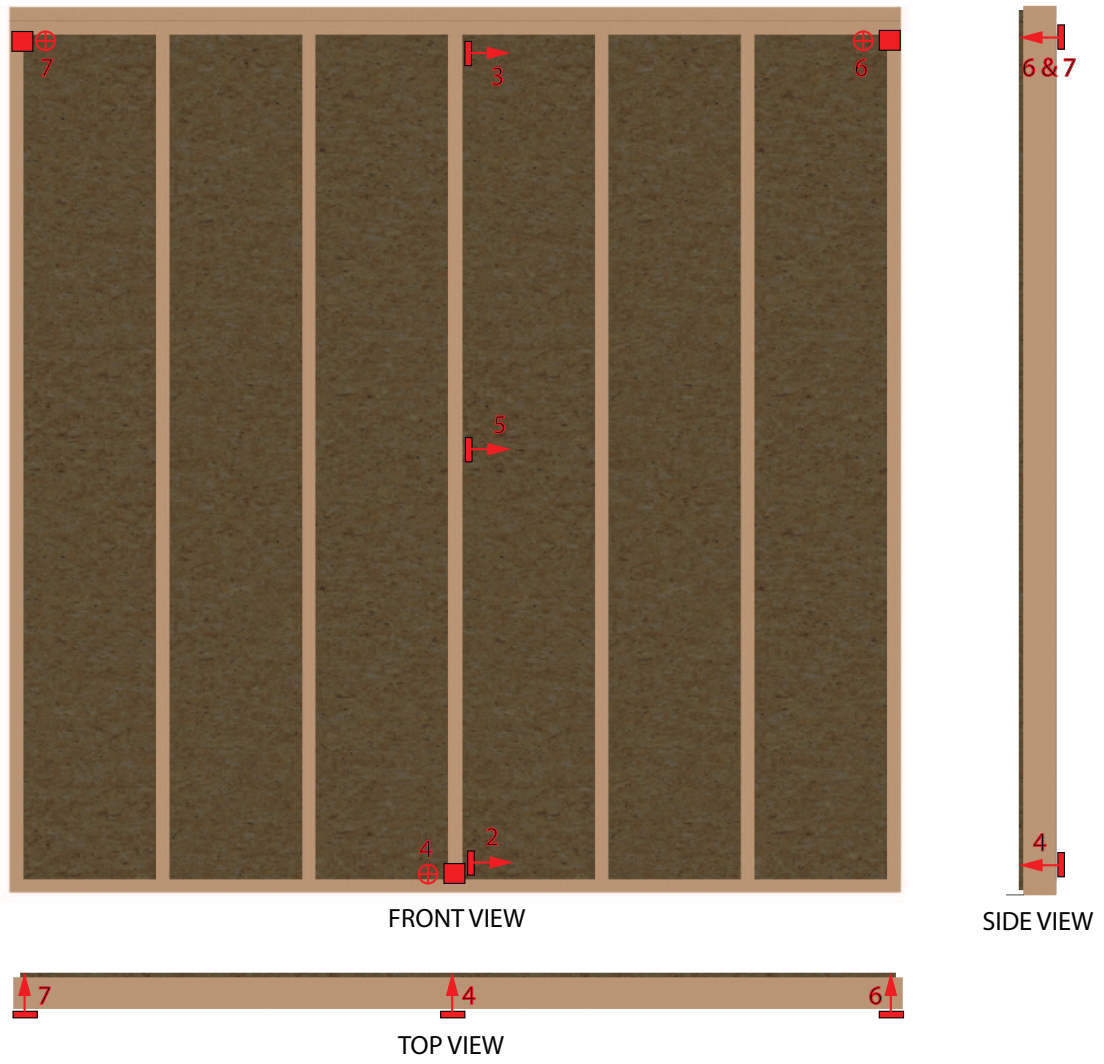


Figure 19: Timber wall sensor layout

Table 9: Description sensor allocation details. †“ai” stands for analog input

Channel ID†	Sensor ID	Location	Orientation
ai1	Hammer	N/A	N/A
ai2	750	base	in-plane
ai3	628	top	in-plane
ai4	751	base	out-of-plane
ai5	753	mid-height	in-plane
ai6	627	top-south	out-of-plane
ai7	754	top-north	out-of-plane

In addition to the accelerometers occupying channels 2 through 7, the modal hammer was connected to channel 1 for force monitoring purpose. An eight-channel differential mode setup was utilized for this particular specimen, however, channel 0 was not used due to its faultiness.

For all accelerometers mounted on the specimen, the following is a description of their primary roles referring to Figure 19 and Table 9:

Sensor 2 measures in-plane ground motion. The data from this sensor enables the exclusion of the translational rigid body motion in the specified direction for the calculation of elastic deformation.

Sensor 3 measures the in-plane acceleration closest to the lumped mass, i.e., on the top plate of the timber wall specimen to obtain the anticipated first mode.

Sensor 4 measures the out-of-plane ground acceleration. The data from this sensor is used as ground reference for all relative out-of-plane accelerations.

Sensor 5 measures the in-plane acceleration at specimen’s mid-height to confirm



the mode shape during data analysis.

Sensor 6 measures the top out-of-plane motion.

Sensor 7 measures the top out-of-plane motion.

The average of the responses obtained from sensors 6 and 7 is used to assess the out-of-plane bending of the specimen, and the difference gives the torsional response.

Figure 20 shows the three loading configurations. In order to mimic the gravity loads that may be bearing upon a typical timber shear wall in service, two loading configurations were created in addition to the specimen's default configuration.

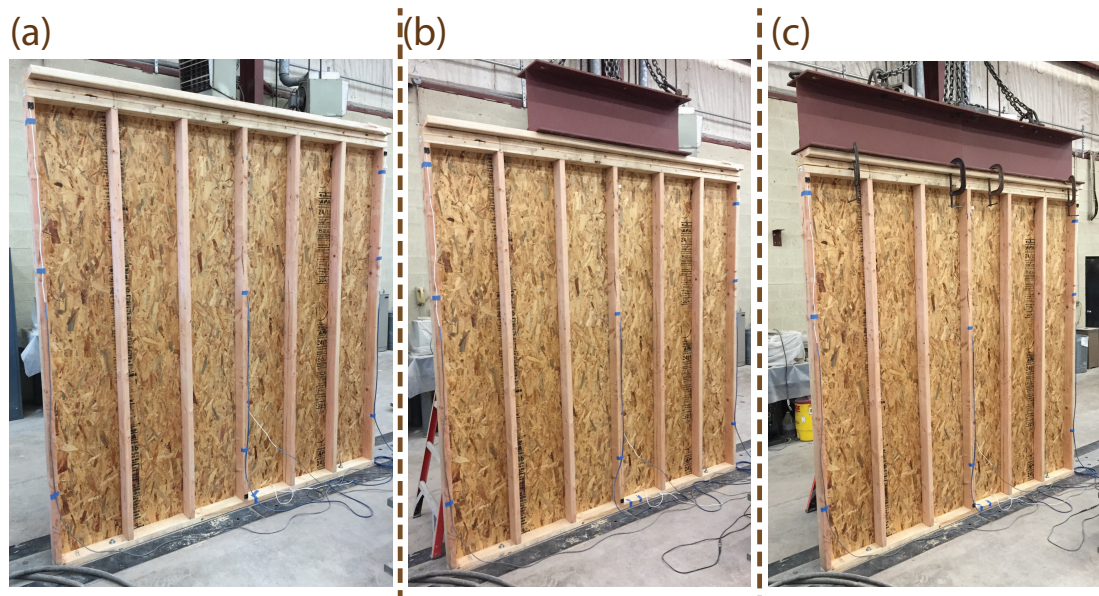


Figure 20: Three loading configurations for the timber wall during the modal hammer test: (a) the specimen is under no distributed load from the top; (b) the specimen is with a 4 ft long  $W15 \times 50$  centered at the top, and (c) the specimen is with two 4 ft long  $W15 \times 50$  placed at the top

These loads were added only during the dynamic test, and were done in three

levels.

Level 1 The specimen was tested with no weight added to the top as illustrated by Figure 20a.

Level 2 A single 4 ft long  $W15 \times 50$  section was used to give a 4 ft long  $50 \frac{lb}{ft}$  distributed load as illustrated by Figure 20b.

Level 3 Two 4 ft long  $W15 \times 50$  sections were used to give it an 8 ft long  $50 \frac{lb}{ft}$  distributed load as illustrated by Figure 20c. This loading condition be considered the most accurate representation of real world situations.

C-clamps were used to secure the loads on the top plate of the specimen to ensure a monolithic reaction during the modal hammer tests. A crane was utilized during loading and unloading the added loads after every test.

## 4.5 Timber Wall: Test Procedure

As mentioned, two types of tests were conducted on the timber wall specimen: lateral shear test and modal hammer test, the procedure of which will be presented in Sections 4.5.1 and 4.5.2, respectively.

### 4.5.1 Lateral shear test

Although not the main focus of this study, the lateral shear test involved applying lateral load to the top of the specimen while the bottom was anchored on the rigid floor. The load was applied using a hydraulic jack in the direction shown earlier in Figure 17. As the specimen was loaded, the load cell was used to record the applied force. A string potentiometer (wirepot) was used to monitor the specimen's



deflection. The specimen was loaded and unloaded successively until failure was reached. During this loading and unloading process, different stages of the specimen's damage state were reached.

#### **4.5.2 Modal hammer test**

The modal hammer tests were executed before, after and in between each of the of the lateral loading cycles. The hammer test involved using the modal hammer to excite the specimen at the designated impact locations to induce free vibration. See Figure 21 for all impact locations and Table 10 for explanations. The impact locations were designed to excite multiple responses to produce a wide scope of analysis for future studies.

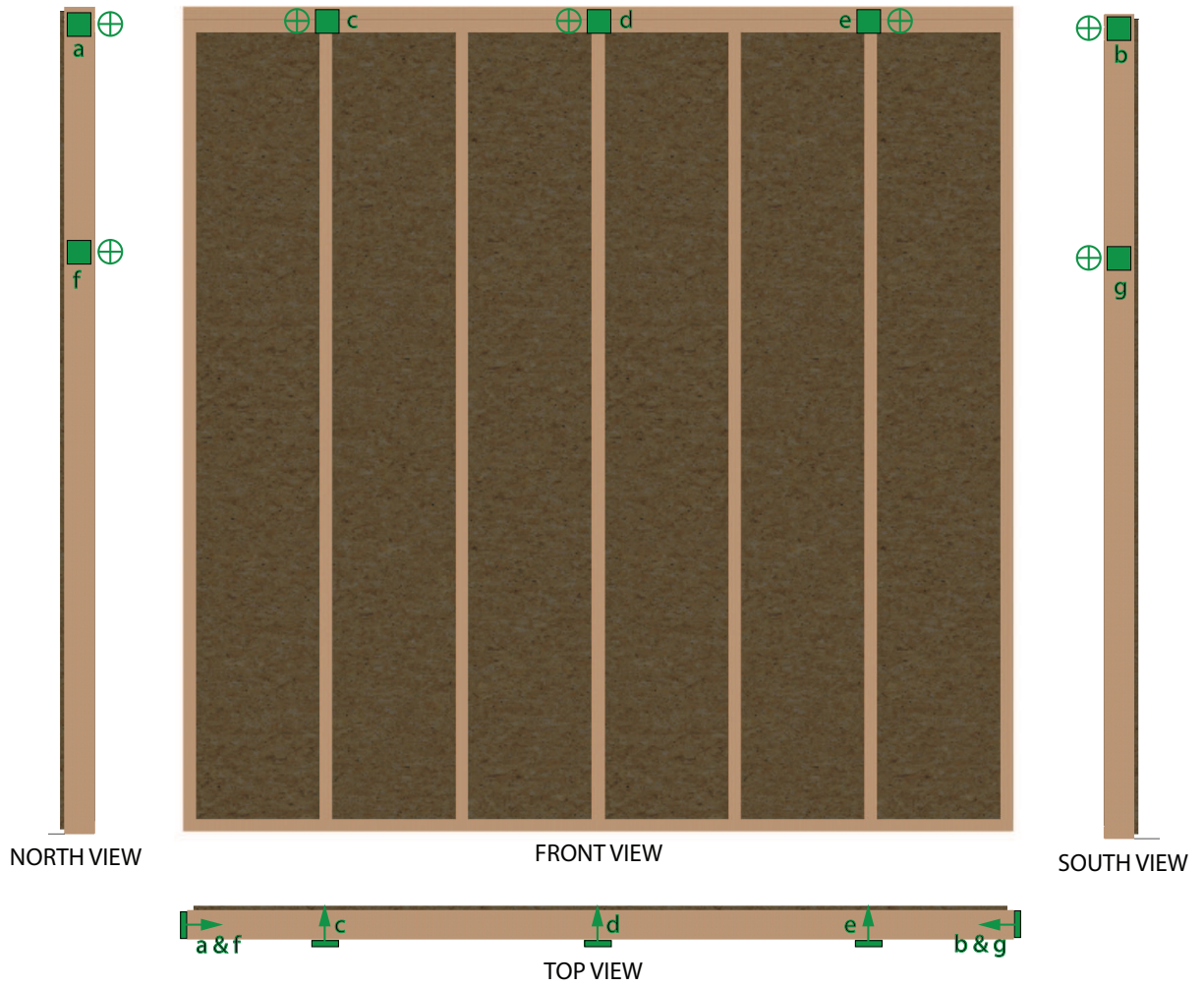


Figure 21: Timber wall impact locations where a cross head is used to indicate each impact location

Table 10: Details on Impact Locations

Location ID	Position on Specimen	Impact direction
a	North - Top	In-plane
b	South - Top	In-plane
c	Second Stud from North - Top	Out-of-plane
d	Middle Stud - Top	Out-of-plane
e	Second Stud from South - Top	Out-of-plane
f	North - 6 <i>ft</i> from bottom	In-plane
g	South - 6 <i>ft</i> from bottom	In-plane

All three loading configurations presented previously in Figure 20 give a broad set of scenarios to model the specimens for real-world situations where the wall is load-bearing. Modal hammer test helps contrast the effect of gravity loads on the modal frequencies. Finally, the different damage states induced by the shear test would further widen the scope of analysis into the study of damaged structure analysis.

#### 4.6 Prestressed Concrete Girder: Specimen Description

As one of the structures tested in this study, Girder C is a “retired” prestressed concrete girder that had served about 47 years on the I-244 bridge over the Arkansas river in Tulsa, Oklahoma (Floyd et al. [2016]) before the bridge was demolished, and the specimen was extracted, transported to, and tested at Fears Structural Engineering Laboratory at the University of Oklahoma. .

Spanning 46 *ft*, Girder C used to be one of the seven girders supporting a 46-*ft* section of the east bound lanes of I-244 (STU [1967]). The girder is an American Association of State Highway and Transportation Officials (AASHTO) Type

II prestressed girder that was precast in the 1960's (STU [1967]). The girder was extracted as the bridge was demolished for a replacement in 2013 (Floyd et al. [2016]). It was, however, extracted with an asymmetric portion of bridge deck and diaphragms (as documented in Figure 22). Figure 22 presents AutoCAD drawings with the exterior dimensions of the girder and some other details relevant to its testing setup. More details on the girder can be found in (Floyd et al. [2016]) where the material properties of the cored samples of Girder C are provided.

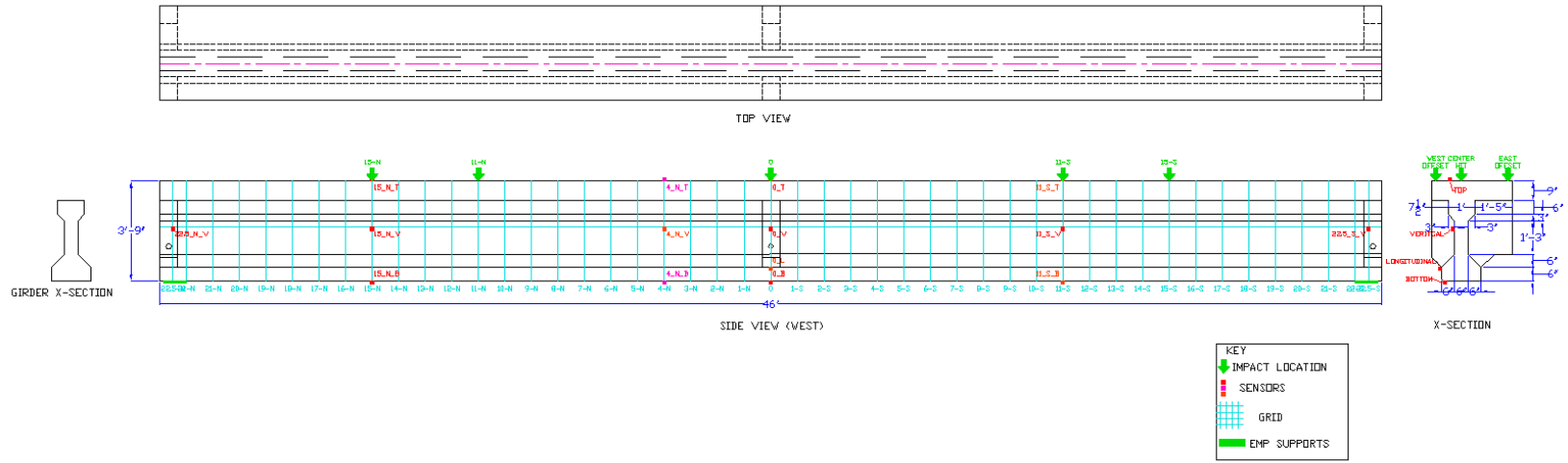


Figure 22: Prestressed girder dimension detailing

## 4.7 Prestressed Concrete Girder: Test Setup

Although the girder was tested both statically and dynamically, they were conducted independently. The dynamic test was only a minor task before the major shear destructive tests. This section discusses only the dynamic test.

Girder C was tested differently from all the other specimens in this study in terms of boundary conditions. In modeling, unlike all the other tested specimens modelled as a cantilever beams/walls, the girder is modeled as a simply-supported beam. The testing protocol is thus different accordingly.

During testing, the girder was placed in Fears Lab high bay and was simply supported on elastomeric pads. These one inch thick pads were utilized to mimic the real-world supporting conditions of the girder in service (Floyd et al. [2016]). These pads were centered at 6 *in* from the ends of the girder, giving the specimen a span of 45 *ft*.

Accelerometers were utilized to capture the free vibration response of the specimen after excitation was applied. The accelerometers were mounted with the use of aluminium plates and Loctite 410 adhesive (given earlier in Figure 14).

The sensor layout for Girder C is presented in Figure 23. Note that notations of N and S imply north and south direction, respectively, based on the orientation of the girder during testing. The numerical values represent the length in *ft* from the mid-span of the girder.

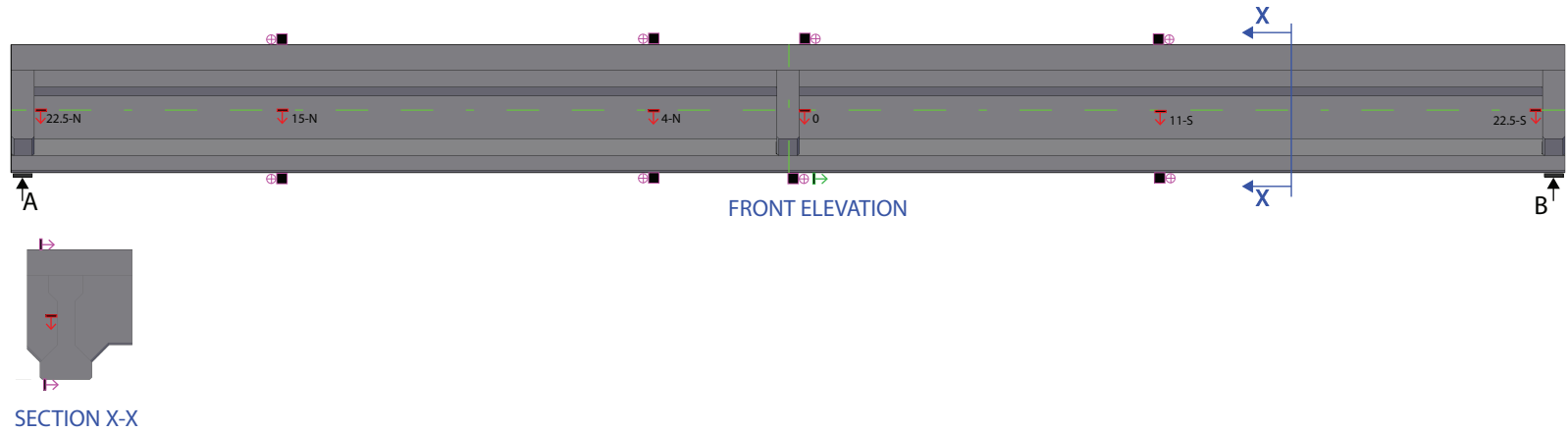


Figure 23: Prestressed sensor layout

Fifteen accelerometers were mounted at key locations of interest on the girder to capture in-plane, out-of-plane, torsion and/or longitudinal accelerations. Together with one channel reserved for the modal hammer, this number of channels makes a total of 16 channels to saturate the single-ended mode capability of SCB-68. Two items played an important role in the placement of sensors: cable lengths and resolution. Accelerometers were generally prioritized based on the importance of the mounted locations in the analysis presented earlier in Section 3.3.

Due to the huge dimensions of the specimen, some sensors had limited reaches because of their short cables. Sensors with longer cables were generally mounted farther from the mid-span and shorter ones were mounted closer to and at the mid-span.

Sensors with shorter ranges of measurement (i.e. 2g sensors) were considered to have a higher resolution and those with long ranges (i.e. 4g and 5g) are considered to have a lower resolution. Higher resolution sensors were mostly used on important locations (i.e. mid-span in-plane, supports in-plane, etc.). Tables 11 and 12 give more information on the location and nature of the accelerometers.



Table 11: Accelerometers with their corresponding channel “ai” designations, resolutions, cable lengths and directions of measurement

Channel No.	Sensor ID	Range	Sensor	Cable length ( <i>ft</i> )	Direction
ai1	626	2g	SD	44	In-plane
ai2	751	2g	SD	24	In-plane
ai3	752	2g	SD	26.5	Out-of-plane
ai4	628	2g	SD	27	Out-of-plane
ai5	539	5g	SD	11	In-plane
ai6	263	4g	ADXL	6	Out-of-plane
ai7	229	4g	ADXL	7	Out-of-plane
ai8	627	2g	SD	7	In-plane
ai9	537	5g	SD	11	Longitudinal
ai10	753	2g	SD	10	Out-of-plane
ai11	750	2g	SD	11.5	Out-of-plane
ai12	749	2g	SD	25	In-plane
ai13	535	5g	SD	12	Out-of-plane
ai14	536	5g	SD	12	Out-of-plane
ai15	754	2g	SD	46	In-plane

Table 12: Locations of all sensors

Coordinate ( <i>ft</i> )	N22.5	N15	N4	0	S11	S22.5
<b>Top flange</b>	N/A	752	263	753	535	N/A
<b>Web</b>	626	751	539	627	749	754
<b>Bottom flange</b>	N/A	628	229	750 & 537	536	N/A

As part of the preliminaries of the experimental work, the specimen was painted white and sharpies were used to draw a grid with a resolution of one foot. Since

the grid was precisely labeled at every one-foot line, it functioned as a ruler and helped avoid repetitive measurement during the dynamic setup. The white paint and grid also helped the trace and document of cracks when the specimen was later tested for shear.

## 4.8 Prestressed Concrete Girder: Test Procedure

The dynamic hammer test on Girder C involved using the modal hammer to excite the specimen at the designated impact locations specified in Figure 24 with the response was captured by the mounted accelerometers.

0 represents mid-span and the others follow a similar coordinates as the specimen's sensor layout. The longitudinal impact locations are designed to excite different modal responses. For each longitudinal location on the girder, three transverse impact locations were chosen; center, offset west and offset east. The center location was positioned through the centroid of the girder (alone without the slab) and the other two were offsets from the centroid. The off-center locations are designed to excite out-of-plane and torsional responses for future models to be used; their analysis in principle would be the same as that in Chapter 5 but omitted in this study..

For each impact location on the girder, the author took the initiative of grinding the surface to ensure smoothness, which would promote proper application of excitation force and mounting of some accelerometers as detailed in Figure 25.

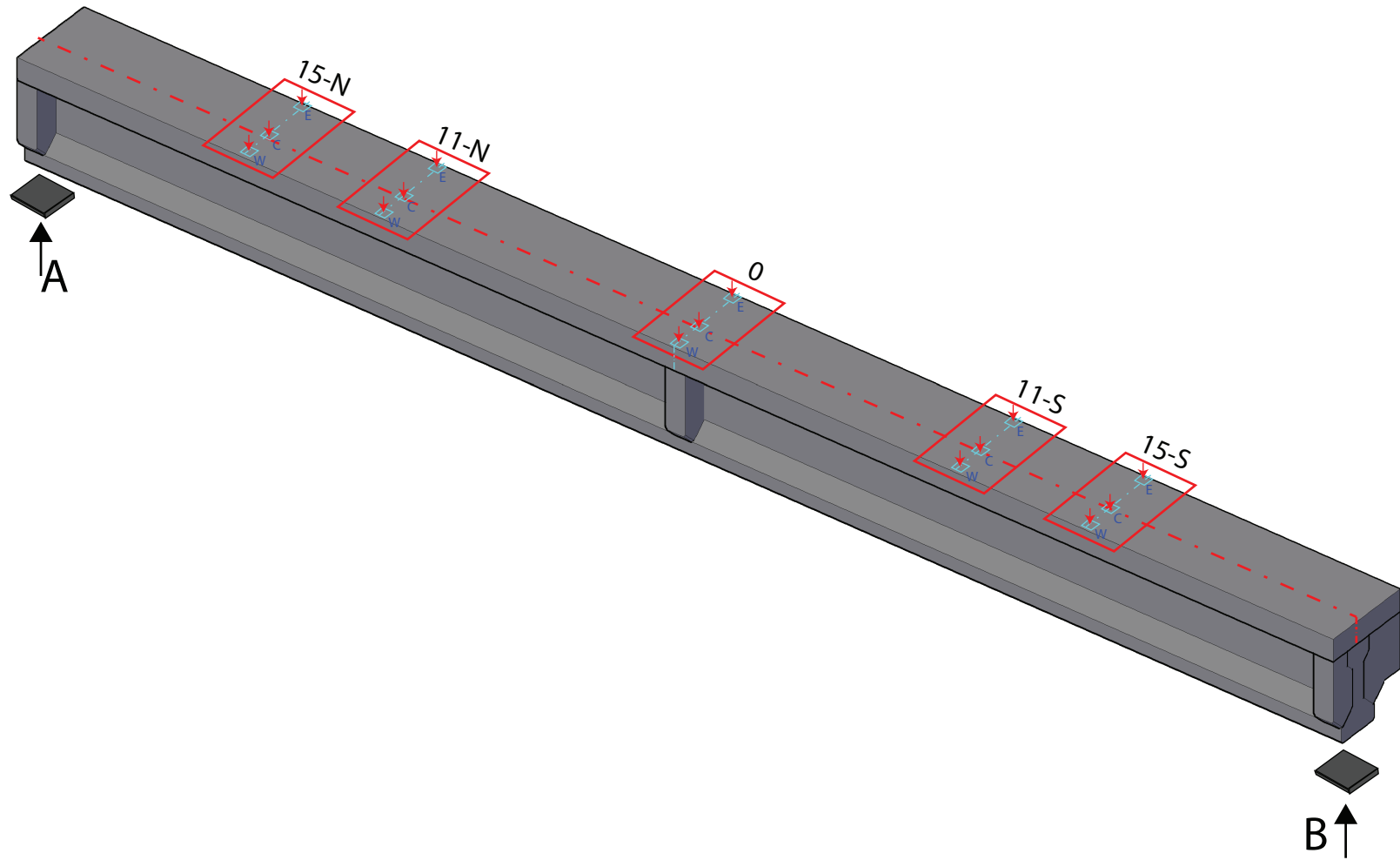


Figure 24: Prestressed girder impact locations



Figure 25: Top view of the prestressed concrete surface sanded and labeled with impact locations and side view of sensor layout: (a) Impact 15N, (b) Impact 11N, (c) Impact 0, (d) Impact 11S, (e) Impact 15S, (f) Sensor at 22.5N, (g) Sensors at 15N, (h) Sensors at 4N, (i) Sensors at 0, (j) Sensors at 11S, (k) Sensor at 22.5S

## 5 DATA PROCESSING

### 5.1 Overview

This study is heavily based on data analysis; therefore, the need for advanced processing tools is mandatory. The goal of this data processing is to better understand the behaviors of the specimens studied. For clarity, the research questions and approach are stated first and foremost.

#### 5.1.1 Research Questions

For this study, the main interests are geared towards studying the dynamic free vibration behaviors of the tested prestressed concrete girder and the masonry wall specimens. The research questions are as follows:

Question 1 What are the fundamental frequencies for Girder C and the masonry wall specimens?

Question 2 What is the nature of the mode shapes corresponding to the two specimens' fundamental frequencies?

Question 3 How does the fundamental frequency vary for the masonry wall through the different damage states?

Question 4 How are the results of the gentle impacts compared with those normal impacts for the masonry wall?

Questions 1 and 2 are not quiet straightforward given the asymmetrical cross section of Girder C, to begin with. Therefore, a procedure is generated to determine the fundamental frequency of the specimen from its SDOF response and verify it

by checking its existence in other degrees of freedom (DOFs). A similar procedure is conducted for the masonry wall specimen.

### **5.1.2 Research Approach**

As a reminder, the specimens were tested for free vibration and to be analyzed as single degree-of-freedom (SDOF) systems. To satisfy the fact that structures naturally have infinite number of DOFs, other DOFs shown up in the selected low mode free vibration response will be checked. By doing so, the author can draw some meaningful conclusions concerning the linear responses of these structural systems.

For the purpose of properly answering the research questions, three types of plotted figures are utilized.

#### **Acceleration-time history plot:**

This is a time-domain plot that displays the measured absolute or calculated relative acceleration of the specimen within various time windows of interest. The longest time window is the original recorded time window, where the response of the specimen can be visualized before, during and after the excitation force was initially applied and until the transient response completely dissipates. There are other acceleration-time history plots using other time windows as will be discussed in later sections.

#### **Power spectrum density (PSD) plots:**

This is a frequency-domain plot that presents the energy level of various frequencies corresponding to the time history that it uses to process. There will be two PSD plots utilized in this analysis for two time windows and will be discussed later.

### **Short-time Fourier transform (STFT) plot:**

STFT plot is a time-frequency domain plot that displays short-time averaged frequency of the response at various time instances. This plot is used to visually distinguish between the existence of forced and free vibration at different time instances and thus, free vibration where the low modes dominate can be separated from the forced vibration response of the recorded acceleration.

The research question is answered in three different analysis phases, where various steps are taken within certain phases.

#### **Phase I**

This phase involves all relative acceleration responses obtained from either of the two specimens. For each test, the recorded response in fact contains both forced and free vibration. The forced vibration, in this context, refers to vibration of the structure during the application of excitation. The duration is very brief; the process is very complicated. As it can be depicted on the STFT plots, it is the area of high energy levels. After the forced vibration, free vibration occurs and takes control of the rest of the response. The free vibration portion of the overall response is when the structure's motion is directly under by the impact force, but rather by an initial condition caused by the impact. The purpose of this phase is to separate the free vibration from the full response in order to extract the fundamental frequency. It is hard to tell when exactly the free vibration starts from the signal, but it is feasible to identify the portion of the free vibration when the fundamental frequency and a few other low modal frequencies dominate. This phase involves three steps as illustrated by Figure 26.

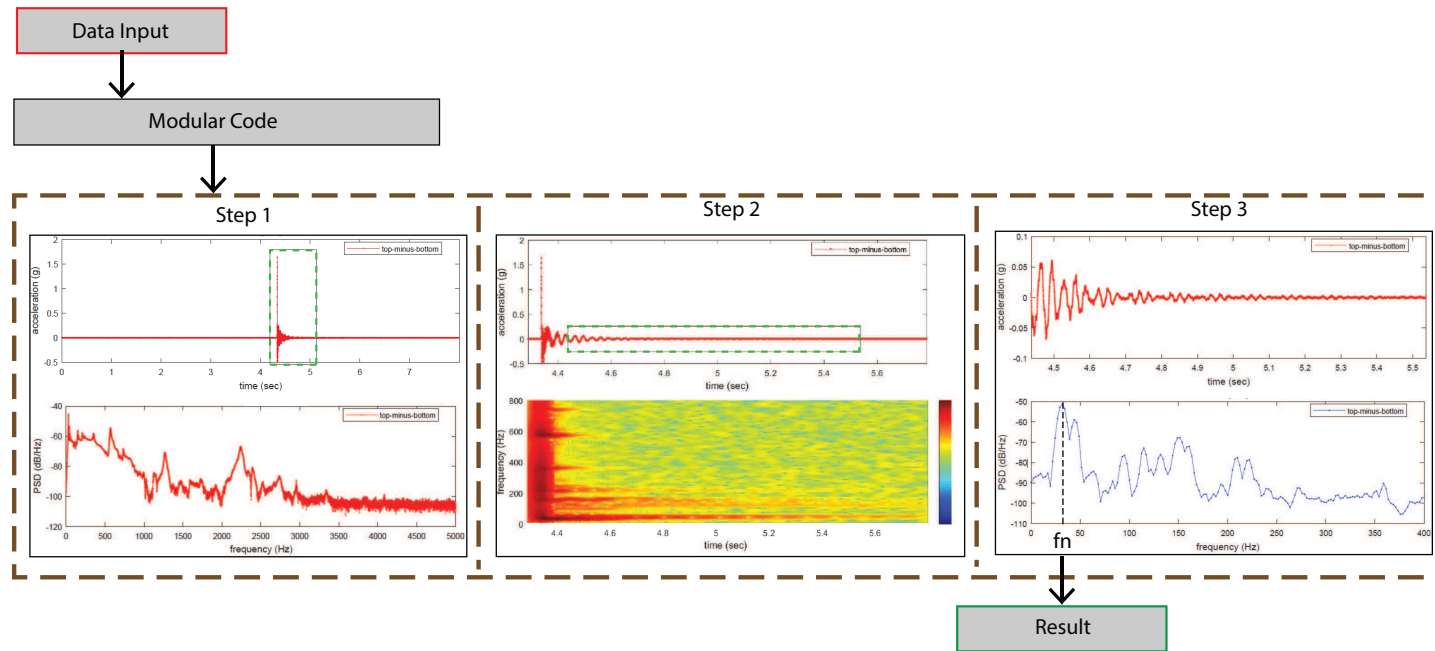


Figure 26: Illustrative summary of phase I steps: (a) show the plotted results: (a.i) full relative acceleration-time history of a particular test and its corresponding PSD plot, (a.ii) zoomed plot of the major response window drawn on plot a.1 and its corresponding STFT plot, and (a.iii) zoomed plot of free vibration window on a.ii and the corresponding PSD plot where fundamental frequency,  $f_n$ , is be obtained



Step 1 entails plotting the full time history that spans from the beginning to the end of the data acquisition duration. This step also involves plotting the frequency-domain (PSD) response for the full time history. The full time history displays all the information in a superficial manner while useful information is hidden inside. The useful information is the major response of the structure from the time of modal hammer impact till the end of its response. For the purpose of extracting the major response, a time window that is suspected to cover the major response is established; this window will be discussed in step 2 below. Step 1 is illustrated in the left panel of Figure 26.

Included in this step, is another short window created on the full time history prior to the application of excitation. This window is called **calibration time window** and is not plotted but is used in making the calibration for zero-g output. The output variable is used to create the zero-gravity acceleration baseline for all the plots in a particular test.

Step 2 involves the use of peak hammer force to detect the time of impact, and create a window ranging from shortly before the time instance of impact till a proper time instance when the majority of the response has dissipated. This time window captures the major acceleration time history and it includes both forced and free vibration responses. The need for separating the free from forced vibration requires not only looking at the acceleration time history but also looking at the STFT plot. STFT is a three dimensional plot and the three dimensions include time (displayed on the x-axis), frequency (displayed on the y axis) and frequency amplitude or energy levels (which occupies the z-axis but displayed using color contours). For the STFT plot, the hot colors signify intense energy levels while the cold colors show the presence of low energy levels (Tang [2015]). The STFT plot shows the distri-

bution of the energy levels through the major response in a time-frequency domain where the fundamental and a few low structural modal frequencies (as depicted by the horizontal peaks) will be revealed to be dominant after a certain time. This time is a sign of the end of the forced vibration response; thus, the free vibration window can be identified. This step is illustrated in the middle panel of Figure 26.

Step 3 involves plotting the free vibration window after it is identified in step 2. As illustrated in the right panel of Figure 26, this step plots both a time history and a PSD spectrum for the free vibration response. For the latter plot, the frequency axis limits are set to low range knowing that the specimen's fundamental frequency will not exceed this range based on the anticipated results computed in Section 3.3.

It is worth noting that these steps are conducted with no use of filtering, i.e., no distortion of the acquired data in the analysis.

In later sections, Step 1 figures will not be presented to avoid repetitiveness.

## Phase II

As illustrated in Figure 27, this phase involves three key analyses to conclude the fundamental frequency and the nature of its corresponding mode shape. Knowing that an intended in-plane excitation could produce both out-of-plane and torsional responses in addition to in-plane responses, in-plane bending (IPB), out-of-plane bending (OPB) and torsional (TOR) response analyses are conducted in this phase. In-plane bending refers to the vertical bending of the girder as demonstrated by the red deflected shape (labeled (1)) in Figure 27(a). Out-of-plane bending refers to the horizontal bending of the specimen as represented by the blue deflected shape (labeled (2)) on the same figure. Torsion refers to the free rotation of the specimen about the x-axis as illustrated by the green arrows (labeled (3)) on the same figure as well. The illustrations of the three motions in Figure 27 do not apply for the masonry wall specimen. Hence, the corresponding three motions for the masonry wall are illustrated as i, ii and iii in Figure 8(a). For each of the described motions, step 3 of phase I results are presented to extract the fundamental frequency. The frequencies obtained from this phase will be compared with the estimated fundamental frequencies of each respective specimen as presented in Section 3.3.

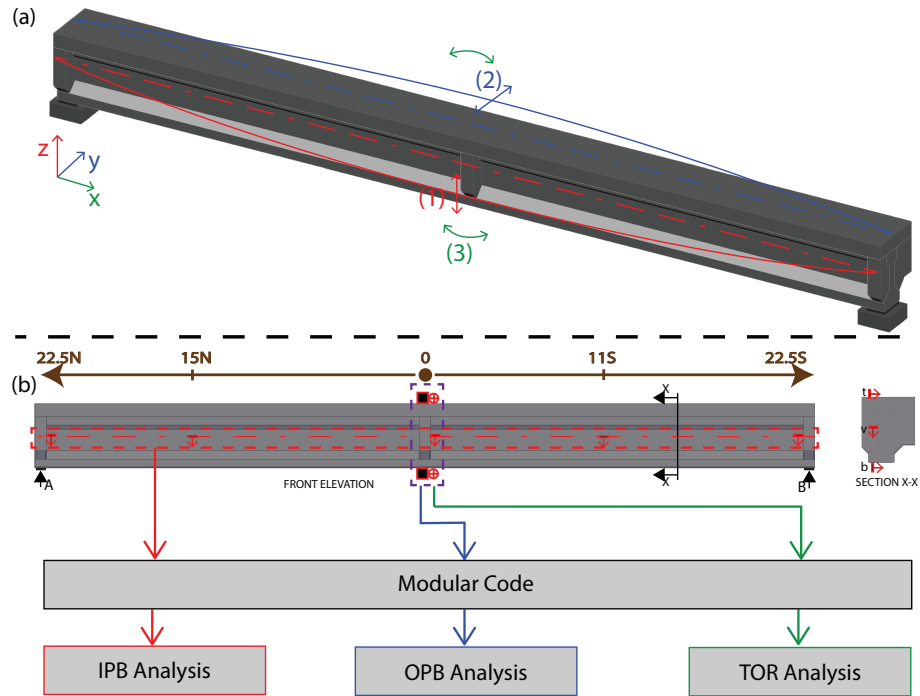


Figure 27: Illustrative summary of the Girder C's analysis procedure: (a) 3D Auto-CAD drawing of specimen showing (1) the in-plane bending deflected shape, (2) the out-of-plane bending deflected shape and (3) the torsional motion about the x-axis of the specimen, (b) showing the sensors of focus for each of the response analyses.

**In-plane bending (IPB) analysis** involves extracting the fundamental frequency from the relative responses of some combinations of the available in-plane sensors. The extraction of fundamental frequencies from each combination is conducted using the procedures in phase I. Given the rough estimations in Section 3.3, this analysis next involves verifying that all the analyzed responses with the same fundamental frequency are in phase to confirm that they belong to the first mode. As it can be seen in Figure 27(b), the in-plane bending involves the accelerometers at locations 15N, 0 and 11S. If these three locations share the same fundamental frequency and are in phase, then it can be justified that the frequency obtained is indeed the fundamental frequency

which corresponds to the first mode. An analysis following a similar concept will be conducted for the masonry wall as well. Note that the author computed the estimated fundamental torsional frequencies for both specimens in Section 3.3 to rule out the possibility of torsion.

**Out-of-plane bending (OPB) analysis** involves checking the presence of the fundamental frequency obtained from the IPB analysis in the out-of-plane response. This is to verify the existence of out-of-plane bending in the first mode, which is a possible observation given the asymmetrical cross section of the girder. If the existence of the fundamental frequency in OPB response is not confirmed, then conclusion can be made that the first mode obtained from IPB is purely in-plane. Otherwise, it is not purely in-plane.

**Torsional (TOR) analysis** also involves checking the presence of the fundamental frequency obtained from the IPB analysis in the torsional response. Again, due to the asymmetrical cross section of the girder, the existence of torsion in the first mode is a possible observation. The same conclusion as the one made for the OPB can be made here if the fundamental frequency is observed in the TOR response.

### **Phase III**

This phase is only applicable to the masonry wall specimen. It involves extracting the fundamental frequencies of the specimen through the different damage states and comparing them. This comparison leads to a better understanding of the change in the fundamental frequency of a structure at different damage states. This will be relevant to structural health monitoring (SHM).

For the masonry wall specimen, this phase is built on phase I and II. First, phase I is utilized to determine the fundamental frequency at an elastic state. Secondly,

phase II procedures are utilized to verify that the fundamental frequency is purely in-plane, or not. Finally, phase III studies the change in the fundamental frequency through its damage states.

## **5.2 Results and Analysis: Prestressed Concrete Girder**

This section presents representative results obtained from all the tests conducted on Girder C. For clarity in presentation, one particular hammer impact at mid-span (i.e. location 0) will be used to start with (see Sections 5.2.2 and 5.2.4). Results from other hammer locations will be presented afterwards (see Section 5.2.5). The meaningful results of this section are only expected to surface through phases II and III analyses. Hence to avoid repetition, results for phase I are only presented for the mid-span relative response when the specimen was excited at the mid-span impact location.

### **5.2.1 Sensor layout**

Figure 28 shows the locations of sensors whose measurements are utilized in this section. The presence of electrical noise was a limitation in using one of the in-plane sensors for this analysis; thus, it was excluded from this analysis. This sensor with a higher noise level was located 4 ft from the mid span toward in the north direction during testing but is not included in Figure 28. Although other out-of-plane sensors were available at other locations, the focus of this study is directed towards mid-span. Supports' out-of-plane motions were not recorded due to limited number of available accelerometers; therefore relative out-of-plane bending and torsion are not utilized in this section.

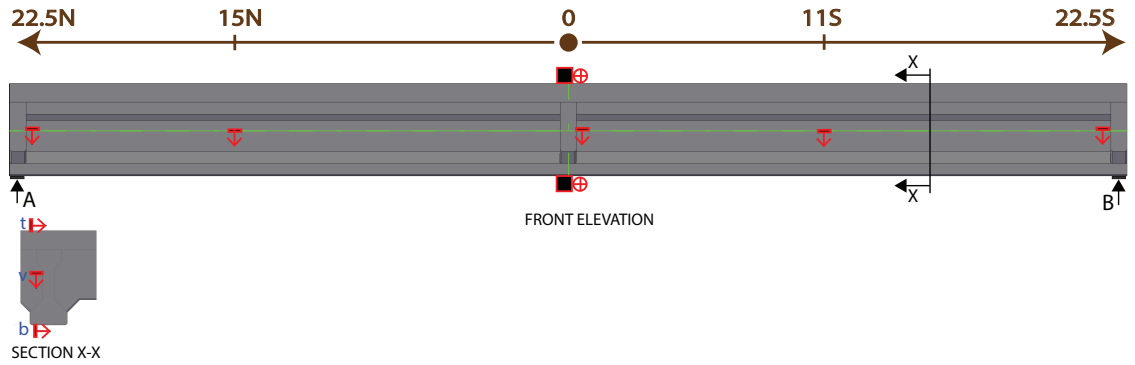


Figure 28: Girder C's sensor locations showing the positions of sensors only analyzed herein

Based on Section 3.3 the in-plane fundamental frequency for Girder C is estimated to be around 11 Hz. This estimated value and the mode shape are to be verified using phases I and II procedures described in Section 5.1.2.

## 5.2.2 Phase I demonstrated using mid-span impact

The three steps in phase I are applied to the analysis of Girder C. As a demonstration, the mid-span impact location is utilized to analyze the recorded response at mid-span relative to the supports. For this specific test, attention is given to the sensor combination of those at locations 0, 22.5N and 22.5S, which represent mid-span, north-end support and south-end support, respectively.

In step 1, full time histories and the corresponding PSD plots are given in Figures 29 and 30, respectively. In each figure, the absolute motions presented for the mid-span and supports in-plane motions are plotted together on the first panel, while the second panel plots a relative in-plane response at mid-span.

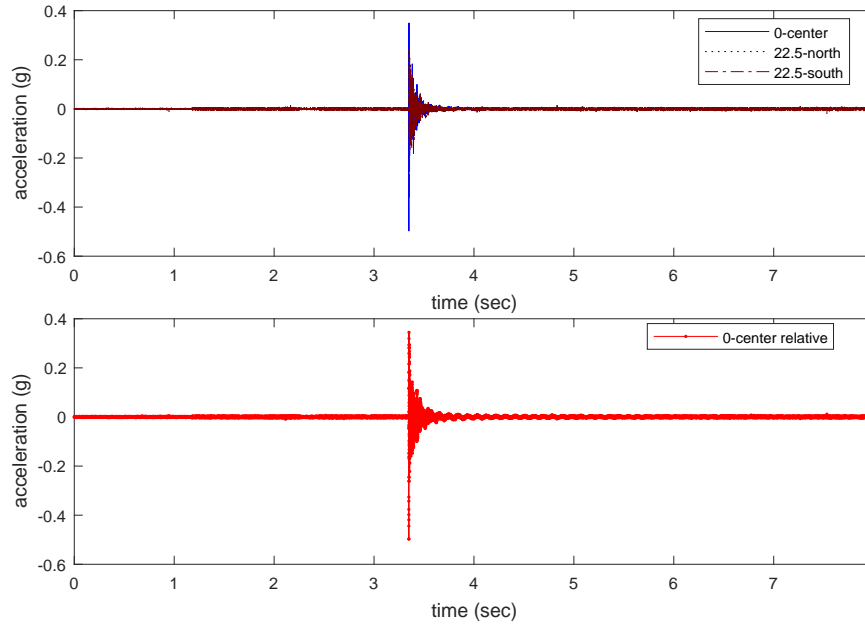


Figure 29: Full in-plane absolute acceleration responses for Girder C at locations 22.5N, 0 and 22.5S (i.e., mid-span and supports), as well as the relative acceleration when specimen was excited at location 0 (i.e., mid-span) - center

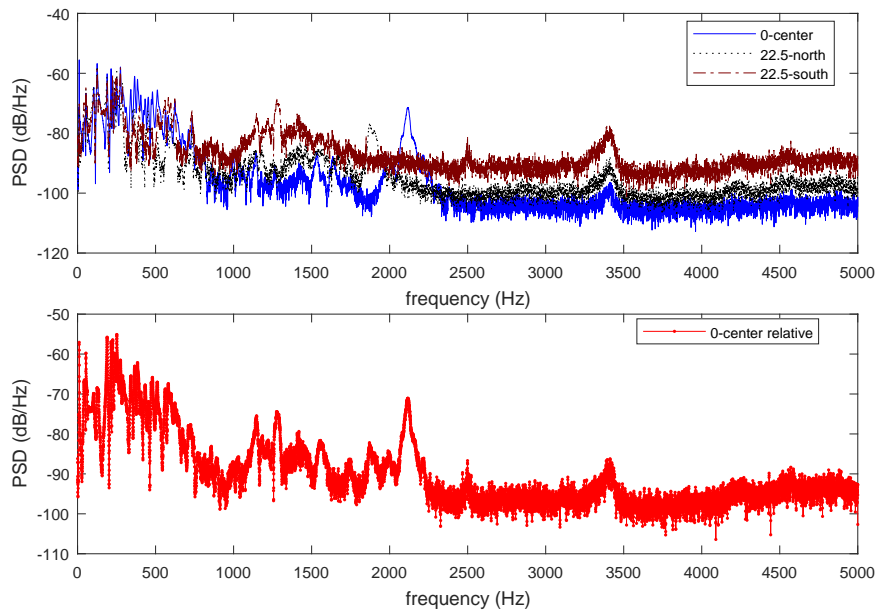


Figure 30: PSD for the response presented in Figure 29

Step 2 is represented by Figure 31 where the major response of the relative mo-



tion is plotted in terms of both time history and STFT response. Using this figure, the author comes up with a “free vibration window” to continue with Step 3. As it can be seen in Figure 31, the free vibration window (i.e. the box drawn on the acceleration time history) corresponds to the portion of the STFT plot where most of the dense energy levels have dissipated and the controlling modal frequencies can be seen as horizontal peaks.

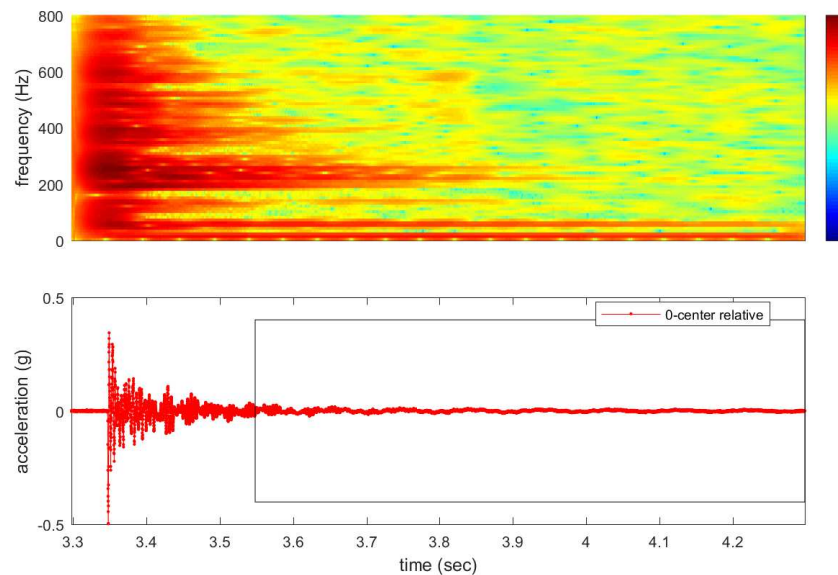


Figure 31: Truncated in-plane relative acceleration response for Girder C at mid-span as well as the STFT plot when specimen was excited at mid-span - center

Step 3, as shown in Figure 32, first presents the identified free vibration response of the relative acceleration. For this portion of the acceleration time history, PSD is performed one more time to extract meaningful structural modal frequencies.

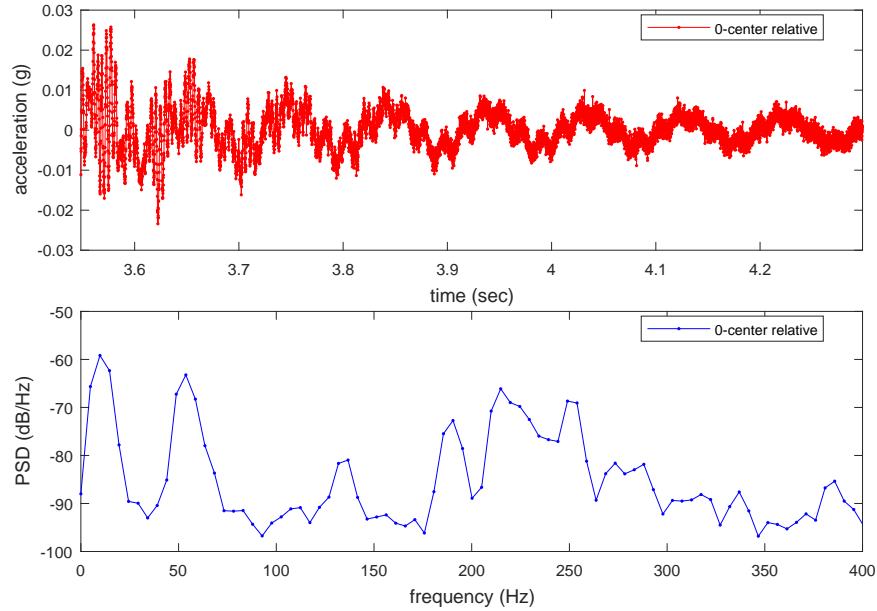


Figure 32: Further truncated response per window in Figure 31 and its truncated PSD spectrum

As it can be seen on the lower panel of Figure 32, the first peak appears to be 9.7656 Hz. This frequency is fairly close to the anticipated result; however, it is not enough to conclude that it is the fundamental frequency. Hence further analyses are to be conducted in Sections 5.2.4 and 5.2.5 to verify this. In addition, the resolution of the PSD plot will be discussed in Section 5.5.3.

### 5.2.3 Governing equations for Girder C relative responses

All relative responses are obtained after correcting the rigid body motion. The interest of this study is in analyzing elastic deformation; thus correcting rigid body motion is necessary. Hence, the need for defining the proper equations for the relative plots with rigid body motion corrections is the key. The rigid body motion includes both translational and rotational movements; thus a linear relationship is assumed. Figure 33 is a trapezoidal approach for doing this correction.

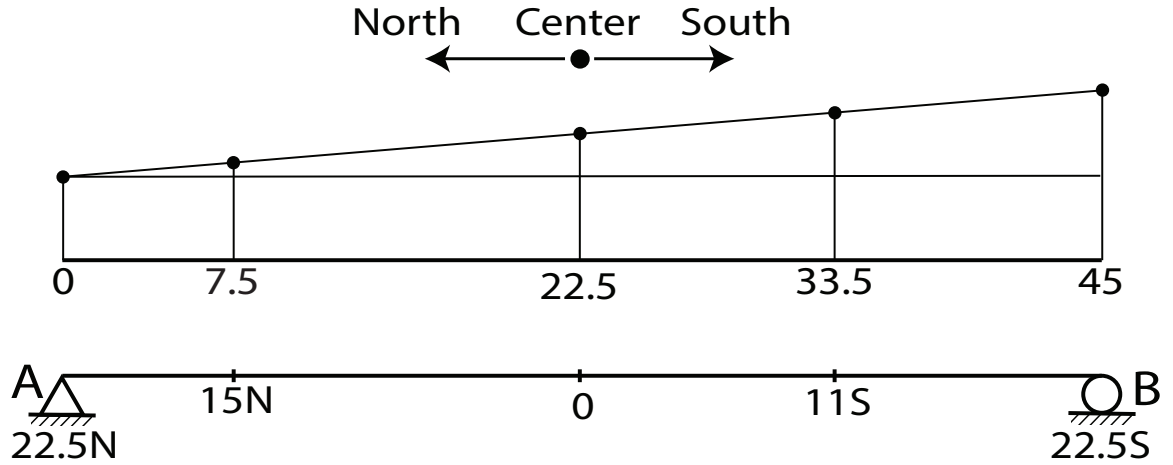


Figure 33: Demonstration of the rigid body motion at various sensor locations induced by support movement; a linear relationship is given by the trapezoid shown here

By using Figure 33, the following equations are obtained. **Note:** The “v”, “t” and “b” refer to vertical, top and bottom, respectively, and imply the transverse location and/or directions of measurements of the sensors at the specified coordinate on the beam as presented in Figure 28. Also the notations “rel” and “abs” refer to the relative and absolute accelerations, respectively. IPB, OPB and TOR refer to in-plane bending, out-of-plane bending and torsion as defined in Section 5.1.2.

### Girder C governing in-plane acceleration equation

$$\ddot{u}_{0,IPB(rel)} = \ddot{u}_{0,v(abs)} - \frac{\ddot{u}_{A,v} + \ddot{u}_{B,v}}{2} \quad (5.1)$$

$$\ddot{u}_{15N,IPB(rel)} = \ddot{u}_{15N,v(abs)} - \left( \ddot{u}_{A,v} + \frac{7.5}{45} (\ddot{u}_{B,v} - \ddot{u}_{A,v}) \right) \quad (5.2)$$

$$\ddot{u}_{11S,IPB(rel)} = \ddot{u}_{11S,v(abs)} - \left( \ddot{u}_{A,v} + \frac{33.5}{45} (\ddot{u}_{B,v} - \ddot{u}_{A,v}) \right) \quad (5.3)$$

For the following governing equations, support motion was not recorded; thus rigid body motion correction cannot be conducted.

#### **Girder C governing out-of-plane acceleration equation**

$$\ddot{u}_{0,OPB} = \frac{\ddot{u}_{0,t(abs)} + \ddot{u}_{0,b(abs)}}{2} \quad (5.4)$$

#### **Girder C governing torsional acceleration equation**

$$\ddot{u}_{0,TOR} = \ddot{u}_{0,t(abs)} - \ddot{u}_{0,b(abs)} \quad (5.5)$$

### **5.2.4 Phase II demonstrated using mid-span**

The purpose of this phase is to conduct analysis on the fundamental frequency of the structure. The goal is to verify that the fundamental frequency obtained in phase I can be characterized as purely for in-plane bending. First mode shape is assumed to begin with. For the mid-span impact location, all three motions: in-plane bending, out-of-plane bending and torsional analyses, are studied, as initially outlined in Section 5.1.2.

**In-plane bending (IPB) analysis** involves analyzing the in-plane motions. Girder C was tested with boundary conditions mimicking a simply supported beam. Therefore, its first mode shape is assumed to be represented by Figure 34b - as a great deal of simplification by neglecting the asymmetrical cross-section.

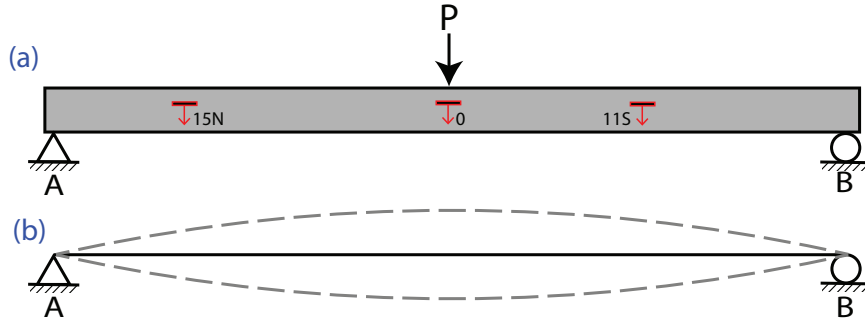


Figure 34: A schematic to show: (a) the locations of the three in-plane sensors and center hammer impact location and (b) the first harmonic mode shape for Girder C

Based on pure in-plane assumptions, an excitation applied at mid-span will only excite the first mode. This analysis entails plotting relative time histories from the in-plane accelerations responses on a single panel. Sensors 15N, 0 and 11S as shown in Figure 34a are used for this analysis. The three corresponding PSD responses are also plotted on a separate panel. The goal is to observe that the three responses share the same fundamental frequency and that the accelerations time histories are in phase assuming that the first mode shape shown in Figure 34b will dominate. The resulting plots for the IPB analysis are presented in Figure 35.

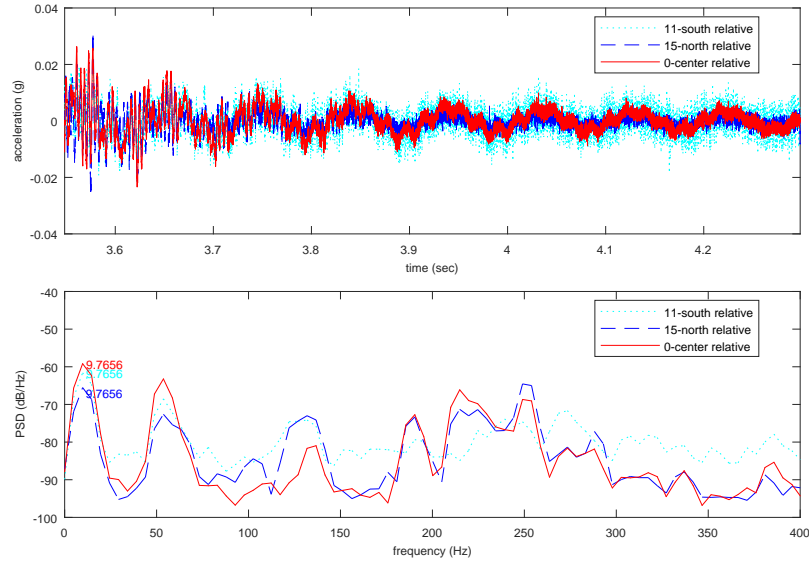


Figure 35: Girder C's phase II analysis for in-plane responses at locations 15N, mid-span and 11S when excitation force was applied at mid-span

The point of this analysis is to check the purity of the in-plane first mode. From Figure 35, it can be said that the dominating frequency for all of the three in-plane responses is 9.7656 Hz (the first peak on the lower panel). In addition to this observation, it can be observed on the upper panel that the three accelerations are in phase with a period of about 0.1s. This confirms that the fundamental frequency is 9.7656 Hz and is indeed first mode. This observation, however, does not confirm that the first mode observed in this analysis is purely for in-plane bending. Thus, out-of-plane bending and torsional responses will be analyzed to check the existence of the 9.7656 Hz frequency in their responses.

**Out-of-plane bending (OPB) and torsional (TOR) analyses** are lumped into one because there are not many sensor combinations for the two as there were in

the IPB analysis. In this analysis, both the out-of-plane bending and torsional motions are plotted on the same panels for both time and frequency domain analyses as presented in Figure 36. The responses for this analysis are only obtained at mid-span.

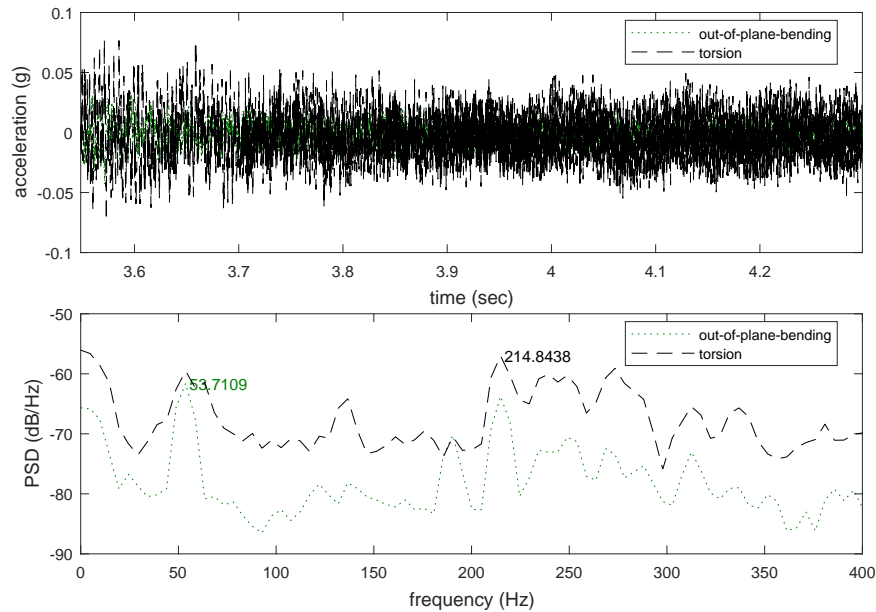


Figure 36: Girder C’s phase II analysis for out of plane and torsional responses at mid-span when excitation force was applied at mid-span

As it can be seen in Figure 36, the out-of-plane bending has its first frequency peak appearing at 53.71 Hz and there is no sign of the 9.7656 Hz frequency. The torsional response has its first small peak at 24.41 Hz and its dominating frequency at 53.71 Hz. There is no sign of the 9.7656 Hz frequency on the torsional motion either. The manifested out-of-plane bending frequency is very large compared to the estimated fundamental frequency of 5.97 Hz. For torsion, however, the experimental frequency is about 122% the estimated value.

These two observations give evidence that the in-plane response of the mid-

span impact location is dominated by a pure in-plane first mode with a fundamental frequency of 9.7656 Hz.

In order to verify that the purity of the fundamental frequency, this procedure is repeated for responses of locations 15N and 11S, as presented in Section 5.2.5.

## 5.2.5 Other phase II results and conclusion

### Phase II results for 15N and 11S impact locations

The phase II procedure conducted for Girder C's mid-span impact location demonstrated in Section 5.2.4 is repeated for 15N and 11S impact locations. The results are presented in Figures 37 through 40.

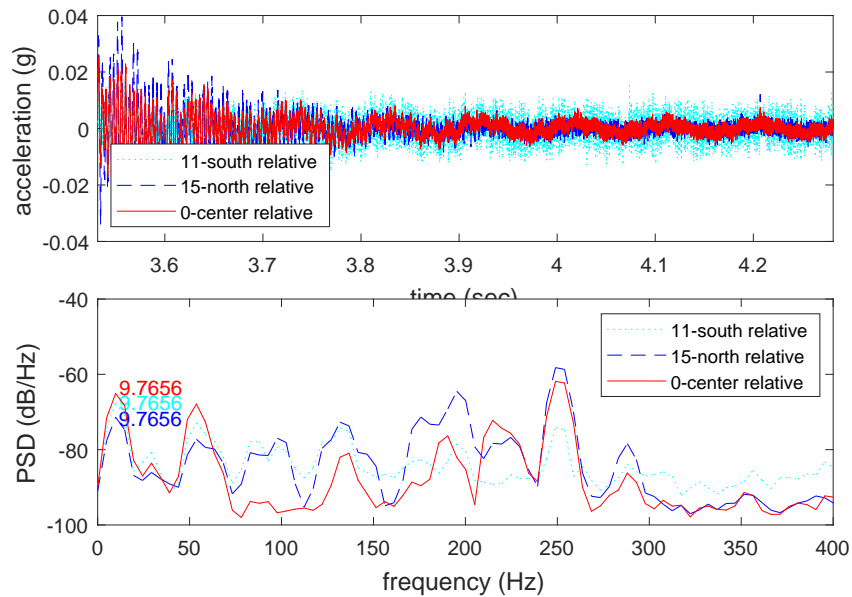


Figure 37: Girder C's phase II analysis for in-plane responses at locations 15N, mid-span and 11S when excitation force was applied at location 15N



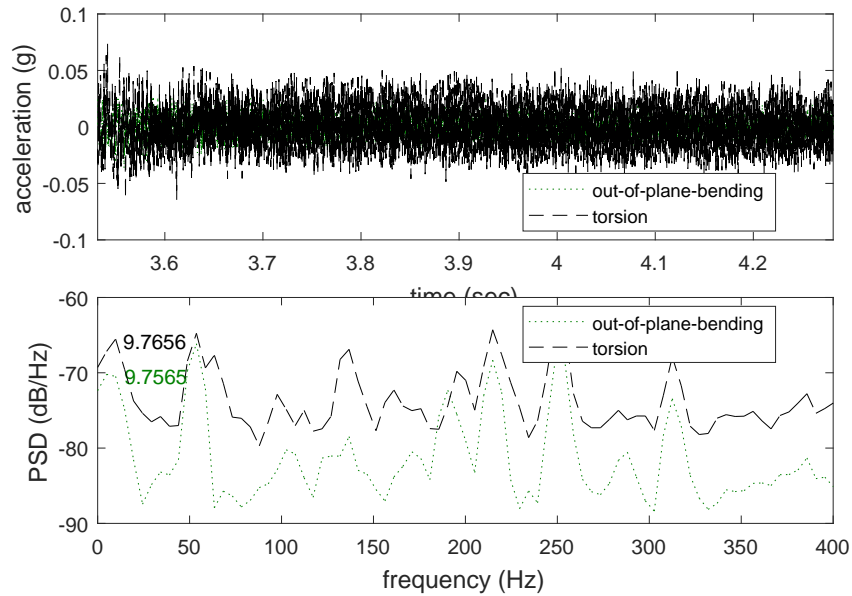


Figure 38: Girder C's phase II analysis for out of plane and torsional responses at mid-span when excitation force was applied at location 15N

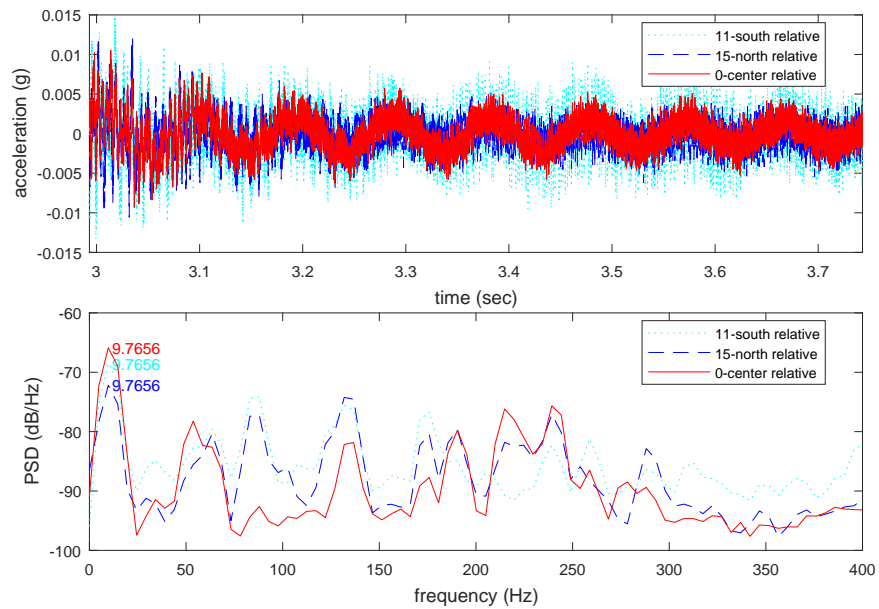


Figure 39: Girder C's phase II analysis for in-plane responses at locations 15N, mid-span and 11S when excitation force was applied at location 11S

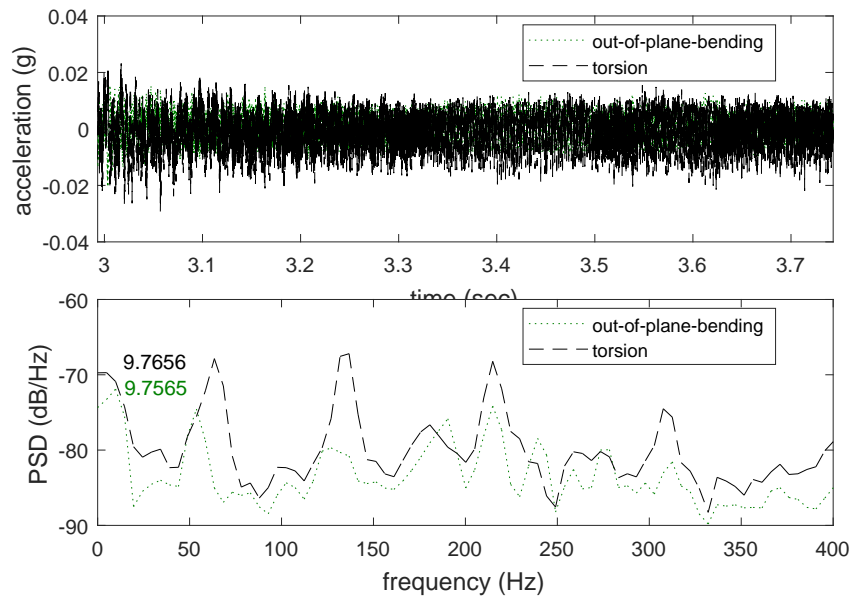


Figure 40: Girder C's phase II analysis for out of plane and torsional responses at mid-span when excitation force was applied at location 11S

In the figures presented above, it can be observed that the fundamental frequency is obvious on the IPB responses for all three sensor locations at both locations 15N and 11S impact locations – similar to the observation made on the mid-span impact results. The OPB and TOR responses for the two named impacts locations, however, indicate results that are different from what is observed for mid-span impact. There is indications of the 9.7656 Hz frequency on both OPB and TOR responses of the girder. This implies that first mode of the prestressed concrete girder is not purely for in-plane bending. It includes some out-of-plane bending and torsional motion. This is not a surprising observation given that the specimen is asymmetric and, therefore, its main flexural strength is not acting at its global centroid (i.e. centroid of the girder plus slab), rather, it is acting at the centroid of the girder only.

### 5.3 Results and Analysis: Masonry Wall

In this section, representative results for the masonry wall experiment are presented. During its modal hammer tests, the specimen was excited on seven locations as detailed in Figure 41. The analysis herein, however, focuses only on the in-plane impact locations *a* and *c* on the figure. Data from other impact locations may be used to conduct similar analysis later in Section 5.5.1 and in future studies.

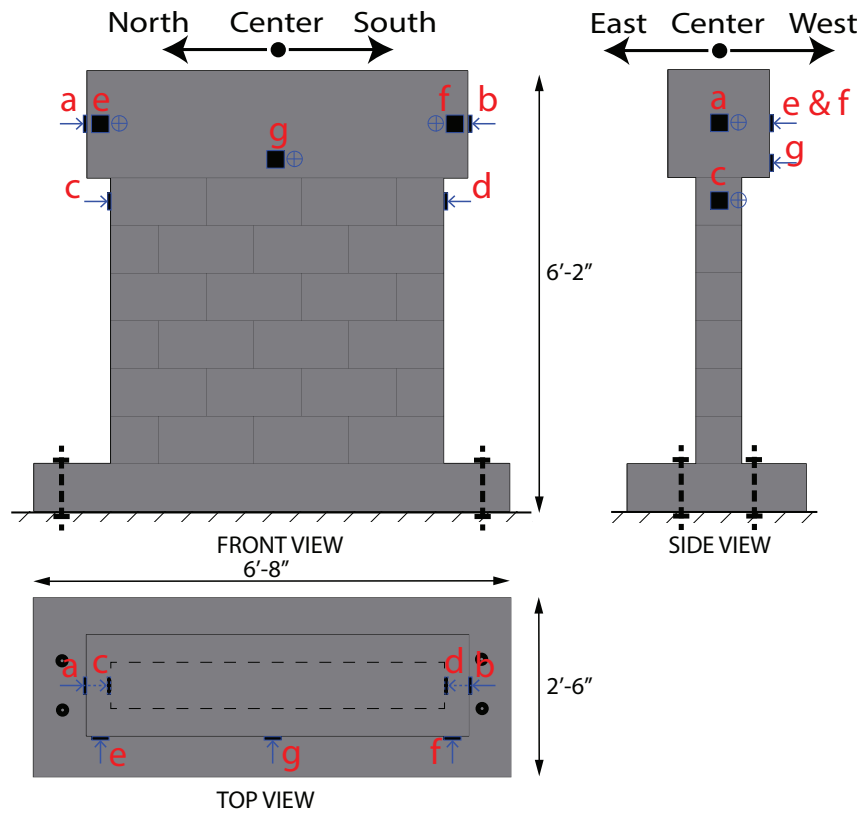


Figure 41: Details showing impact locations from a to g where the highlighted location a and c are the main focus in this section

The excitation force was applied with two intensities. Although these forces were applied using human control, which guarantees no accuracy in repeating the same force intensity, there were significant differences, on average, in the amount force between the two as intended. The intensities were named after *normal impact*

and *gentle impact* and their forces ranged from 2700 *lbf* to 3500 *lbf* and 900 *lbf* to 1200 *lbf*, respectively. More details will be given in Section 5.5.2.

Gentle impact was conducted for the purpose of studying its feasibility in the field of structural health monitoring (SHM). To be able to conduct a modal hammer test on a building with high occupancy (i.e. an apartment or an office building) by applying low enough impact force that will generate the least amount of disturbance (in terms of sound noise and vibration) and obtain the same result is the goal.

Most of the tests were carried out using the normal impact; however, the gentle impact was applied in a number of the tests. For the analyses in this section, comparison will be made between the results of the normal impact and gentle impact.

As mentioned in Section A.2 for the masonry wall specifically, intermittent modal hammer tests were conducted in between the static lateral loading cycles. Thus, it enabled dynamic analyses of the different damage states. This section eventually compares the specimen's fundamental frequencies obtained from every damage state and how they evolve. The motivation of this analysis is to verify the known structural damage by using the observed lowered fundamental frequency in the progressive damage of a structure.

### 5.3.1 Masonry wall setup

Figures 41 and 42 display the impact locations and accelerometer layout, respectively. The impact locations were designed to excite the specimen for different responses, such as in-plane bending, out-of-plane bending and torsion. The sensor layout was designed to allow the measurement of each of the responses mentioned above. Table 13 provides additional information to the sensor arrangement and details.

Although only in-plane impact locations (i.e. locations a and c) are analyzed in this section, the analysis will involve in-plane bending, out-of-plane bending and torsion, as conducted for Girder C.

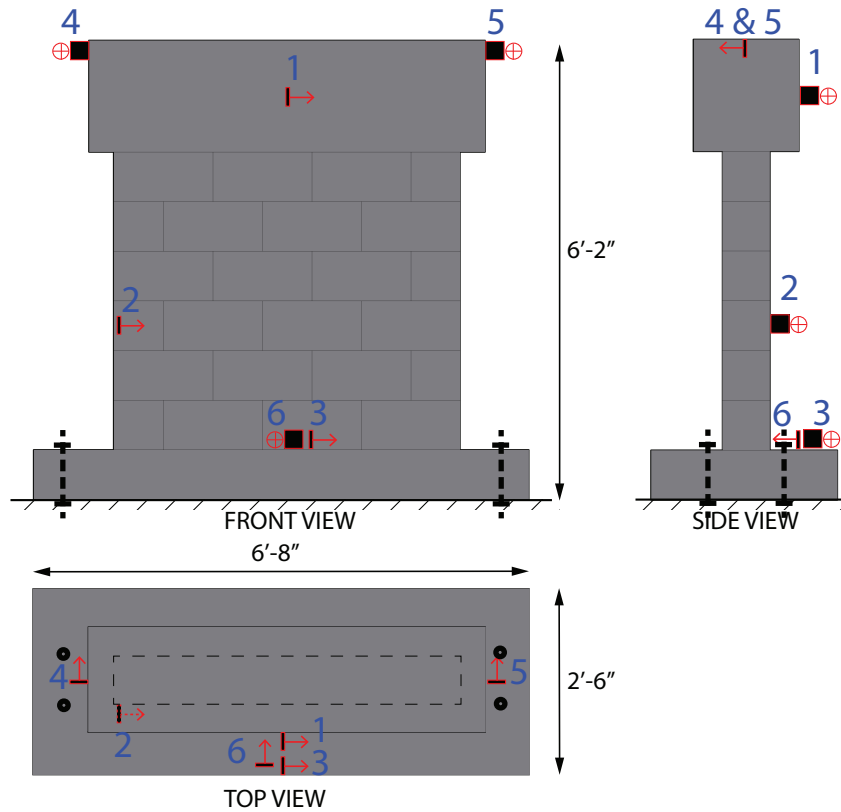


Figure 42: Details of the mounted sensor locations on the masonry wall, refer to Table 13 for the list of the corresponding sensor details

Table 13: Masonry wall list of sensors IDs, channel IDs and measured acceleration, †channel 1 reserved for hammer and channel 0 is not functioning

No.	Sensor ID	Allocated Channel †	Measured Acceleration
1	750	2	in-plane motion at the top
2	753	5	in-plane motion at mid-height
3	628	3	in-plane motion at the base
4	754	7	out-of-plane motion at the north end
5	627	6	out-of-plane motion at the south end
6	751	4	out-of-plane at the base

### 5.3.2 Governing equations for masonry wall relative responses

For all of the response analyses conducted for the masonry wall specimen, relative acceleration is used rather than absolute. For the purpose of data processing, Equations (5.1) to (5.9) are prepared for converting absolute accelerations into relative acceleration. Due to the limited number of properly functioning sensor channels on the DAQ system, only a single accelerometer was mounted to capture base in-plane motion. This resulted in a limitation of not being able to correct rotational rigid body motion. Thus, only translational motion correction is made. The subscripts used in the equations represent the designated sensor numbers according to Figure 42 and Table 13. The other subscripts carry the same meaning as previously defined in Section 5.2.3.

#### Masonry wall governing relative top in-plane acceleration equation

$$\ddot{u}_{1,IPB(rel)} = \ddot{u}_{1(abs)} - \ddot{u}_{3(abs)} \quad (5.6)$$

### Masonry wall governing relative mid-height in-plane acceleration equation

$$\ddot{u}_{2,IPB(rel)} = \ddot{u}_{2(abs)} - \ddot{u}_{3(abs)} \quad (5.7)$$

### Masonry wall governing relative out-of-plane acceleration equation

$$\ddot{u}_{OPB(rel)} = \frac{\ddot{u}_{4(abs)} + \ddot{u}_{5(abs)}}{2} - \ddot{u}_6 \quad (5.8)$$

### Masonry wall governing relative torsional acceleration equation

$$\ddot{u}_{TOR(rel)} = (\ddot{u}_{4(abs)} - \ddot{u}_{5(abs)}) - \ddot{u}_{6(abs)} \quad (5.9)$$

The masonry wall is analyzed in a similar manner as Girder C to identify the in-plane bending fundamental frequency first and foremost. This is necessary to eventually analyze different damage states. Both phases I and II are utilized just like for Girder C to obtain and confirm whether the fundamental frequency is purely for in-plane bending. Presentation of phase I for the masonry wall is skipped to avoid repetitiveness while phase II is demonstrated next:

#### 5.3.3 Phase II demonstrated using masonry wall

Similar to Girder C, in-plane bending (IPB), out-of-plane bending (OPB) and torsional (TOR) analyses are conducted for the masonry wall specimen.

**In-plane bending (IPB) analysis:** Discussions on different boundary conditions used in analyzing the IPB was given previously in Section 3.3. Figure 43 supports the two models adopted there. It is important to note that these models are nonetheless preliminary and must be improved in the future work, e.g.,

by considering the deep beam effect.

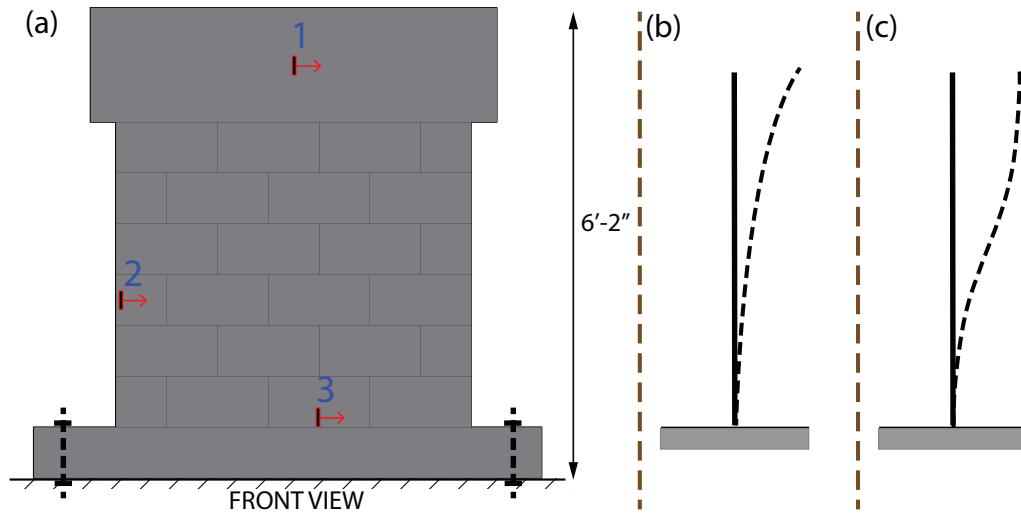


Figure 43: An illustration of the wall's bending and sidesway mode shapes in conjunction to the in-plane sensors: (a) Shows the wall with the three in-plane sensors, (b) shows the fundamental bending mode shape and (c) shows the fundamental sidesway mode shape

In IPB, the relative top and mid-height in-plane responses are plotted together to study the fundamental frequency and verify if they are in-phase. Figures 44 and 45 present the results of the IPB analysis when the specimen was excited with normal and gentle impacts, respectively.



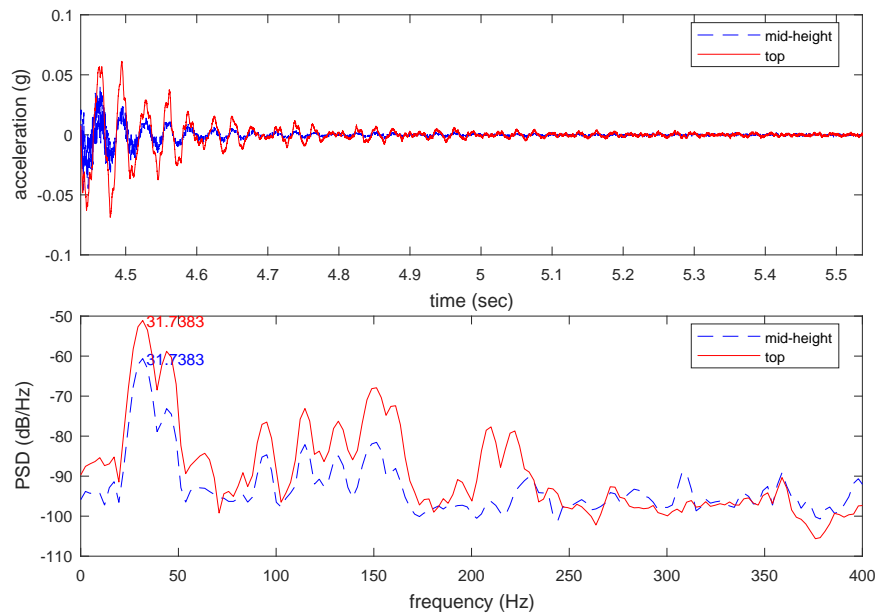


Figure 44: Phase II IPB results for masonry the masonry wall when normal impact was applied at location a

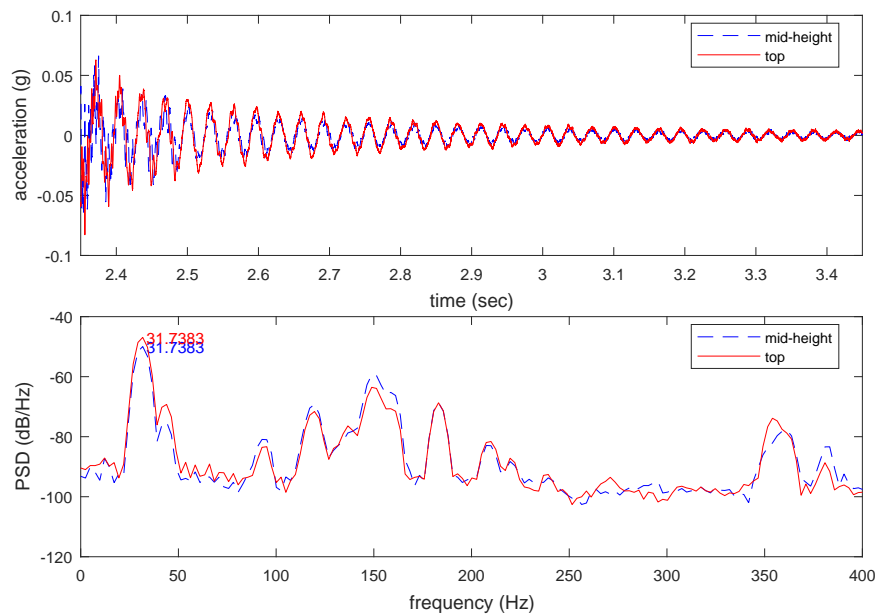


Figure 45: Phase II IPB results for the masonry wall when gentle impact was applied at location c

It can be seen in Figures 44 and 45 that both the mid-height and top responses for the masonry wall share an identical fundamental frequency of 31.74 Hz. The top and mid-height responses appear to be in phase, thus indicating that the first mode controls the response. This observation is made for results obtained from both the normal and gentle impacts. This frequency comparable to the estimated sidesway fundamental frequency of 34.44 Hz, thus showing that the sidesway mode controls in the in-plane response of the wall.

**Out-of-plane bending (OPB) and torsion (TOR) analyses:** Due to the section properties of the specimen and nature of the impact, out-of-plane bending and torsion are two responses expected to show even when the specimen was excited in-plane through its neutral axis. Since the excitation force was applied manually, despite the fact that the intended direction of force is in-plane through the neutral axis direction, human imperfections could have directed the force slightly out of plane. This, in addition to the fact that the specimen is inherently weaker in the out-of-plane, make a case for us to study the out-of-plane and torsional behaviors.

As before, OPB and TOR are presented in the same figure. The goal is to examine whether the fundamental frequency observed on the in-plane analysis is also observed on either out-of-plane bending or torsion. Figures 46 and 47 present the results of this analysis when the specimen was excited with normal and gentle impacts, respectively.

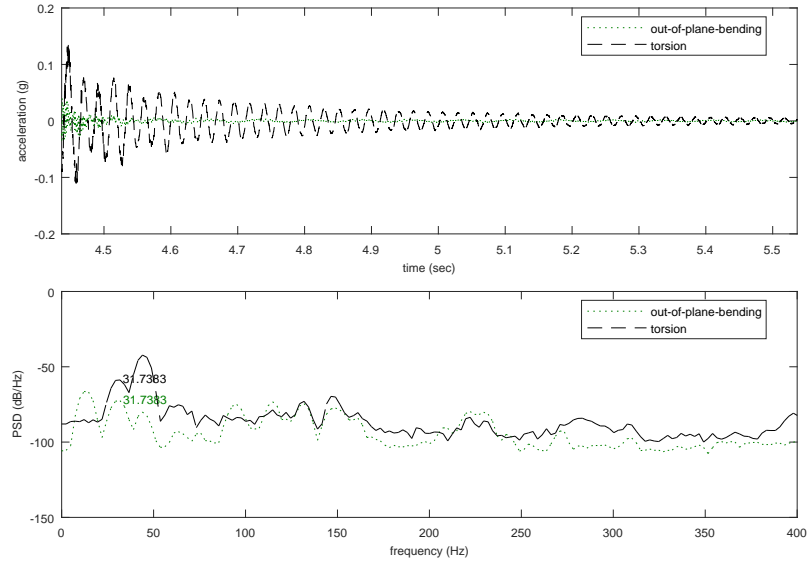


Figure 46: Phase II OPB and TOR results for the masonry wall when normal impact was applied at impact location a

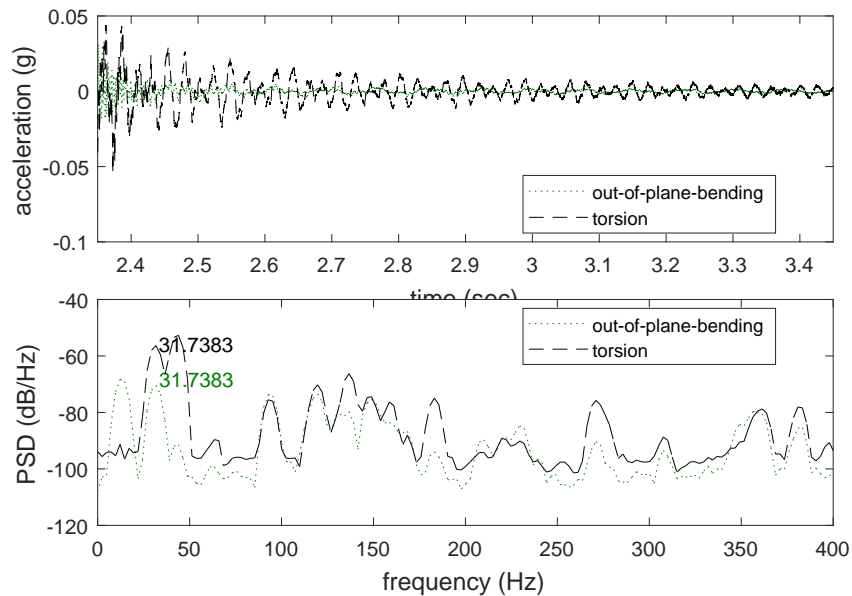


Figure 47: Phase II OPB and TOR results for the masonry wall when gentle impact was applied at impact location c

Figures 46 and 47 indicate the presence of the frequency, 31.74 Hz in the out-of-plane and torsional responses for both normal and gentle impacts. This observation implies that 31.74 Hz is not a pure in-plane frequency. In other words, the 31.74 Hz frequency is a combination of in-plane bending, out-of-plane bending and torsion.

### 5.3.4 Phase III demonstrated using masonry wall

The masonry wall was subjected to an incremental lateral pushover tests conducted by others – with the modal hammer tests conducted by the author fitted into every intersession. After five progressive lateral pushover loadings to failure, five different damage states were defined and illustrated in Figure 48 and described in Table 14. The purpose of phase III is to study the evolution of the

fundamental frequency of the wall at each damage state.

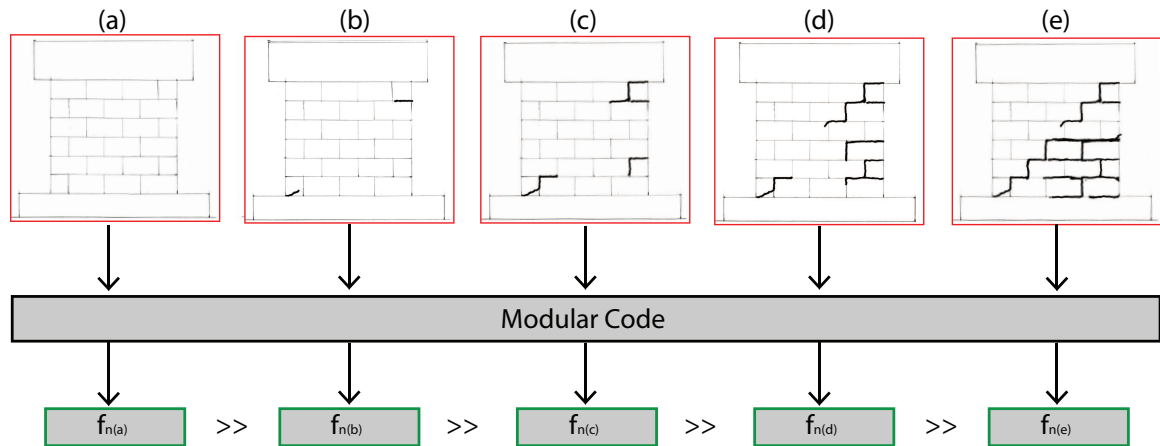


Figure 48: Phase III analysis illustration for the masonry wall with hand traced crack patterns that are based on the recorded ultimate crack pattern, see Table 14 for labeling description

**Note:** Although the crack pattern for all damage states are presented in Figure 48, only damage states (a), where there was no cracks, and (e), where all cracks had occurred, are confirmed. Panel (a) shows no cracks because it was during the elastic state and (e) represents the exact final crack pattern as recorded after ultimate loading. The crack patterns in between were not recorded during testing but are drawn for illustration purpose only.

Table 14: Damage states on the masonry wall specimen

Label	Damage State Nickname	Occurrence	Load, (kips)
(a)	Elastic	Prior to initial loading	4.03
(b)	First crack	After first crack	7.04
(c)	Post-crack	After further cracks	12.17
(d)	Post-crack 2	Before ultimate failure	17.08
(e)	Ultimate	After ultimate failure	20.14

Figure 48 displays an illustration of the processes involved in phase III analysis for the masonry wall and Table 14 presents brief description of each damage state. After the fundamental frequency of the specimen has been determined, the five different damage states are analyzed using their in-plane bending responses only. The modular code developed in this study (described in Section 5.4) was utilized for this analysis and all the previous analyses. It is anticipated that the fundamental frequency of the specimen will decrease after every damage state due to reduction of stiffness arising from increment in cracks. Figures 49 and 50 represent the results of phase III analysis for the normal and gentle impacts, respectively.

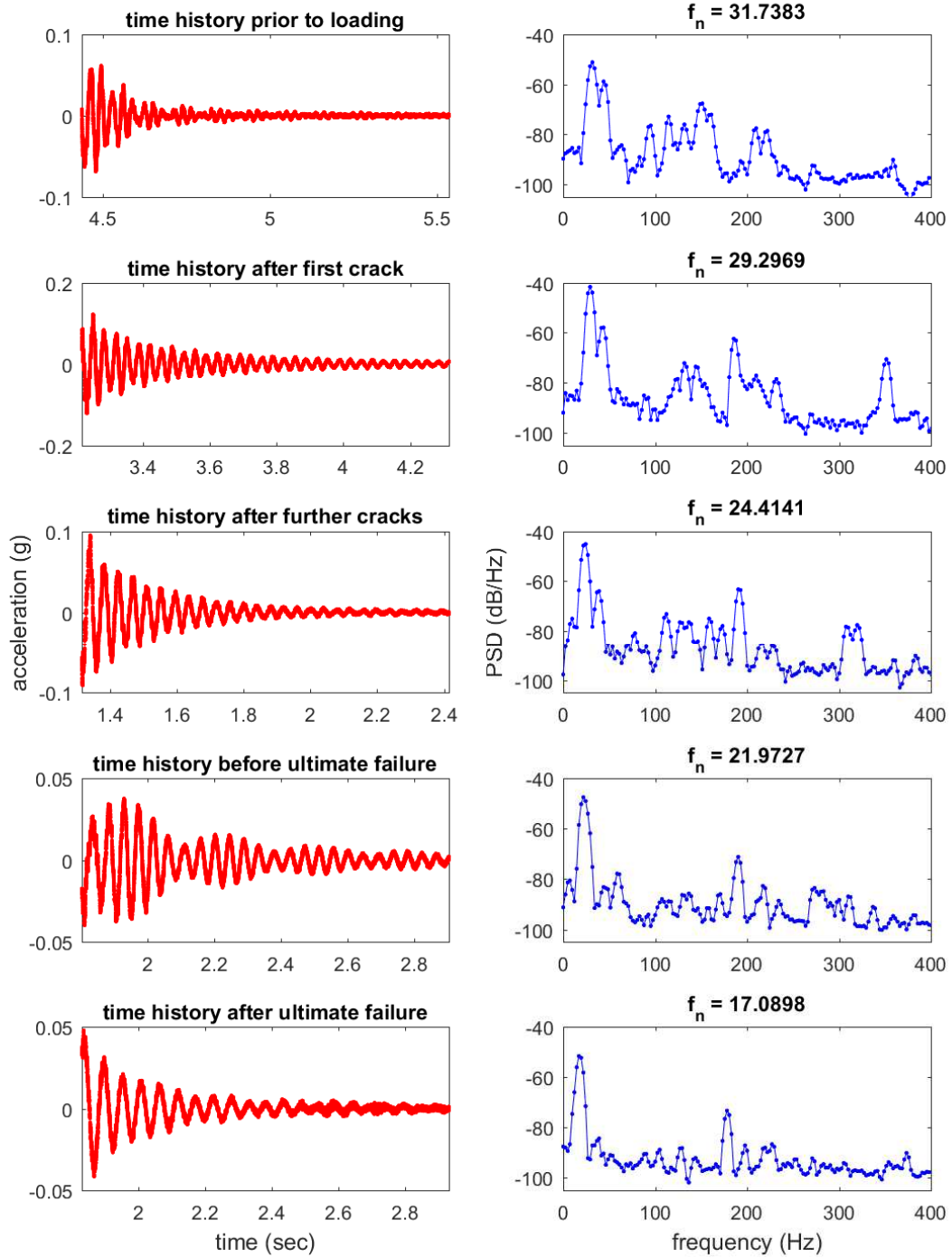


Figure 49: Summary of the masonry wall results at all five damage states when excitation force ranging from 2700 *lbf* to 3500 *lbf* (so-called normal impact) was applied

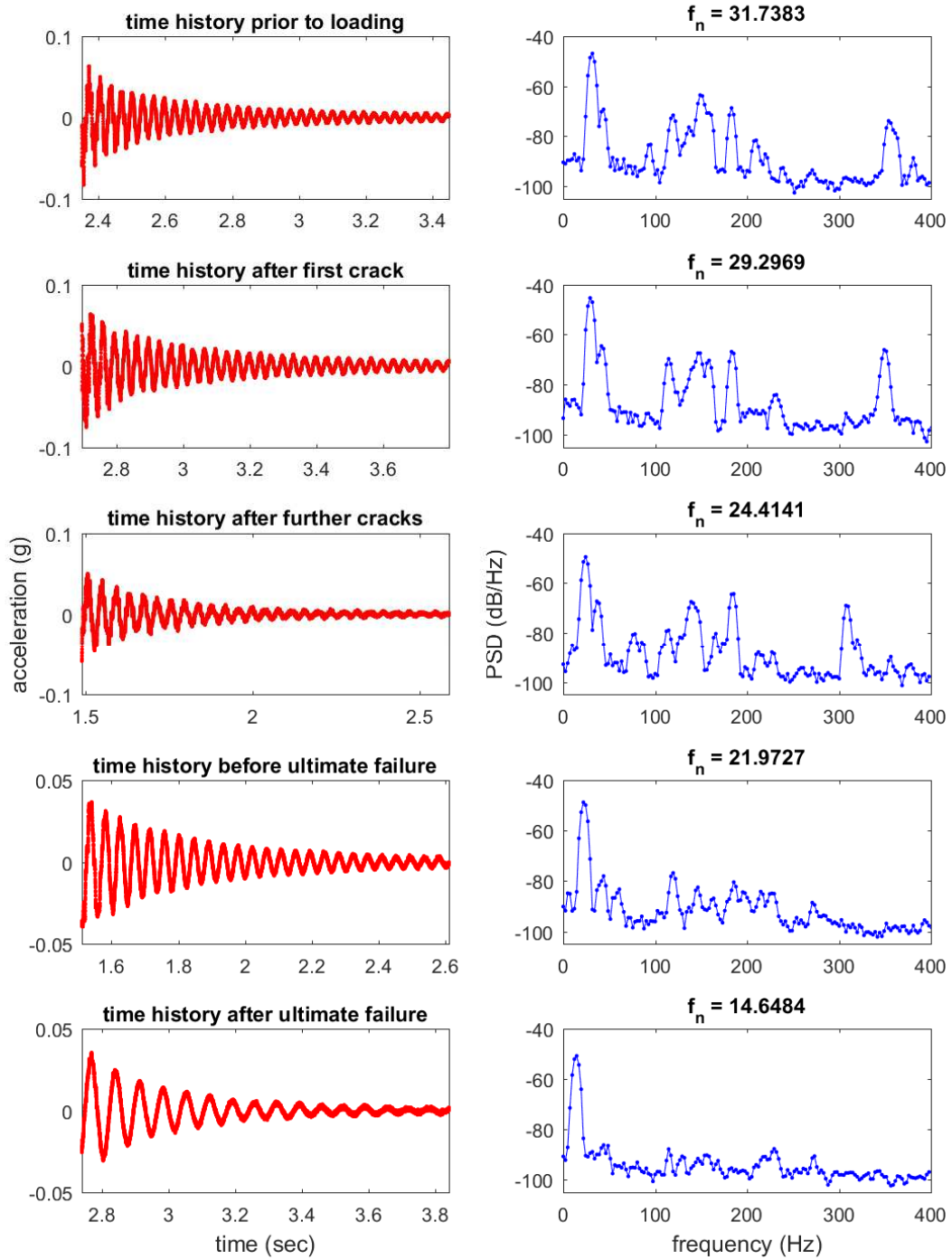


Figure 50: Summary of the masonry wall results at all five damage states when excitation force approximately ranging from 900 *lbf* to 1200 *lbf* (so-called gentle impact) was applied



Figures 49 and 50 indicate that the fundamental frequency of the wall has progressively decreases as the specimen's damage increased. The same observation is made regardless of the intensity of the excitation.

### 5.3.5 Masonry wall: Results conclusion

In this section, phases II and III results for the masonry wall were conducted. The masonry wall's fundamental frequency was determined to be 31.74 *Hz* according to phase II analysis, which turned out to be 92% of the anticipated fundamental frequency for sidesway and 136% of the anticipated fundamental frequency for the bending mode. This shows that the wall's deflected shape is relatable to sidesway rather than bending. The same analysis shows that the determined fundamental frequency is the first mode but not a purely in-plane first mode since it was observed to occur in the out-of-plane bending and torsional responses.

Comparison is made between normal and gentle impact intensities in this section as well. Generally, gentle impact averaged to be about one-third of the normal impact force magnitude. This is done to study the applicability of using gentle excitation, which causes less environmental noise and vibration than normal excitation, in SHM for damage detection. The results within the analysis scope of this study shows consistency between the two excitation intensities, except at ultimate failure – which, at that point the specimen is unpredictable. Thus, it can be said that gentle impact can be applied in SHM for damage detection as it has been.

An interesting observation made while comparing the results of normal and gentle impacts is that beating occurred on some of the results arising from the normal impact. This observation was not made on the gentle impacts, however. This observation is inconclusive within the scope of this study.

Another interesting observation made is the existence of another frequency in

the response, 43.95 Hz. This frequency was observed to fade away after a few damage states. This observation is inconclusive in this analysis.

## 5.4 Modular Code

### 5.4.1 Architecture

The modular code is developed using an automated interaction among a series of mfiles coded using MATLAB<sup>®</sup>. The code is prepared for use in this study and can be conveniently adapted for future study involving similar tests and collected data format. Figure 51 presents its architecture in its simplest form.

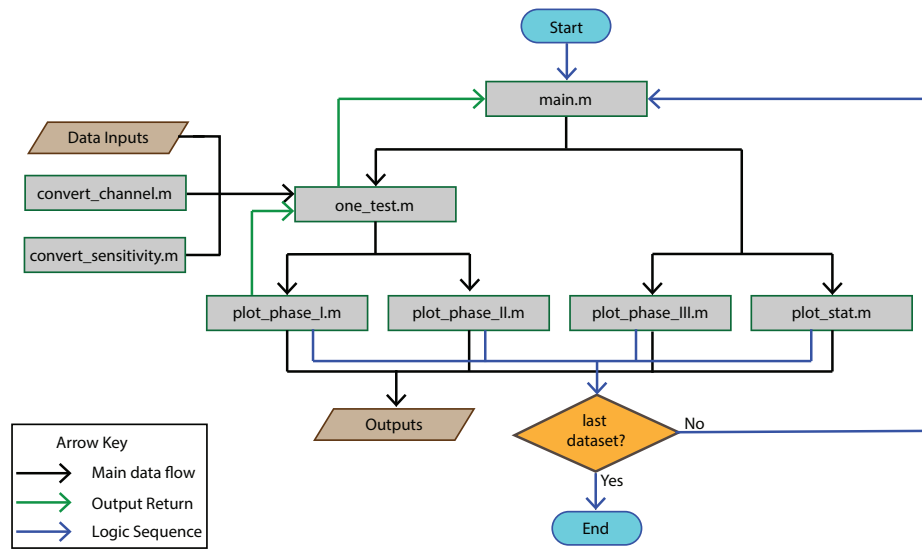


Figure 51: Flowchart showing the overall architecture of the modular code

The key purpose of this modular code is to conduct time-domain, frequency-domain and time-frequency domain analyses, generating acceleration time histories, PSD, and STFT plots, respectively.

The inputs to the entire modular code are the data inputs and supplemental quantitative inputs that are illustrated on the left side of Figure 51. The data inputs

are lvm files consisting of voltage outputs from the sensors that are sorted column-wise according to the DAQ's channel sequence. The supplemental inputs are the "convert\_channel" and "convert\_sensitivity" mfiles that are used to accommodate different sensor channel assignments and calibration values, respectively.

The outputs of the modular code are mainly plots and identified critical values as illustrated in phase I analysis overview, Figure 26, and are direct products of four different mfiles in the code.

The main processing flow of the code follows a tree shape with six mfiles interacting with each other in a hierarchy. The black arrows carry the main data flow, the blue arrows show logic sequences for the loop and the green arrows show the direction of output returns. The logic sequence, in this context refers to the sequence of the data sets as defined in the "main" file and looped to load the data for processing in the order in which they are defined. Output returns are utilized when a branch in the processing is desired and the outputs of a subsequent file is needed for the deviation. The different types of specimens are accommodated inside the "main" file and plotting functions through the use of switching. The individual mfiles are described in further detail in following section.

#### 5.4.2 Description of individual data processing files

**Channel Conversion file "convert\_channel.m"** converts the sensor IDs, i.e. hammer, 750, etc., into the actual analog channel ID corresponding to the hammer force and sensor reading, i.e. 1, 2, respectively, which will be used for data extraction purposes. Different specimens have different channel assignments; all assignments are programmed into this mfile under a switch function using specimen ID for selection.

**Sensitivity Conversion file “convert\_sensitivity.m”** calculates sensitivity value for each accelerometer so that the voltage outputs of the individual sensors can be later converted into an acceleration vector. +g and -g voltage readings obtained prior to each test are used in the calculation. The sensitivity, in conjunction with the zero-g value, will be used to convert voltage to acceleration by following the common practice of field calibration.

#### **Main file “main.m”**

- takes the specimen IDs as the inputs
- defines the test ID vector for each test using the specimen IDs
- defines the beginning and ending time instances for the major response windows (MRW) and the free vibration windows (FVW)
- calls one\_test.m in a loop that runs for each test
- calls plot\_phase\_III.m and plot\_stat.m for when applicable

#### **Plotting preliminaries file “one\_test.m”**

- calls both convert\_channel.m and convert\_sensitivity.m for hammer channel assignment and sensor sensitivity values, respectively
- plots the hammer data-time history for each test
- uses the MRW and FVW variables given in main.m in conjunction with the time instance of the peak hammer force occurrence to define time instances for the two named plotting windows to be drawn by subsequent files

- defines the calibration time window which would be used in conjunction with `convert_sensitivity.m` to obtain zero-g output values for calibration purpose
- calls `plot_phase.I.m` and `plot_phase.II.m` for the proper plotting commands to be executed

### **Phase I plotting file “plot\_phase.I.m”**

- calls both `convert_channel.m` and `convert_sensitivity.m` for collecting the accelerometer channel assignment and sensitivity value, respectively, of each involved accelerometer
- calculates the zero-g voltage values for all accelerometers used in each dataset by utilizing the calibration time window defined in `one_test.m`
- plots the full, truncated (i.e., main response) and further truncated (i.e., free vibration response) time histories for both absolute and relative accelerations
- plots PSD for the full and free vibration time histories
- plots STFT for the main response

**Phase II plotting file “plot\_phase.II.m”** generates figures such as the free vibration response and its corresponding PSD for phase II analysis, as the name implies.

**Phase III plotting file “plot\_phase.III.m”** generates figures such as the free vibration response and its corresponding PSD for the individual damage states in phase III analysis, as the name implies.

**Statistics plotting file “plot\_phase\_III.m”** plots a histogram for the impact hammer force magnitudes for a group of tests on one specimen.

Table 15 lists the inputs and outputs of each mfile in the modular code, while the following list offers a short descriptions of items in Table 15:

Table 15: Mfiles' inputs and outputs

<b>Mfile</b>	<b>Inputs</b>	<b>Outputs</b>
convert_channel.m	Specimen ID, and (2) Sensor ID	Channel IDs
convert_sensitivity.m	Specimen ID, and (2) Sensor ID	sensor sensitivity values estimated from the dataset
main.m	Specimen ID	(1) Test IDs, and (2) Truncation Variables
one_test.m	(1) Specimen ID; (2) Test IDs; (3) Sampling rate, and (4) Truncation Variables	(1) Loaded dataset; (2) Test IDs; (3) Time; (4) Time window, and (5) Calibration time window
plot_phase_I.m	(1) Specimen ID; (2) Sensor ID; (3) Title; (4) Test IDs; (5) Figure ID; (6) Time; (7) Time window; (8) Calibration time window; (9) Dataset; (10) Sampling rate; (11) Situation, and (12) Legend cell	(1) Time history plots (relative and absolute motions); (2) PSD plots, and (3) STFT plots
plot_phase_II.m	(1) Specimen ID; (2) Impact intensity; (3) Time; (4) Acceleration, and (6) Fundamental frequencies;	(1) further truncated time history, and (2) corresponding PSD plot
plot_stat.m	(1) Specimen ID, and (2) Impact force vector	Statistic plot for hammer forces from a collection of tests

### 5.4.3 Data processing inputs, outputs and their definitions

The modular code includes a number of inputs and outputs that may not be self-explanatory; therefore, their names, code representations and descriptions are presented below. The names in quotation are is the variable names as used in the modular code.

The identification (ID) strings are part of the inputs and given as follows:

**Specimen ID string “specimenID\_str”:** For the modular code to work for all specimens, this string is added as an input to run the files in a way that is tailored for each of the specimens using the switch command. Specimen IDs are GC, MW, TW and TJ, which represent Prestressed concrete girder (Girder C), masonry wall, timber wall and timber joints, respectively.

**Test ID “testID”:** With many datasets named distinctly for each specimens, the test ID variable is created in the main file (main.m) as a vector of strings that match the name of each of the datasets to be processed for data loading purpose. Test ID is a vector that contains all the IDs for the dataset to be analyzed. Each specimen has a defined test ID vector. The test ID templates and meanings for each character given in Tables 16, 17,18 and 19, for TW, GC, MW and TJ, respectively.

**Sensor ID “sensorID”:** As an input in the plotting file, this is a vector variable that includes the sensor IDs for all the sensors that would be involved in a particular data loading.

**Situation “situation”:** This is a scalar variable utilized to classify the different governing equations used to calculate relative acceleration. For example situation 1 in the plot\_phase.I.m file refers to the Girder C governing in-plane acceleration.



Other input and output items are as follows:

**Datasets:** These are the selected acceleration time histories analyzed by the modular code.

**Sampling rate “fs”:** This is a constant following the DAQ setting. All datasets in the experimental investigation of this study are acquired using a sampling rate of 10,000Hz. This is used in the modular code to imply that the input has a 10,000 data points per second.

**Maximum hammer force “hammer\_force\_vec”:** This is used as an input for the plot\_stat.m and it carries the maximum hammer forces for the individual tests collectively as a vector.

**Impact intensity switch “hit\_intensity\_switch”:** This is a scalar used in the plot\_phase\_III.m to switch between the two impact intensities.

**Impact intensity “impact\_intensity”:** This is a string input (i.e. “normal\_impact and gentle\_impact”) used in automating the title generation for the plots generated by plot\_phase\_III.m.

**Acceleration “accel”:** This is the acceleration time history used as an input in the plot\_phase\_III.m file.

**Fundamental frequency “fn”:** This is a fundamental frequency input variable used in the plot\_phase\_III.m file which is an output of one\_test.m.

Output plots are as follows:

**Acceleration time history plots:** Acceleration time histories - full, truncated, and further truncated are the outputs of Steps 1, 2, and 3 in Phase I respectively. Phases II and III output further truncated acceleration time histories

**Power spectral density (PSD) plots:** PSD plots are done by directly utilizing the MATLAB<sup>®</sup> built-in function called “pwelch”. The PSD plots are generated from Steps 1 and 3 of Phase I. The PSD plots are further used in Phase II with interested peak values annotated to the dominating frequencies for the a response. PSD plots are also used in phase III analysis in a similar manner as in phase II.

**Frequency (STFT) plots:** The plots are done by directly utilizing an mfile developed by (Tang [2015]), the STFT plots were generated for each of the zoomed plots to manifest areas of higher and lower energy levels using a multicolored frequency distribution. The STFT plots are generated from Step 2 of Phase I.

The following are for plotting input parameters:

**Figure ID number “figID\_num”:** This variable is used to automate the figure plotting and saving.

**Legend cell “legend\_cell”:** This is a column cell that facilitates the automation of figure saving and plotting with an adaptive legend block.

**Title strings “title\_str & title\_str\_”:** Similar to the test ID strings, these two strings are used to facilitate the automation of figure plotting and saving with the proper figure title in the figure and file name, respectively. The focus is given to the classification of IPB, OPB, and TOR.

**Test ID strings “testID\_str & testID\_str\_”:** These two variables facilitate the automation of figure plotting and saving with the proper figure title in the figure and file name, respectively. The focus is given to answering the question “which test is this figure from?”

All time variables utilized are as follows:

**Time “time”:** The time variable is a crucial part of the data processing, as it occupies the x-axis in all the acceleration history plots. This refers to the full time history thus is defined based on the size of the dataset. It represents the exact length of time that the dataset lasted during its acquisition.

**Truncation variables “MRW\_1, MRW\_2 FVW\_3 and FVW\_4”:** These are variables that define the beginning and ending time of the major response and free vibration windows that are required in Steps 2 and 3, respectively, under Phase I analysis. Although the window span should vary from test to test, a unified range is chosen for each specimen and used throughout the data processing for a specific specimen as a roughly automated process and verified by the author’s visual inspection.

**Major and free vibration time windows “time\_window” and “time\_window\_new”:** These two serve as time-windows for the major response and free vibration window that are required in Steps 2, and 3 under Phase I, respectively. .

**Calibration time window “time\_window\_calibration”:** This is a time window from the initial part of every input whose voltage is used as zero-g calibration. The acceleration within this time window is expected to be zero since there is no excitation force applied yet.

#### 5.4.4 Test nomenclature

Test data files were named in a manner that facilitates automation during their processing. The test names were utilized during loading of each of the datasets. The nomenclature used in processing and described in this section does not follow the

original nomenclature established during testing. Although the original names are still maintained by the original files, the names are modified for easier processing.

Each of the files are named according the corresponding specimen ID (i.e., GC, TW, etc.) as well as all the testing configuration in the form of numbers. This ensured distinction between the test names and that no particular test has the same name as a different test.

The timber wall specimen (TW) is the most complicated in terms of naming and labelling. Thus, Table 16 presents its ID system as the most comprehensive example. Similar tables for the remaining specimens can be found in Appendix B.1.

Table 16: Test IDs for Timber Wall (Test ID template = TWtest“a” “b” “c” “d”)

<b>TWtest</b>	<b>“a”</b>	<b>“b”</b>	<b>“c”</b>	<b>“d”</b>
<b>Representation</b>	Condition ID	Setup ID	Impact ID	Trial ID
<b>Range</b>	<b>0 - 5</b>	<b>0 - 2</b>	<b>1 - 7</b>	<b>1 - 3</b>
Number	0	0	1	1
Representation	elastic	no weight added	location a	first trial
Number	1	1	2	2
Representation	pre-yield	4 feet of 50plf section added	location b	second trial
Number	2	2	3	3
Representation	yield	8 feet of 50plf section added	location c	third trial
Number	3		4	
Representation	post yield		location d	
Number	4		5	
Representation	post yield 2		location e	
Number	5		6	
Representation	ultimate		location f	
Number			7	
Representation			location g	

## 5.5 Other Analysis

### 5.5.1 Masonry out-of-plane responses under out-of-plane impacts

Section 5.3 presents the responses generated from test setup when in-plane responses were anticipated for the masonry wall specimen. In this section, representative Phase II results of the wall after out-of-plane excitations are presented. Specifically, results from impact locations e, f and g (illustrated in Figure 41) during its elastic damage state. It is anticipated that impact locations e and f mainly excite torsional motions while location g mainly excites out-of-plane bending. The purpose of this analysis is to gain a better understanding of the out-of-plane bending and torsional behaviors of the wall when out of plane excitations are applied. The results obtained in this section will be compared with the estimated modal frequencies presented in Section 3.3.2. The results of one impact each at the three impact locations, e, f, and g, are presented in Figures 52 to and 54.

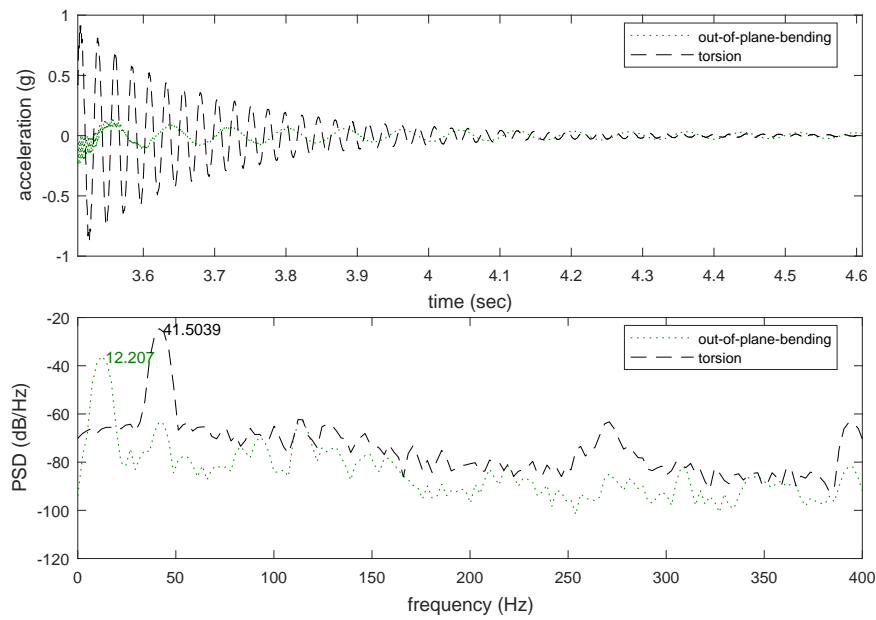


Figure 52: Phase II OPB and TOR results for the masonry wall when normal impact was applied at impact location e, when torsion was anticipated

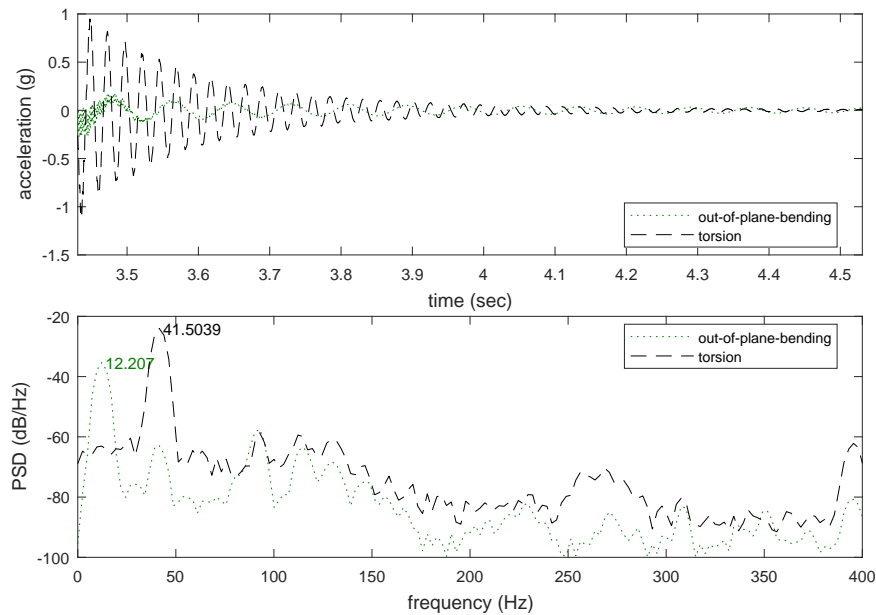


Figure 53: Phase II OPB and TOR results for the masonry wall when normal impact was applied at impact location f, when torsion was anticipated

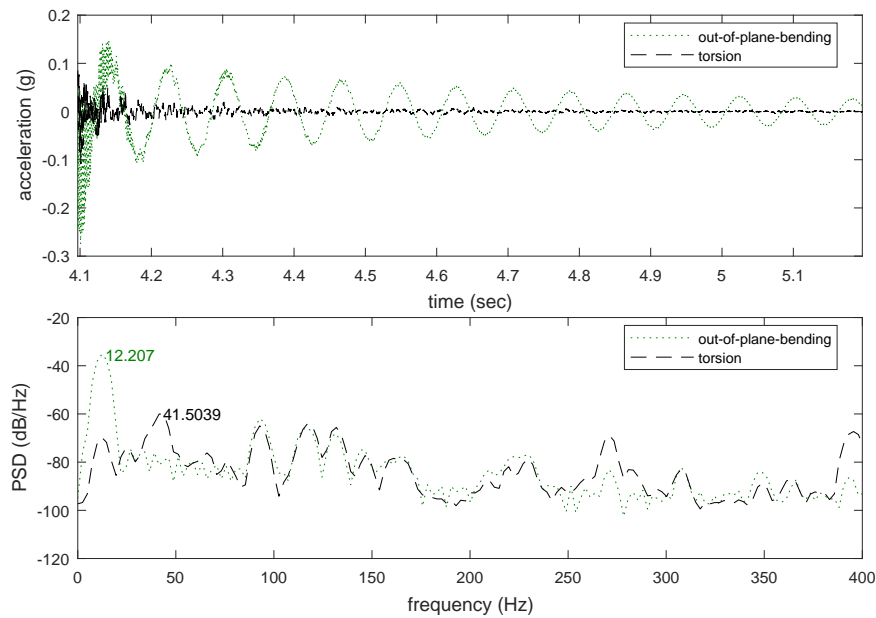


Figure 54: Phase II OPB and TOR results for the masonry wall when normal impact was applied at impact location g, when out-of-plane bending was anticipated

The author anticipates the torsional response to be the dominant motion when the excitation is applied on locations e and f. On the other hand, the out-of-plane bending motion is anticipated to be dominant when the specimen was excited at impact location g. The dominance is indicated by the highest peak on the PSD plots. The out-of-plane bending and torsional fundamental frequencies have thus been identified as 12.21 Hz and 41.50 Hz, respectively, from these three plots. Neither the out-of-plane bending nor the torsional fundamental frequencies conform to their anticipated values of 2.34 Hz and 11.15 Hz, respectively. Further work can start with using a more accurate estimation for torsional constant,  $J$ . The out-of-plane bending and torsional fundamental frequencies observed in Section 5.3.3 – results of in-plane impacts – differ slightly from the results of the out-of-plane impacts presented here.



### **5.5.2 Comparison of force magnitudes between normal and gentle impacts applied on masonry wall specimen**

As presented and discussed in Section 5.3, normal and gentle impacts are used by the author to assess the feasibility of applying gentle taps in modal hammer tests as a potential application in SHM. Since the excitations were applied manually, their magnitudes varied at the different trials. In this section, the force magnitudes of the normal and gentle impacts are presented quantitatively and compared. Figure 55 presents the magnitudes of the applied excitation force of both the normal and gentle for the datasets studied.

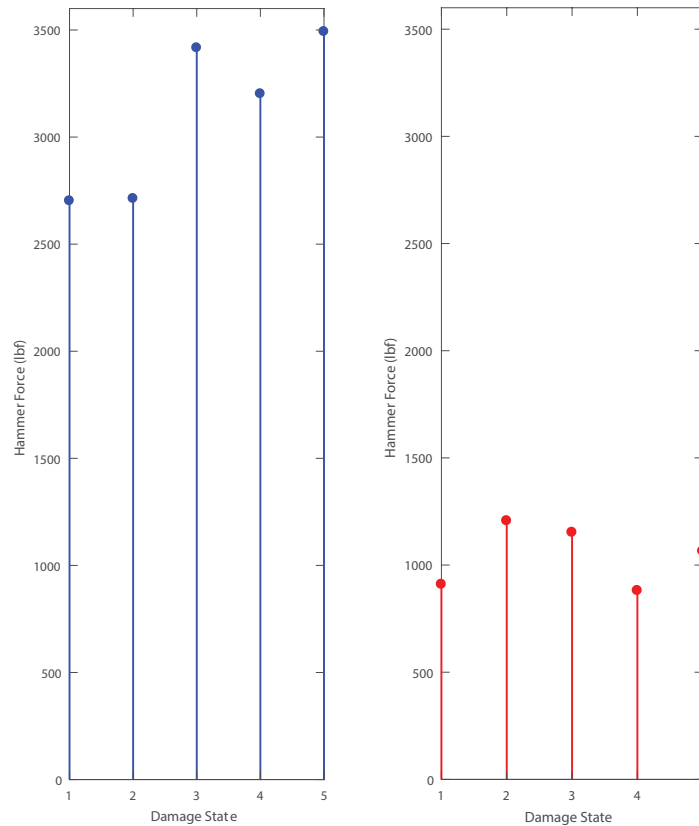


Figure 55: Comparison between normal and gentle impacts: force magnitudes for normal impact shown in blue, and force magnitudes for normal impact shown in blue, applied at the different damage states labeled from 1 to 5 representing elastic to ultimate state.

As seen in Figure 55, the magnitudes of applied excitation forces vary through. However, the differences in magnitudes between normal and gentle impacts is visually distinguishable. The normal impact force magnitudes ranged from approximately 2700 *lbf* to about 3500 *lbf* with an average of 3105 *lbf*, while that of the gentle impact ranged from approximately 900 *lbf* to about 1200 *lbf* with an average of 1043 *lbf*.

### 5.5.3 More details on PSD plots

Power spectral density (PSD) can be plotted using a number of ways. In this study, a MATLAB<sup>®</sup> built-in function named `pwelch` is utilized in plotting all PSD plots of the studied specimens. `Pwelch` is chosen for this study due to its popularity in practice. In the default setting of `pwelch`, which is adopted throughout this study, an entire dataset is divided into eight segments with 50% overlap, after which the FFT results of all segments are averaged for PSD. This choice in DSP and the available data length dictate the resolution of the PSD plot in this study.

For demonstration of how `pwelch` works and how the resolution could be improved one dataset from the prestressed concrete girder's tests is utilized in this comparison. To begin with, the length of the free vibration window that was utilized in processing the girder's response is utilized. This length is 0.75 second. Figure 56 presents the full and truncated frequency responses generated by the default `pwelch` command. This plot indicates 11 data points between 0 and 50 Hz.

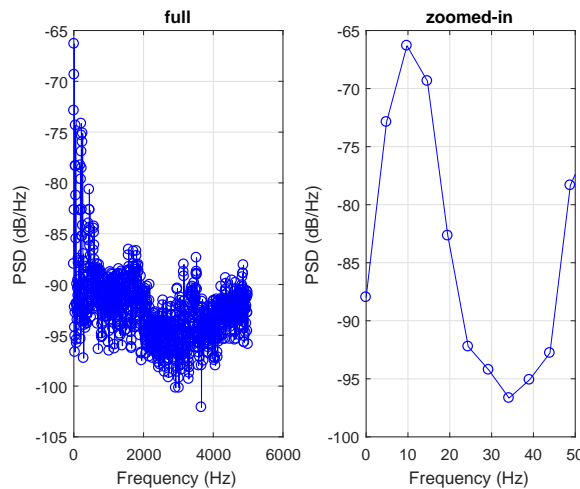


Figure 56: Figure showing the `pwelch` frequency plots with a free vibration window length of 0.75s

With a sampling rate,  $f_s$  of 10,000 Hz, the length the data for Figure 56 is 7500

data points. The “readable frequencies” range from 0 to 5,000 *Hz* which is half of  $f_s$ , the so-called “Nyquist frequency.” Since *pwelch* divides the entire length into eight segments with 50% overlap, each segment has 1666 data points. This number is rounded down from  $\frac{7500}{4.5}$ , and then zero padded to the closest  $2^{n+1}$  for FFT. For each of the segments, the default *pwelch* length is then  $2^n + 1$ . through a DSP concept called “zero padding” when necessary. For this case, the maximum possible  $n$  that will fit the segment length is 10, which gives the PSD (as used in this study) a maximum length of 1025 data points to display from 0 to 5,000 *Hz*. Thus, for a window of 0 to 50 *Hz*, only 11 data points can be used.

In order to improve the PSD resolution still under the default *pwelch*, the data length must then be extended. Given the involvement of zero padding, the increment of data length and improvement of PSD resolution do not have a linear relationship. For example, Figures 57 and 58 contrast two choices in data length: 0.92 and 0.923 second, between which the resolution is doubled. Future studies can look into a user-defined setting of *pwelch* or other choices in plotting PSD.

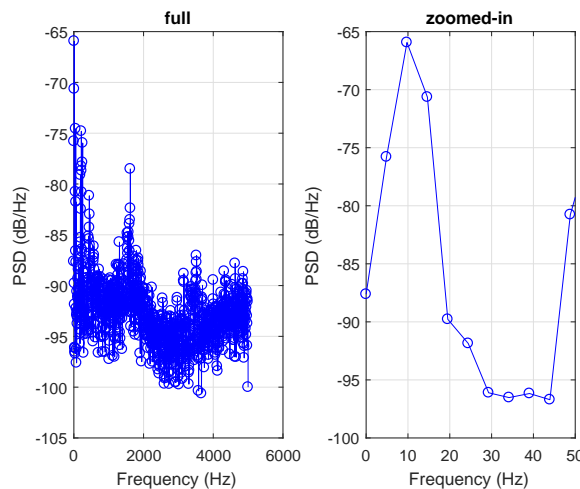


Figure 57: Figure showing the default *pwelch* PSD plots with a free vibration window length of 0.92s

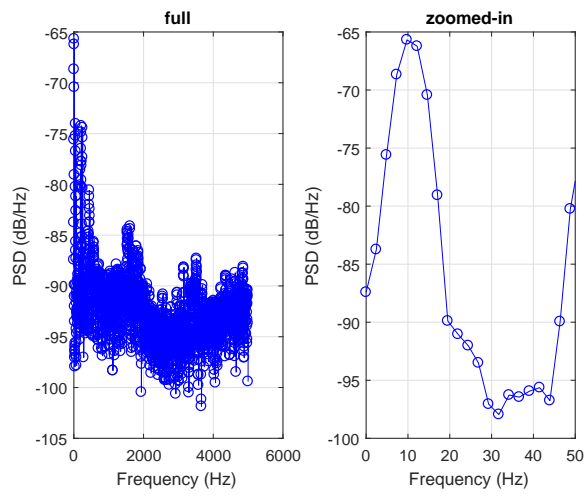


Figure 58: Figure showing the default pwelch PSD plots with a free vibration window length of 0.923s

## 6 DISCUSSION

Although a few limitations of this study have been mentioned in the previous chapters, a comprehensive list of limitations are presented in this chapter, in addition to recommendations for future work.

### 6.1 Limitations of this Study

The limitations in this study can be divided into three categories: instrumentation, specimen and data analysis.

#### 6.1.1 Instrumental limitations

The instrumental limitations are a major problem encountered during the experimental investigation of this study. They are described as follows:

**Sensor noise interference:** During testing, the accelerometers captured electrical noise, footsteps, vibration from other motorized lab equipment and any other vibrations within a fairly close range. To mitigate this problem, the author avoided conducting modal hammer tests during a busy time in the lab. Additionally, once the data acquisition system was started for a particular test, the author avoided stepping heavily on the floor.

**Saturated accelerometers:** 2g accelerometers were mostly used in this study due to their higher resolution than other available modules. Their constraints, however, were that they cannot measure acceleration outside of the  $\pm 2g$  limit. Higher acceleration was encountered during the timber joint testing when the responses exceeded the measurable limits of the accelerometer, thus causing saturation. In order to avoid the saturation, the impact force

intensity was manually reduced by the author. This reduction reduced resulted in less acceleration induced to the specimen, thus, not exceeding the accelerometer's  $\pm 2g$  limit.

**Equipment malfunction:** Equipment constraints were encountered throughout the experimentations in this study. Malfunctions encountered include wire pinching, occasional accelerometer irresponsiveness and DAQ channel malfunction. The wire pinch problem was experienced once and was caused by a table leg that rested on the accelerometer wire. This pinch resulted in dense high-frequency noise during data acquisition.

**Modal hammer response drift:** Throughout the experimental investigations, the modal hammer response has indicated incremental drifts whose root cause is yet to be determined.

**Limited number of accelerometers, cable length, and capability of SCB-68:** These DAQ constraints limited the number of locations on the tested specimens whose responses could be measured. Due to this limitation, the rotational rigid body motion for the out-of-plane response of the girder and masonry wall could not be measured and cannot be analyzed.

**Manually-controlled excitation:** The modal hammer excitation was applied using human effort. The author strived to perfect the excitation magnitude and direction, yet the human imperfections did not guarantee consistency.

### 6.1.2 Specimen limitations

**Component testing:** In this study, the masonry wall was tested as an isolated component. In reality, it is part of a system including a slab and continuous walls. The component nature might be different from a real-world nature of a typi-

cal shear wall that is part of a building system. Paquette and Bruneau [2003] studied a four sided masonry wall with continuous slabs for its seismic behavior and concluded that the continuous corners have negligible effect in the walls lateral strength. However, in this study, where both in-plane and out-of-plane motions are studied, the behavior of the wall is expected to change given that it had continuous corners. This limitation applies to the timber wall specimen, and may also apply to the prestressed concrete girder and timber joint specimens.

### 6.1.3 Analysis limitations

**Limitation of SDOF models:** SDOF models are known for their effectiveness for many practical applications and great popularity as the first approximation of real-world structural dynamics. However, structures inherently have infinite number of DOFs. Thus, the accuracy of SDOF models is not guaranteed for application scenarios. There maybe potential limitations with some of the assumptions made during the estimation of the fundamental frequencies of the specimen presented in Section 3.3.2.

**Linear analysis:** Not all structures behave linearly. Prestressed concrete specimens typically behave linearly as long as the section remains uncracked (Nawy [2006]). Masonry and timber materials are known to behave inherently non-linear Marotta et al. [2011]. Thus, linear analysis cannot offer a comprehensive study on the masonry and timber specimens.



## 6.2 Future Work

This study has laid a solid foundation for a number of future studies that can either be built on or separate from this study. Similar to the layout of this study, the future studies can be categorized into two parts: experimental investigation and data processing, and are described as follows:

### **For experimental investigation:**

- Structural free vibration testing should be conducted with a more comprehensive accelerometer layout if instrumentation allows it. This will allow more detailed analyses to be conducted and MDOF models to be adopted.
- More robust acquisition systems that are highly sensitive but immune to noise should be used for future experiments similar to this study. Wireless sensors may be feasible to avoid wiring noise interference, pinches and cable length constraints, although the limitations of wireless sensors can be can apply.
- A simple masonry and timber house should be tested to study the behavior of the structures as part of a system. A bridge should also be tested in a similar way to study the behavior of the girder as part of a system. Results obtained from these studies should be compared with results from this study.
- Symmetrical girder specimens should be tested and analyzed in a similar way and results obtained should be compared with results from this study.

### **For data processing:**

- As it has been mentioned before, the scope of the data collected is too large

for this study. With emphasis specified on SDOF modeling, the analysis in this study is only focused on selected in-plane and out-of-plane impact locations. Other impact locations from the collected datasets should be studied to generate a comprehensive analysis of the tested structural elements thus validating the developed modular code. Other tested specimens tested but not analyzed in this study are recommended for analysis in future studies.

- The modular code developed in this study should be expanded to analyze other inconclusive observations in this study, such as: why beating occurred on the normal impact and not the gentle impact, and why another frequency is observed on the masonry wall's response at the elastic and early stages of damage but faded away after extensive damage has occurred.
- This study is only focused on linear analysis. Nonlinear analysis should be conducted, especially for the masonry and timber specimens due to their inherent nonlinear nature.

## 7 CONCLUSION

The author has conducted free vibration tests on four types of common structural elements and linear dynamics data analysis on two of the specimens. Motivated by an increasing number of environmental events that accelerate structural deterioration, in conjunction with the need to make structures more resilient to these events, this study strives to better understand some real world structural free vibration responses. The tested structures include a retired prestressed concrete girder, a masonry wall, a timber wall and a set of timber connection specimens. The author has conducted modal hammer tests on the named structures with careful planning for modeling purpose and a thorough execution taking into account challenging practical constraints to generate a large amount of high quality datasets for this study and future studies. In addition, a comprehensive linear SDOF analysis has been conducted on two of the named specimens, the prestressed concrete girder and the masonry wall, using a modular MATLAB code that has been generated with general applications in mind.

The experimental investigation was conducted with a scope intended to accommodate a wide range of analysis. Specimens were tested for free vibration with the use of a modal hammer to excite them and record their motions using accelerometers. The specimens were excited at designated impact locations that are each expected to have a certain effect to its behavior. The motions were recorded at critical locations through mounted accelerometers. The tests were designed with the goal of conducting linear SDOF analysis in this study and nonlinear analysis in future studies.

Data processing, in this study, was facilitated by a modular code that was developed in this study. The modular code was largely based on proper digital signal processing (DSP) tools that enabled a sequential procedure that is divided into

three phases. Phase I, which laid a foundation for the remaining two, was conducted to extract meaningful results from a typical dataset with the use of two windows: major response and free vibration windows. The free vibration window was considered the core of the analysis and from it, the fundamental frequency was extracted. Phase II used the free vibration window to extract the fundamental frequency of in-plane bending and confirmed its consistency in all in-plane measured locations. In addition to this extraction, phase II checked to confirm that all measured in-plane motions were in phase to verify the occurrence of first mode. Phase II continued to analyze out-of-plane bending and torsion to check the presence of the fundamental frequency where, the confirmation of its absence would imply a pure in-plane first mode. Phase III was mainly a contribution to SHM as it mainly analyzed the changes in fundamental frequency through the different damage states of a structure. From the three phases described, valid conclusions were drawn for both the prestressed concrete girder and masonry wall specimens.

For both of the analyzed specimens, it was concluded that the obtained fundamental frequencies were not purely for in-plane bending. Instead, both of the specimens' first modes were a combination of in-plane bending, out-of-plane bending and torsion. Both of the experimentally obtained fundamental frequencies were less than the anticipated fundamental frequencies. With assumption that sidesway would control the in the response of the masonry wall, the experimentally obtained fundamental frequency of the masonry wall, however, was about 8% lower than the anticipated value. The fundamental frequency of the masonry wall was observed gradually decrease through the different damage states as expected.

For the sake of SHM, the author compared the results of the masonry wall specimen arising from two levels of excitation impact forces: normal impact and gentle impact. Gentle impact was averaged about a third of the normal impact's force

magnitude. The observed consistency in the results indicates that gentle impact is a possible application in SHM.

Two interesting observations made were: (1) normal impact was observed to cause beating for some of the masonry wall responses while gentle impact did not create that effect, and (2) the masonry wall results indicated the existence of another frequency which disappeared after the specimen has gone through extensive damage. These two observations were inconclusive in this study.

With properly designed testing procedures, acquired data, analysis procedure and modular code, this study provides opportunities for further testing and analysis to be continued for a long-term goal of more resilient civil infrastructure.

## Bibliography

Plan: prestressed concrete girders. Structural Drawing, 1967.

American Concrete Institute. Building code requirements for structural concrete (aci 318-14) and commentary, 2014.

American Wood Council. National design specification (nds) supplement: Design values for wood construction, 2014.

*Manual for engineered wood construction.* American wood council, 2015.

James C Anderson and Farzad Naeim. *Basic structural dynamics.* John Wiley & Sons, 2012.

R. D. Andrews and A. Holland. Summary statement on oklahoma seismicity. Web, April 2015.

ASCE. 2017 infrastructure report card. web: <https://www.infrastructurereportcard.org/>, 2017.

A. P. Boresi and R. J. Schmidt. *Advanced mechanics of materials.* Wiley New York, 6 edition, 2003.

A. K. Chopra. *Dynamics of structures: theory and applications to earthquake engineering.* Prentice-Hall, 2012.

City of Moore. Ordinance no. 768 (14), section 5-204 adoption of dwelling code, 03 2014.

Dytran Instruments, Inc. *Performance specification, model 5800b4.* 21592 Marilla St. Chatsworth, CA 91311, a.

- Dytran Instruments, Inc. *Operating guide, model 5803A instrumented impulse hammer, twelve pound sledge*. 21592 Marilla St. Chatsworth, CA 91311, b.
- R. W. Floyd. *Masonry wall design, construction and shear testing*. 2017.
- R. W. Floyd, J. S. Pei, C. D. Murray, B Cranor, and P. F. Tang. Understanding the behavior of prestressed girders after years of service. Tech report, University of Oklahoma, 12 2016.
- N. F. Grace and B. Ross. Dynamic characteristics of post-tensioned girders with web openings. *Journal of Structural Engineering*, 122(6):643–650, 1996.
- N. Hajdin. A method for numerical solution of boundary value problems. *Trans. Civ. Engng. Dept*, 4:1–58, 1958.
- S. M. Han, H. Benaroya, and T. Wei. Dynamics of transversely vibrating beams using four engineering theories. *Journal of sound and vibration*, 225(5):935–988, 1999.
- G. W. Housner, L. A. Bergman, T. K. Caughey, A. G. Chassiakos, R. O. Claus, S. F. Masri, R. E. Skelton, T. T. Soong, B. F. Spencer, and J. T. P. Yao. Structural control: past, present, and future. *Journal of engineering mechanics*, 123(9):897–971, 1997.
- S. Jacobs, S. Matthys, G. De Roeck, L. Taerwe, W. De Waele, and J. Degrieck. Testing of a prestressed concrete girder to study the enhanced performance of monitoring by integrating optical fiber sensors. *Journal of structural engineering*, 133(4): 541–549, 2007.
- M. Kato and S. Shimada. Vibration of pc bridge during failure process. *Journal of Structural Engineering*, 112(7):1692–1703, 1986.

- J. P. Lynch and K. J. Loh. A summary review of wireless sensors and sensor networks for structural health monitoring. *Shock and Vibration Digest*, 38(2):91–130, 2006.
- E. C. Mai, Y. P. Sugeng, J. S. Pei, S. M. Zimmermann, C. V. Borchard, Y. Li, and K. Piyawat. Development of small wood models to demonstrate nonlinear dynamics. Proceedings of IMAC-XXVI: A Conference & Exposition on Structural Dynamics, Orlando, FL, Feb 2008.
- T. W. Marotta, J. C. Coffey, C. Brown LaFleur, and C. LaPlante. *Basuc construction materials*. Pearson prentice hall, 5 edition, 2011. ISBN 0135129699.
- Masonry Standards Joint Committee. *Building code requirements and specification for masonry structures*. The Masonry Society, Boulder, CO, 2008.
- S. H. Mirtalaie, M. Mohammadi, M. A. Hajabasi, and F. Hejripour. Coupled lateral-torsional free vibrations analysis of laminated composite beam using differential quadrature method. *World Academy of Science, Engineering and Technology, International Journal of Mechanical, Aerospace, Industrial, Mechatronic and Manufacturing Engineering*, 6(7):1143–1148, 2012.
- S.P. Narayanan and M. Sirajuddin. Properties of brick masonry for fe modeling. *American Journal of Engineering Research (AJER)*, pages 2320–0847, 2013.
- National Instruments. National instruments - scb-68 block. Web.
- E. G. Nawy. *Prestressed concrete: a fundamental approach*. Pearson prentice hall, 5 edition, 2006. ISBN 0131497596.
- J. Paquette and M. Bruneau. Pseudo-dynamic testing of unreinforced masonry building with flexible diaphragm. *Journal of structural engineering*, 129(6):708–716, 2003.



- B. Peeters. System identification and damage detection in civil engineering. 2000.
- Precast/Prestressed Concrete Institute. Pci design handbook: precast and prestressed concrete, 2010.
- A. Prokic, M. Besevic, and D. Lukic. A numerical method for free vibration analysis of beams. *Latin American Journal of Solids and Structures*, 11:1432 – 1444, 12 2014. ISSN 1679-7825.
- S. S. Rao. *Vibration of continuous systems*. John Wiley & Sons, 2007.
- H. G. Russell, A. R. Anderson, J. O. Banning, I. G. Cantor, R. L. Carrasquillo, J. E. Cook, G. C. Frantz, W. T. Hester, K. L. Saucier, P. C. Aitcin, et al. State-of-the-art report on high-strength concrete. *Chicago Committee on High-Rise Buildings*, 1977.
- M. Saiidi, B. Douglas, and S. Feng. Prestress force effect on vibration frequency of concrete bridges. *Journal of structural Engineering*, 120(7):2233–2241, 1994.
- O. S. Salawu. Detection of structural damage through changes in frequency: a review. *Engineering structures*, 19(9):718–723, 1997.
- O. S. Salawu and C. Williams. Review of full-scale dynamic testing of bridge structures. *Engineering Structures*, 17(2):113–121, 1995.
- Silicon Designs, Inc. *Model 2210 Analog Accelerometer Module*. 1445 NW Mall St. Issaquah, WA 98027, 2006.
- Y. P. Sugeng. Shaking table tests of timber joints to understand nonlinear dynamics. Ms thesis, University of Oklahoma, 2006.
- P. F. Tang. *Analysis of Backbone Technique: A Hilbert Transform and Discrete Hilbert Transform-Based Technique*. PhD thesis, University of Oklahoma, Norman, OK, December 2015.

J. K. Wight. *Reinforced concrete: Mechanics and design*. Pearson, 2016.

K. Worden, C. R. Farrar, G. Manson, and G. Park. The fundamental axioms of structural health monitoring. In *Proceedings of the Royal Society of London A: Mathematical, Physical and Engineering Sciences*, volume 463, pages 1639–1664. The Royal Society, 2007.

Y. Yu, J. P. Ou, C. W. Zhang, and L. Y. Li. Wireless inclinometer sensor and its data acquisition system for swing monitoring of large scale structures. In *Earth & Space 2008: Engineering, Science, Construction, and Operations in Challenging Environments*, pages 1–7. 2008.

## 8 APPENDICES

### A EXPERIMENTAL INVESTIGATIONS OF MASONRY WALL AND TIMBER JOINT SPECIMENS

#### A.1 Masonry Wall: Specimen Description

The masonry wall specimen was designed to mimic the portion of a masonry building in between two door openings. The entire specimen consists of a reinforced concrete base, a 4 *ft* tall reinforced masonry wall section and a reinforced concrete block section on top of the wall as shown in Figure 59.

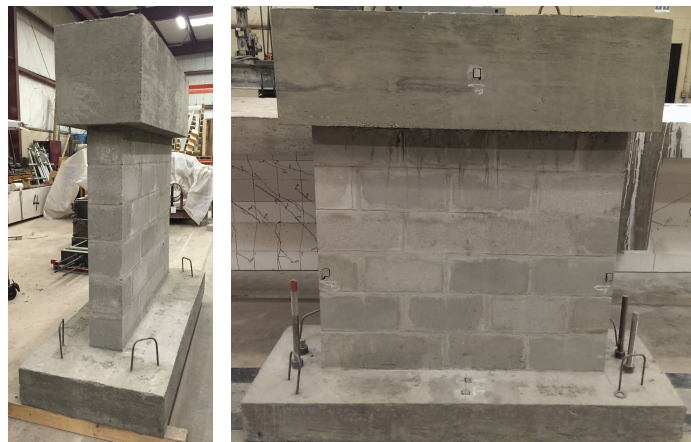


Figure 59: Pictures of the masonry wall specimen

The 4 *ft* tall masonry portion of the wall is to represent a typical 8 *ft* wall; and is built to half-scale due to lab head room constraint. The single wythe wall is designed with 8 *in* wide hollowed concrete masonry units (CMU) and is reinforced using three #4 bars. The concrete block at the top is designed to mimic the gravity loads that bear on the wall in a real-world scenario.

The free-hand sketch presented in Figure 60 gives the full dimensions of the specimen. The specimen's impact location and sensor layout (do be discussed in Appendix A.2) are also illustrated on the sketch.

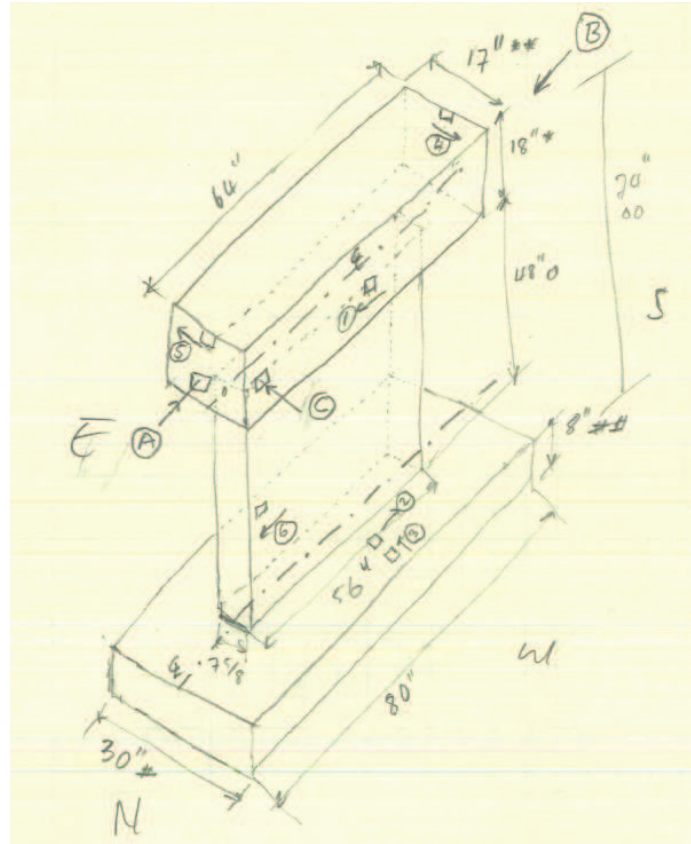


Figure 60: Free-hand sketch of the masonry wall specimen by the author (not to scale)

## A.2 Masonry Wall: Test Setup and Procedure

The masonry wall was tested in a similar manner as the timber wall for both static and modal hammer tests.

The masonry wall underwent a series of static lateral loading in between its modal hammer tests. The loading process was similar to the one conducted on the timber wall specimen. Thus, the modal hammer tests was conducted at different

damage states of the specimen. Figure 61 presents the lateral loading setup.



Figure 61: The masonry wall lateral test setup: (a) string potentiometer for measuring deflection; (b) hydraulic loading piston for applying lateral force; (c) load cell for measuring the applied lateral force, and (d) shear loading plate for transferring the shear load to the specimen

Figures detailing the masonry wall's impact locations and sensor layout can be found in Section 5.3.1. Modal hammer impacts were applied at designated impact locations. As shown in Figure 41, these impact locations were designed to produce in-plane bending, out-of-plane bending and torsional responses for the specimen.

Similar to the procedure conducted on the prestressed concrete girder, the masonry wall was sanded at necessary locations using a grinding tool to ensure proper application of excitation force and mounting of accelerometers.

To capture the in-plane, out-of-plane and torsional motions of the specimen, six accelerometers were mounted on the specimen at different locations of interest. The sensor layout for the masonry wall is given in Figure 42 and Table 13 presents further details of each sensor's measured motion. Together with the one channel reserved for the modal hammer reading, there was a total of seven channels

making it possible to use the differential mode of the SCB-68 when there was one malfunctioning channel.

### A.3 Timber Joints: Specimen Descriptions

Designed and fabricated by Sugeng [2006] and Mai et al. [2008] to assess their non-linear behaviors, the timber joint specimens are of two types: a T-shaped and a frame model. Three T-shaped and two frame models were tested in this study. All connected lumber arms are 12 *in* long. The timber joint specimens are made of 2 × 4 Spruce Pine Fir lumber and are designed with varying connection types. Figure 62 presents drawings of the connection details on all five specimens. Figure 62(a) shows the T-shaped specimen connected using L-plates (A21Z angle) (Sugeng [2006]) on both the bottom and top connections. Figure 62(b) and (c) show the specimens using mending plates (MP14) (Sugeng [2006]) on both connections, and mending plates on the bottom connection and an L-plate at the top plate, respectively. In addition to the connectors, all three T-shaped specimens used two 12D nails (Sugeng [2006]) at every connection. The two frame models only used two 12D nails in its connections.

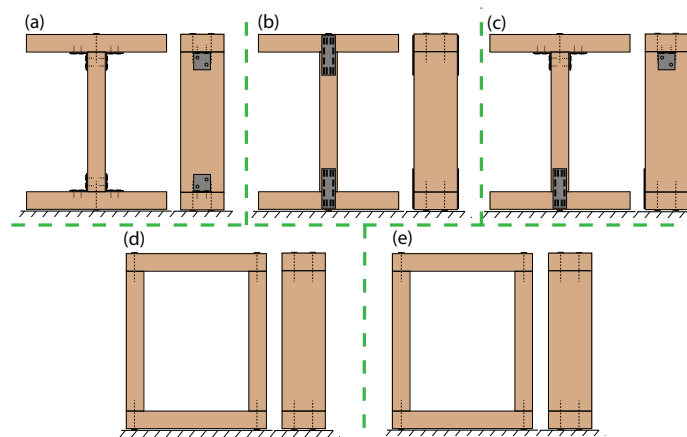


Figure 62: Connection details for the five timber joint specimens tested

## A.4 Timber Joints: Test Setup and Procedure

As shown in Figures 63 and 64, the specimens were tested with an added mass at the top; a steel block weighs 8.93 *lb*.

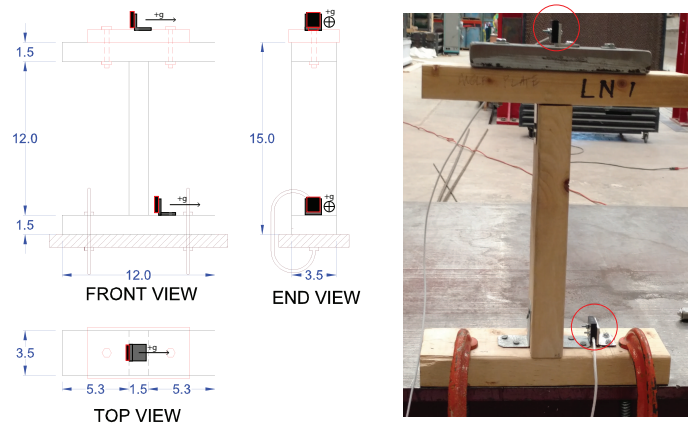


Figure 63: Test configuration for a typical T-shaped timber joint specimen; all dimensions are in inches

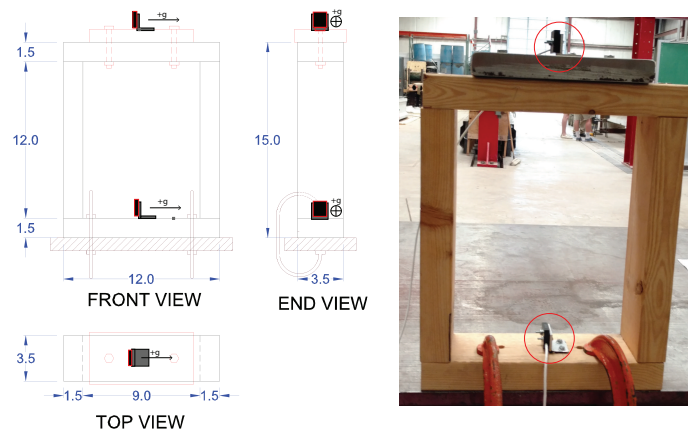


Figure 64: Test configuration for a frame timber joint specimen; all dimensions are in inches

All five timber joint specimens were tested in the same manner. During testing, each specimen was clamped to a semi-rigid table at Fears Structural Engineering Laboratory at the University of Oklahoma and excited laterally at one location only

- the top lumber. Excitation was applied using the small Dynapulse hammer described in Section 4.2.1. Different hammer heads of varying hardness were used during testing. Two uniaxial  $\pm 2g$  range SD accelerometers were utilized in each test; one mounted at the base and one at the top lumber of each specimen as highlighted in Figures 63 and 64. The base accelerometer was utilized to correct the translational rigid body motion in data processing.



## B OTHER INFORMATION RELEVANT TO Chapter 5

### B.1 Other Specimens' Test Nomenclature

Table 17: Test IDs for Girder C specimens (Test ID template = GCtest "a" "b" "c")

<b>GCtest</b>	<b>"a"</b>	<b>"b"</b>	<b>"c"</b>
<b>Representation</b>	Impact ID (long.)	Impact ID (trans.)	Date ID
<b>Range</b>	1 - 3	1 - 3	1 - 2
Number	1	1	1
Representation	0	center	June 24th, 2015
Number	2	2	2
Representation	15feet north	west offset	June 25th, 2015
Number	3	3	
Representation	15feet south	east offset	

Table 18: Test IDs for Masonry Wall (Test ID template = MWtest “a” “b” “c” “d”)

<b>MWtest</b>	<b>“a”</b>	<b>“b”</b>	<b>“c”</b>	<b>“d”</b>
<b>Representation</b>	Condition ID	Impact ID	Hit Force ID	Trial ID
<b>Range</b>	0 - 4	1 - 7	1 - 2	1 - 3
Number	0	1	1	1
Representation	elastic	location 1	normal impact	first trial
Number	1	2	2	2
Representation	first crack	location 2	gentle impact	second trial
Number	2	3		3
Representation	post crack	location 3		third trial
Number	3	4		
Representation	post crack 2	location 4		
Number	4	5		
Representation	ultimate	location 5		
Number		6		
Representation		location 6		
Number		7		
Representation		location 7		

Table 19: Test IDs explanation for tested Timber Joint specimens (Test ID template = TJtest“a” “b” “c”) †see Figure 62

<b>TJtest</b>	<b>“a”</b>	<b>“b”</b>	<b>“c”</b>
<b>Representation</b>	Specimen ID†	Hammer head ID	Trial ID
<b>Range</b>	1 - 5	1 - 3	1 - 2
Number	1	1	1
Representation	Specimen (a)	aluminum head	first trial
Number	2	2	2
Representation	Specimen (b)	rubber head	second trial
Number	3	3	
Representation	Specimen (c)	white head	
Number	4		
Representation	Specimen (d)		
Number	5		
Representation	Specimen (e)		